Differentiationsprozesse alkalischer bis peralkalischer Magmen, untersucht am Ilímaussaq-Komplex der Gardar-Provinz in Süd-Grönland

Dissertation

zur Erlangung des Grades eines Doktors der Naturwissenschaften

der Geowissenschaftlichen Fakultät
der Eberhard-Karls-Universität Tübingen

vorgelegt von
Thomas V. Krumrei
aus Dresden

2007

Tag der mündlichen Prüfung: 29.06.2007

Dekan: Prof. Dr. Peter Grathwohl

1. Berichterstatter: Prof. Dr. Gregor Markl

2. Berichterstatter: PD Dr. Thomas Wenzel

Danksagung

Zuerst möchte ich Gregor Markl für die Aufnahme in seine Arbeitsgruppe, für die Zurverfügungstellung des Themas und die Betreuung der Arbeit sehr herzlich danken. Thomas Wenzel sei für die Übernahme des Koreferates mein herzlichster Dank ausgesprochen. Außerdem zeichnet er für die gute und verlässliche Qualität der Mikrosondenanalytik verantwortlich, wofür ihm ebenfalls mein Dank gewiss ist. Für die Unterstützung bei der Ar-Ar-Datierung und die Hilfe bei der Auswertung der Daten möchte ich Igor Villa ganz herzlich danken. Wolfgang Siebel danke ich für die U-Pb-Analytik und die Diskussionen dazu. Für die Spurenelementanalytik der Sodalithe mittels Neutronenaktivierung danke ich Ernst Pernicka sehr herzlich. Helene Brätz verdanke ich die Spurenelementanalysen von Amphibolen mit Laser-ICP-MS. Florian Wehland danke ich für die Hilfe zur Abkühlungsmodellierung, Thomas Wagner für thermodynamische Berechnungen und Bernd Binder für die Unterstützung bei der Ramanspektroskopie. Gisela Bartholomae hat bei der Probenaufbereitung und –separierung wertvolle Tipps gegeben.

Ein besonderer Dank geht an meine Büropartnerin Gesa Graser, die nicht nur mit fachlichem Rat zur Seite stand, sondern mir auch über eine persönlich schwere Zeit hinweghalf und auch immer auf das leibliche Wohl bedacht war. Schließlich möchte ich allen Kollegen der Arbeitsgruppe sehr für stets offene Ohren, die Bereitschaft zu Diskussionen und nicht zuletzt für das angenehme Arbeitsklima danken. Ein großes Dankeschön geht auch an das Geländeteam vom Sommer 2003, das perfekt harmoniert hat und damit die Arbeit sehr produktiv werden ließ. John Bailey, Henning Sørensen und John Rose-Hansen möchte ich meinen Dank aussprechen für die Einladung nach Kopenhagen und die Möglichkeit, Proben aus Bohrkernen zu bekommen. Brian Upton ist für Diskussionen und Anregungen mein Dank gewiss.

Ein herzliches Dankeschön geht an meine Frau Ingrid, die mir stets zur Seite stand und mir Kraft und Motivation schenkte. Nicht zuletzt danke ich auch meinen Eltern und Großeltern, die mir nicht nur das Studium ermöglicht haben, sondern mich auch während der Promotion weiterhin großzügig unterstützten.

Ziel der Arbeit

Für die Ilímaussaq-Intrusion wurden in Promotionen der letzten Jahre in petrologischen und isotopengeochemischen Arbeiten die intensiven Parameter sowie die Bedeutung von Assimilation und Fraktionierung auf die chemische Differenzierung quantifiziert. Aufbauend darauf soll eine detaillierte geochronologische Aufschlüsselung der intrusiven Ereignisse in Ilímaussaq es ermöglichen, die Differentiations-, Assimilations- und Aufstiegsprozesse zeitlich fassen zu können. Frühere Datierungen, die in der Arbeitsgruppe von Prof. Markl durchgeführt wurden, deuten darauf hin, dass möglicherweise über 30 Ma zwischen der Intrusion des ersten und des letzten Magmenschubes in Ilímaussaq liegen, obwohl sie isotopen-geochemisch und petrologisch eindeutig zusammenhängen. Für die Datierungen bietet sich die Ar-Ar-Methode, angewendet an Amphibolen, an, da die Amphibole ein Hauptmineral aller Gesteinstypen der Intrusion sind und zudem über einen für die Methode ausreichenden Gehalt an Kalium verfügen.

Nach der Erfassung des zeitlichen Rahmens der Intrusion sollen anhand von detaillierten Flüssigkeits-Einschlussuntersuchungen und der Analyse der chemischen Zusammensetzung ausgewählter Minerale die Entwicklung der Magmen und der koexistierenden fluiden Phasen näher betrachtet werden, um damit die Intrusionsgeschichte der agpaitischen Intrusionsphase in größerem Detail zu erhellen. Auch hier werfen vorläufige Studien Fragen auf, denn mittels ersten Untersuchungen von Flüssigkeitseinschlüssen scheint sich der Kristallisationsbeginn von Sodalith aus dem Dachbereich der Intrusion bereits bei einer Tiefe von etwa 3 kbar abzuzeichnen, obwohl die endgültige Platznahme der Intrusion bei 1 kbar erfolgte. Somit soll in dieser Arbeit untersucht werden, wie und in welcher Geschwindigkeit die Fraktionierung in der Tiefe bzw. im finalen Intrusionsniveau erfolgte.

Neben den sodalithreichen Gesteinen der Dachkumulate, soll auch das durch starke magmatische Schichtung gekennzeichnete Kumulat am Boden der Magmenkammer untersucht werden, um Fraktionierungsprozesse und Schmelzentwicklung in der Ilímaussaq-Intrusion besser zu verstehen.

Insgesamt soll die Arbeit eine detaillierte und quantitative Beschreibung der chemischen und physikalischen Entwicklung einer komplex zusammengesetzten, hoch differenzierten Alkali-Intrusion ergeben. Besonderes Augenmerk soll dabei auf die peralkalinen Gesteine gelegt werden, die den Hauptteil der Intrusion ausmachen.

Geologischer Rahmen

Seit 200 Jahren ist die Ilímaussaqintrusion schon Gegenstand geowissenschaftlicher Untersuchungen. Karl Ludwig Giesecke (1761 – 1833) besuchte zu Beginn des 19. Jahrhunderts mehrfach die Intrusion, um Minerale und Gesteinsproben zu sammeln. Auf ihn gehen die Erstbeschreibungen der in der Intrusion gesteinsbildend vorkommenden Minerale Arfvedsonit, Eudialyt und Sodalith zurück. In den folgenden Jahrzehnten fanden weitere mineralogische Exkursionen statt, die zu neuerlichen Mineral-Neuentdeckungen führten. Ussing war es schließlich, der 1912 eine erste geologische Karte und eine petrographische Beschreibung der Gesteine von Ilímaussaq veröffentlichte. Auf ihn geht auch der Begriff „agpaitisch" zurück. In der Mitte des 20. Jahrhunderts fanden umfangreiche Prospektionen inklusive eines Bohrprogrammes sowie Versuche zur Aufbereitung und Wertstoffextraktion statt. Als ein Ergebnis dieser Arbeiten publizierte Ferguson (1964) eine geologische Karte im Maßstab 1:20.000, die auch heute noch als Basis für geologische Untersuchungen Verwendung findet. Kurz darauf erschienen auch erste geochemische Arbeiten am Ilímaussaqkomplex (Hamilton, 1964; Ferguson, 1970), sowie weitere Erstbeschreibungen von Mineralen. Bis heute wurde die Anzahl an Mineralen, für die der Ilímaussaqkomplex die Typlokalität darstellt, auf etwa 30 erhöht (Petersen, 2001). In den vergangenen 40 Jahren nahm auch die Anzahl wissenschaftlicher Publikationen, die sich mit den unterschiedlichsten Aspekten der Intrusion beschäftigen, stetig zu. Die Reihe „ Contributions to the Mineralogy of Ilímaussaq", die wesentliche Titel der in verschiedenen Zeitschriften erschienen Artikel zum Thema zusammenfasst, enthält heute mehr als 130 Aufsätze. Eine Literaturliste wurde von Rose-Hansen et al. (2001) veröffentlicht.

Die Ilímaussaqintrusion ist Teil der Gardarprovinz an der Südspitze Grönlands. Bestehend aus archaischen Gesteinen im Norden und dem ketilidischen Graniten des Julianehåb-Batholides stellt die Gardarprovinz eine kontinentale Riftzone dar, deren Aktivität im Mittelproterozoikum lag. Neben zahlreichen Ganggesteinen unterschiedlicher chemischer Zusammensetzung intrudierten 12 größere, alkaline bis peralkaline Komplexe in einer Zeitspanne von 1280 Ma bis 1140 Ma. Die zugehörigen Extrusiva wurden weitestgehend erodiert und finden sich heute lediglich in einem durch tektonische Aktivität versetzten Block im Zentrum der Gardarprovinz (Escher & Watt, 1976). Es handelt sich bei diesen Extrusiva um die als Eriksfjord-Formation bezeichnete Wechsellagerung von Basalten und Sandsteinen, die in submarinem bis subaerischem Milieu gebildet wurden (Poulsen, 1964), deren genaue Altersstellung aber nach wie vor unklar ist (Upton et al. 2003). Nach dem Ende der magmatischen Aktivität vor

etwa 1140 Ma erfuhr die Gardarprovinz keine weitere Überprägung durch magmatische oder metamorphe Ereignisse.

An einer der großen Störungszonen, die heute die Eriksfjord-Formation begrenzen (Sörensen, 1966), intrudierte der Ilímaussaq-Komplex während der zweiten Hauptperiode der magmatischen Aktivität der Gardar-Provinz um 1160 ± 5 Ma (Blaxland et al., 1976; Krumrei et al., 2006, siehe Kapitel 1). Er ist heute auf einer Fläche von 17 x 8 km aufgeschlossen, und die Mächtigkeit des Körpers wird mit 1700 m angegeben. Durch die Analyse von Flüssigkeitseinschlüssen und die Rekonstruktion der sedimentären Überdeckung kann ein finales Intrusionslevel von ca. 1 kbar festgemacht werden. Im Gegensatz zu allen anderen Intrusivkomplexen der Gardarprovinz zeichnet sich der Ilímaussaq-Komplex dadurch aus, dass er sowohl aus Si-untersättigten als auch leicht Si-übersättigten Gesteinen besteht. Nach dem klassischen Modell entstand die Ilímaussaqintrusion in drei Phasen. Zuerst intrudierte ein Augitsyenit, der von einem Alkaligranit gefolgt wurde. Letzterer wurde von Marks et al. (2004) als krustal kontaminiertes Äquivalent zum Augitsyenit interpretiert. Schließlich entstand in einer dritten Phase der peralkaline Hauptteil des Komplexes. Die meisten der Gesteine der dritten Phase zeigen Texturen, die sie als Kumulate kennzeichnen. Vom Dachbereich der Magmenkammer nach unten kristallisierend entstanden Pulaskit, Foyait, Sodalitfoyait und Naujait. Am Boden der Magmenkammer bildeten sich die Kakortokite. Zwischen diesen Gesteinen liegen die Lujavrite, die gelegentlich immer noch Kumulatstrukturen zeigen, aber als hochmobile Restschmelzen in die Gesteine des Hangenden gangförmig eindringen konnten (Larsen & Sörensen, 1987). Unter den Kakortokiten werden, angezeigt von einer Gravitationsanomalie, weitere Kumulate vermutet. Neue Arbeiten deuten jedoch darauf hin, dass die dritte Intrusionsphase nicht als Einzelevent zu sehen ist, sondern weiter unterteilt werden muss. So trennen Sörensen et al. (2006) die Gesteine vom Dachbereich von den Kakortokiten und den Lujavriten. Zudem scheint es auch in der Entstehung der Dachkumulate eine Diskontinuität zu geben (Bailey et al., 2001; Bailey, 2006; Krumrei et al., 2007, siehe auch Kapitel 2).

Die Mineralogie der Gesteine der dritten Phase ist zugleich einfach und komplex. Sie alle bestehen aus den Hauptmineralen Alkalifeldspat, Klinopyroxenen (Aegirin), Na-Fe-Amphibolen, Eudialyt, Nephelin und Sodalith, unterscheiden sich aber stark in den Texturen und Modalanteilen dieser Minerale. Dazu kommt eine Vielzahl seltener Minerale wie Rinkit, Villiaumit, Aenigmatit, Neptunit und andere (siehe Mineralienliste in Petersen, 2001).

Die Entwicklung der Schmelzen ist anfangs gekennzeichnet durch sehr geringe Wasseraktivität (aH$_2$O), SiO$_2$-Aktivität (aSiO$_2$) und ebenfalls sehr geringe Sauerstofffugazität (fO$_2$). Alle

drei Werte steigen im Laufe der Entwicklung an (Markl et al., 2001a, b; Marks & Markl, 2001). Diese Bedingungen haben zur Konsequenz, dass zu Beginn der Entwicklung ein Fluid bestehend aus Kohlenwasserstoffen – hauptsächlich Methan – im Gleichgewicht mit der Schmelze steht und erst später im Verlauf der Fraktionierung zusätzlich ein wässriges Fluid aus der Schmelze entmischt (Krumrei et al., 2007, siehe Kapitel 2). Dabei ist aus isotopengeochemischen Untersuchungen klar, dass die Schmelzen der einzelnen Instrusionsphasen alle aus einer Quelle stammen (Nielsen & Steenfelt, 1979; Larsen & Sörenen, 1987; Stevenson et al., 1997; Marks et al., 2004).

Erweiterte Zusammenfassung

Kapitel 1 – Datierung des Komplexes

Nach einer intensiven „Grunddatierung" der Provinz durch Blaxland et al. (1976) mit der Rb/Sr-Methode wurde erst in neuester Zeit begonnen, diese Daten durch U/Pb-Untersuchungen zu vervollständigen und in ihrer Präzision zu verbessern. Alle derzeit verfügbaren Daten sind in einer Arbeit von Upton et al. (2003) zusammengefasst. Es ist offensichtlich, dass es eine große

Altersspanne der magmatischen Aktivität zwischen etwa 1140 und 1280 Ma gibt. Dabei wurden immer wieder vorhandene Strukturen in der Region um Ilímaussaq (wozu neben Ilímaussaq auch Tugtutôq gehört) als Aufstiegspfade für Magmen benutzt. Zeitlich kann die magmatische Aktivität grob in zwei Phasen unterteilt werden. Zum einen intrudierten um 1280 Ma eine ganze Reihe von Ganggesteinen (BDo-Gänge von Tugtutôq, Kangerluarssuk und Qaqortoq) sowie Teile der Motzfeldintrusion. Zum anderen lässt sich eine Zeitspanne von etwa 1180 bis 1130 Ma aushalten, in der unter anderem auch der Ilímaussaq-Komplex entstand. Blaxland et al. (1976) gibt für diese Intrusion ein Alter von 1158 ± 24 Ma an (neu berechnet mit der revidierten Zerfallskonstante für 87Rb von Begemann et al., 2001). Dieses Alter wird auch durch ein bisher allerdings nur in Form einer persönlichen Mitteilung veröffentlichten U-Pb Alters des Alkaligranites bestätigt (1166 ± 9 Ma, Heaman & Upton, zitiert in Upton et al., 2003). Weiterhin existieren zwei Alter aus Sm-Nd Daten mit 1130 ± 50 Ma (Paslick et al., 1993) und 1160 ± 30 Ma (Marks et al., 2004). Detailliertere Datierungen an einem aus mehreren Magmenschüben zusammengesetzten Komplex wie z. B. Ilímaussaq gibt es in der Gardar-Provinz nicht, d. h. es gibt bisher keine Untersuchungen zur Fraktionierungs- und Abkühlgeschichte innerhalb solch eines „composite plutons". Aufbauend auf die bisher gewonnenen Einzeldatierungen wurden, neben U-Pb Altern des Augitsyenites,

Ar-Ar- Alter von allen wichtigen Phasen in der Intrusionsgeschichte der Ilímaussaq-Intrusion bestimmt.

In Ar-Ar- und U-Pb-Studien an peralkalinen „composite plutons" außerhalb der Gardarprovinz zeigen sich sehr deutliche Unterschiede in der geochronologischen Entwicklung von Instrusivkomplexen. Die Spanne in der Entwicklungsdauer reicht dabei von quasi gleichzeitig über Systeme mit abwechselnden Intrusiv- und Ruhephasen bis zu mehrere Zehner-Millionen-Jahre dauernden Aktivitäten. In der Arbeit von Schmitt et al. (2000) am Brandberg-Komplex in Namibia wird deutlich, dass die Intrusion aller Teile des Komplexes innerhalb einer Million Jahre ablief. Dagegen konnte Henry et al. (1997) für den Solitario-Lakkolith in Texas zeigen, dass dort einzelne Intrusionsphasen durch bis zu 1 Ma dauernde Ruhephasen getrennt sind. McDowell & Mauger (1994) untersuchten den über etwa 40 Ma dauernden tertiären Magmatismus im zentralen Chihuahua, Mexiko. Der Ilímaussaq-Komplex bietet nun eine exzellente Möglichkeit, diesen Datensätzen einen weiteren hinzuzufügen, mit der Besonderheit, dass der Fraktionierungsgrad der Gesteine z.T. sehr viel höher ist als in den genannten Komplexen.

Die Alter, die mit der Ar-Ar Methode gewonnen werden können, sind Abkühlalter, d.h. das Ergebnis stellt den Zeitpunkt dar, ab dem ein Mineral unter eine bestimmte Temperatur - die sog. Schließtemperatur - abgekühlt ist. Unterhalb dieser Temperatur kann das aus dem radioaktiven Zerfall hauptsächlich von ^{40}K entstandene Ar nicht mehr aus dem Kristallgitter entweichen. Für Amphibole liegt die Schließtemperatur allgemein bei etwa 600 °C (Villa, 1998), jedoch muss für Alkaliamphibole, die für die Ilímaussaqintrusion typisch sind, eine erhöhte Porosität in Betracht gezogen werden (Dahl, 1997), die die Schließtemperatur auf 500 – 550 °C verringert. Trotzdem handelt es sich bei den an diesen Amphibolen bestimmten Altern um tatsächliche Bildungsalter, da der Solvus peralkaliner Gesteine bei außergewöhnlich niedrigen Temperaturen bis zu ~450 °C liegen kann (Boily & Williams-Jones, 1994).

Die mit der Ar-Ar Methode bestimmten Alter weisen nun eine systematische Abweichung von ca. 15 Ma von den mit anderen Methoden durchgeführten Datierungen auf. Während Datierungen mit Rb-Sr und U-Pb übereinstimmend 1160 Ma als Intrusionsalter ergeben, liegen die Ar-Ar Alter um 1145 Ma. Da aber, wie oben gezeigt, die Ar-Ar Datierung an den Amphibolen tatsächliche Bildungsalter liefert, scheidet eine langsame Abkühlung als Erklärung für diese Diskrepanz aus. Um diese Möglichkeit trotzdem zu prüfen, wurde eine Abkühlungsmodellierung durchgeführt, die ergab, dass der Komplex innerhalb weniger 100.000 Jahre unter

die Schließtemperatur abgekühlt sein muss. Die schnelle Abkühlung resultiert zum einen aus dem relativ flachen Intrusionsniveau von ca. 3 km, zum zweiten aus der wahrscheinlich schnell erfolgten Ausbildung von Konvektionszellen in den wasserreichen Sedimenten und Basalten der subaerisch bis submarin entstandenen Eriksfjord-Formation - ein sehr effektiver Prozess zum Abtransport von thermischer Energie - und schließlich auch aus der flachen Geometrie der Magmenkammer, die bezogen auf das Volumen eine große Oberfläche bietet.

Als weitere mögliche Erklärung für die Abweichung in den Altern bietet sich eine 15 Ma während Pause der magmatischen Aktivität an. In diesem Fall wären der Augitsyenit und der Alkaligranit quasi gleichzeitig um 1160 Ma entstanden und die Gesteine der dritten Instrusionsphase erst nach dieser Pause 15 Ma später. Da aber die Amphibole aus dem Augitsyenit und dem Alkaligranit Ar-Ar Alter haben, die ebenfalls 1145 Ma anzeigen, muss zusätzlich noch angenommen werden, dass durch die vom Magmenkörper der dritten Intrusionsphase ausgehende Hitze die Amphibole in beiden früheren Gesteinen deutlich über deren Schließtemperatur aufgeheizt worden sind, d.h. über etwa 550 – 600 °C, um das Isotopensystem in den Amphibolen komplett zurückzusetzen. Für eine derartige thermische Überprägung von Augitsyenit und Alkaligranit gibt es aber keinerlei Belege in den Gesteinen. Somit muss die Möglichkeit einer diskontinuierlichen magmatischen Aktivität auch ausgeschlossen werden. Alle drei Intrusionsphasen müssen in so kurzen Abständen entstanden sein, dass diese nicht mehr mit den derzeitigen geochronologischen Methoden auflösbar sind. Dass trotz der kurzen Abstände zwischen den einzelnen Magmenschüben zwischen den Einheiten Intrusivkontakte ausgebildet sind, ist ein zusätzlicher Beleg für die oben diskutierte schnelle Abkühlung.

Da davon ausgegangen werden kann, dass sowohl die Ar-Ar Alter als auch die Vergleichsalter analytisch richtig sind, bleibt nur noch die Unvereinbarkeit der verschiedenen Datierungsmethoden, bzw. fehlerbehaftete Voraussetzungen für die Berechnung der Alter. Damit sind die aufgrund sehr langer Halbwertszeiten nur sehr schwer messtechnisch bestimmbaren Zerfallskonstanten und speziell bei der Ar-Ar Methode die Verwendung von Standards mit durch unabhängige Methoden bekannten, aber mit den gleichen Problemen bei den Zerfallskonstanten belasteten Altern gemeint. In der Tat wird seit einigen Jahren in der Literatur über die Höhe der Zerfallskonstante von ^{40}K diskutiert (Min et al., 2000, Kwon et al., 2002; Villa & Renne, 2005). Dabei zeichnet sich immer mehr ab, dass die bisher als Standard für die K-Ar Datierungsmethode und deren „Ableger", das Ar-Ar-System, verwendete Konstante von $5{,}543 \times 10^{-10}$ a^{-1} (Steiger & Jäger, 1977) etwas zu junge Alter liefert. Als Bezugspunkt für die

Standards – auch den in dieser Studie verwendeten MMhb1 - wird der Sanidin aus dem Fish Canyon Tuff (FCT) verwendet, dessen Alter auf 28,02 ± 0,16 Ma bestimmt wurde (Renne et al., 1998). Aber auch das korrekte Alter des FCT wird diskutiert (Kwon et al., 2002; Kuiper et al., 2004).

Die Daten dieser Studie bieten nun eine gute Gelegenheit, zur Lösung der Probleme mit der Zerfallskonstante von 40K und dem Alter des FCT-Standards, und damit zum Abgleich zwischen verschiedenen geochonologischen Methoden beizutragen. Zusammengefasst erlauben folgende Argumente, Aussagen und Anpassungen an beiden Werten vorzunehmen bzw. stellen günstige Voraussetzungen dazu dar:

- alle Gesteine der Ilímaussaqintrusion führen für die Methode geeignete Minerale (Amphibole) mit ausreichend hohen K-Gehalten.

- Die Schließtemperatur der Amphibole für das Ar-Ar-System liegt in einem Temperatur bereich, der aufgrund der außerordentlichen Spanne (~ 1000 bis ~ 450 °C, Boily & Williams-Jones, 1994; Markl et al., 2001a) noch über dem Solvus vieler Gesteine des Komplexes - insbesondere bei denen der dritten Intrusionsphase - liegt, d.h. die Datierung liefert tatsächliche Bildungsalter.

- Der Komplex ist sehr alt, und damit wird der zu erwartende absolute Unterschied in den mit unterschiedlichen Zerfallskonstanten berechneten Altern deutlich größer als der analytische Fehler und damit wiederum aussagekräftig.

- Es liegen bereits einige Datierungen mit anderen unabhängigen Methoden vor, die als Vergleich dienen.

- Seit der Intrusion der Gesteine ist keinerlei magmatische oder metamorphe Überprägung in der Gardarprovinz zu verzeichnen (Upton et al., 2003), die das K-Ar System hätte beeinflussen können.

Um die Ar-Ar Alter mit den anderen Datierungen durch die Anpassung beider Parameter in Übereinstimmung zu bringen, kann man unterschiedliche Ansätze verfolgen, nämlich (1) nur die Zerfallskonstante anzupassen, (2) nur das Alter des FCT zu korrigieren oder (3) beide Parameter zu ändern. Letztere Variante wurde bereits von Kwon et al. (2002) durchgeführt, der dabei Werte von (5,476 ± 0,034) x 10^{-10} a^{-1} (Zefallskonstante) und 28,27 ± 0,13 Ma (Alter des FCT) erhielt. Diese Zahlen auf die Ergebnisse unserer Studie angewendet, ergaben Alter um 1170 Ma, also etwa 10 Ma zu alt. Kuiper et al. (2004) folgten dem Ansatz (2) und ermittelten als Alter des FCT 28,24 ± 0,01 Ma unter Beibehaltung der Zerfallskonstante von Steiger & Jäger (1977). Damit berechnet liegen die Ar-Ar Alter dieser Studie bei 1155 Ma. Versuche mit

dem Ansatz (1) sind dagegen in der Literatur noch nicht belegt. Eine Anpassung der Zerfallskonstante unter Beibehaltung des von Renne et al. (1998) publizierten FCT-Alters ergibt einen Wert, der sehr nahe an der von Kwon et al. (2002) veröffentlichten Zerfallskonstante liegt. Anhand dieser Ergebnisse genaue Festlegungen bezüglich FCT-Alter und 40K Zerfallskonstante zu treffen, ist zwar nicht möglich, jedoch zeigen die Daten die Größenordnung der notwendigen Änderungen auf. Und sie zeigen auf, dass die Verwendung der herkömmlichen Parameter systematisch zu junge Alter liefert, wobei die Abweichung etwa 1,5 % beträgt.

Kapitel 2 – Die Dachkumulate

Der Ilímaussaq-Komplex ist die Typlokalität für Sodalith. Als Hauptbestandteil des Naujaites tritt dieses Mineral in Ilímaussaq gesteinsbildend in großem Umfang auf. Der Naujaitkörper hat eine Mächtigkeit von mindestens 600 m und besteht bis zu 75 % aus Sodalith; der durchschnittliche Sodalithanteil liegt bei etwa 50 %. Sörensen et al. (2006) gehen sogar von einer ursprünglich noch größeren Mächtigkeit aus, die durch „piecemeal stoping" während der Intrusion der Lujavrit- und Kakortokitmagmen verringert wurde. Die Sodalithkristalle messen durchschnittlich etwa 1 cm im Durchmesser und sind meist idiomorph ausgebildet. Aufgrund ihrer geringeren Dichte als die Schmelze, aus der sie kristallisierten, stiegen sie zum Dach der Magmenkammer auf und akkumulierten dort. Mit fortschreitender Abkühlung und Kristallisation wurden sie poikilitisch von Arfvedsonit-, Alkalifeldspat- und Eudialyt-Kristallen eingeschlossen, die wiederum bis zu 10 cm groß werden.

Anhand vom im Rahmen einer früheren Diplomarbeit gemachten Flüssigkeitseinschluss-Untersuchungen an den Sodalithkristallen aus dem Naujait deutete sich an, dass ein Teil der Sodalithkristalle möglicherweise schon in deutlich größerer Tiefe gebildet wurde als es dem finalen Intrusionsniveau von ca. 3 km Tiefe entspricht. Daraus ließe sich dann schließen, dass der Sodalith, zumindest teilweise, bereits beim Aufstieg oder in einer mittelkrustalen Magmenkammer gebildet wurde. Daher sollte er Information in Form von Fluid-Einschlüssen oder auch solche mineralchemischer Art aus größeren Tiefen enthalten. Schmelzversuche an Naujaitproben zeigten, dass der Liquidus dieses Gesteins bei 1190 °C bei atmosphärischem Druck bzw. bei 900 °C bei 1 kbar liegt (Piotrowski & Edgar, 1970), wobei Sodalith die erste Phase ist, die aus der Schmelze zu kristallisieren beginnt. Da es sich beim Naujait um ein Kumulat handelt, können diese Schmelzversuche nur eine Annäherung an die tatsächlichen Kristallisationsbedingungen sein. Jedoch kommen Sharp et al. (1989), die einen anderen Ansatz wählten und die Stabilität von Sodalith im System $NaAlSiO_4$ – $NaCl$ untersuchten,

bezüglich der Kristallisationstemperatur von Sodalith zu ganz ähnlichen Ergebnissen (800 – 1000 °C), betonen aber zusätzlich, dass in der Schmelze eine hohe Aktivität von NaCl (aNaCl) für die Sodalithbildung benötigt wird. Die hohe aNaCl am Beginn und das Absinken dieses Parameters im weiteren Verlauf der Entwicklung des dritten Magmenschubes wurden von Markl et al. (2001) quantifiziert. Außerdem geht aus dieser und anderen Arbeiten hervor, dass die Schmelze durch sehr geringe fO_2 und aH_2O gekennzeichnet ist, wobei beide Werte mit zunehmender Fraktionierung ansteigen.

Um diesen Fragen nach der Fraktionierungsgeschichte und der Fluidentwicklung nachzugehen, wurden Proben aus Bohrkernen genommen (Rose-Hansen & Sörensen, 2002), die, ergänzt durch Proben von der Oberfläche, ein vollständiges Profil durch den Naujaitkörper ergeben. An diesen Proben wurden Flüssigkeitseinschluss-Untersuchungen, Mikrosondenanalysen, Analytik der Spurenelemente mittels Neutronenaktivierung (NAA), Kathodolumineszenz (CL) und Ramanspektroskopie durchgeführt.

Im CL-Bild sind klare Zonierungen der Sodalithkristalle zu erkennen, die nicht im Lichtmikroskop zu sehen sind. Die Kernbereiche haben dunklere Farben (bräunlich-orange bis violett) als die Ränder (hell orange). Oftmals zeichnen diese Zonierungen die idiomorphe Kornform nach, d.h. es handelt sich um Wachstumszonierungen.

In der Mineralchemie und im Fluideinschluss-Inventar zeigen sich systematische Variationen entlang des Vertikalprofiles durch den Naujait. So sind etwa die S-Gehalte in den mittels CL ausgehaltenen Kernbereichen der Sodalithkristalle und das Cl/Br-Verhältnis im oberen Teil des Profils weitestgehend konstant, während im unteren Teil deutlich höhere und variablere S-Gehalte in den Kernen enthalten sind und das Cl/Br-Verhältnis nach einem rapiden Anstieg mit zunehmender Tiefe wieder auf das Ausgangsniveau absinkt. Die Kernbereiche der Sodalithe führen neben kristallographisch orientiert eingeschlossenen, winzigen Aegirinnadeln auch primäre, d.h. während der Kristallisation des umschließenden Mediums entstandene Fluideinschlüsse, die mit Methan gefüllt sind und Einschlussdrucke von bis zu 4 kbar anzeigen. Dagegen fehlen in den Randbereichen der Sodalithkörner die Aegirinnadeln und auch die primären Methaneinschlüsse. Stattdessen finden sich zwei unterschiedliche Typen sekundär gebildeter Fluideinschlüsse: zum einen mit einer Mischung aus Methan und variablen Anteilen von höheren Kohlenwasserstoffen (Ethan und Propan) gefüllte Einschlüsse und zum anderen Einschlüsse mit einer mittel- bis hochsalinaren wässrigen Lösung.
Daraus ergibt sich eine zweistufige Bildung des Naujaitkörpers. Die systematischen Varia-

tionen im S-Gehalt und im Cl/Br-Verhältnis deuten darauf hin, dass es während der Soda-lithkristallisation zum Nachströmen von etwas weniger differenzierter Schmelze gekommen sein muss. Zudem lässt sich aus den Einschlussbedingungen der Flüssigkeitseinschlüsse ableiten, dass die Sodalithkristallisation schon in größerer Tiefe – beispielsweise während des Aufstiegs oder in einer tiefkrustalen Magmenkammer – begann und sich im finalen Intrusionsniveau noch fortsetzte. Aufgrund der sehr niedrigen Sauerstofffugazität und der ebenfalls sehr geringen Wasseraktivität (Markl et al. 2001), stand die Schmelze dabei mit einem aus Kohlenwasserstoffen bestehenden Fluid im Gleichgewicht, welches wegen der höheren Stabilität gegenüber höheren Kohlenwasserstoffen bei den gegebenen Bedingungen (800-1000°C und 1-4 kbar) im Wesentlichen aus Methan bestand. Dieses Fluid ist bis heute in den primären Einschlüssen in den Sodalithkernen erhalten. Mit fortschreitender Fraktionierung stiegen sowohl fO_2 als auch aH_2O an. Vor allem letzteres ist für die weitere Entwicklung der fluiden Phase und letztlich auch der Magmenzusammensetzung von Bedeutung, denn der Anstieg in aH2O in der Schmelze führt schließlich dazu, dass diese nicht mehr sämliches Wasser in gelöster Form halten kann: es kommt zur Entmischung einer wässrigen fluiden Phase aus der Schmelze. Da nun NaCl stark in solch eine wässrige Fluidphase partitioniert (Kilinc & Burnham, 1972), werden der Schmelze beide Elemente entzogen. Als Konsequenz ist die Schmelze schließlich nicht mehr in der Lage, weiter Sodalith zu kristallisieren, d.h. die Entmischung der wässrigen Phase beendet die großmaßstäbliche Sodalithkristallisation und damit die Naujaitbildung. In allen später gebildeten Gesteinen (Kakortokite und Lujavrite) findet sich Sodalith nur noch in geringen Mengen.

Neben der wässrigen Phase existierte weiterhin das an Kohlenwasserstoffen reiche Fluid. Beide Phasen sind nicht mischbar und wurden getrennt voneinander im Sodalith eingeschlossen. Konnerup-Madsen et al. (1979) berichten von sehr seltenen Flüssigkeitseinschlüssen, die beide Phasen enthalten und damit das gleichzeitige Vorhandensein beider Fluide belegen.

Kohlenwasserstoffreiche Fluide sind typisch für peralkaline Gesteine und wurden neben der Ilímaussaqintrusion auch von anderen peralkalischen Kompexen beschrieben, z.B. vom Strange Lake Pluton, Kanada (Salvi & Williams-Jones, 2006) oder vom Lovozero Komplex, Russland (z.B. Potter et al., 2004). Während über den abiogenen Ursprung dieser Kohlenwasserstoffe (KW) in der Literatur Einigkeit besteht, wird heftig darüber diskutiert, wie sie entstehen, bzw. welchen Ursprung sie haben. Konnerup-Madsen & Rose-Hansen (1982) erklärten das Auftreten von Kohlenwasserstoffen in der Ilímaussaqintrusion durch eine

spätmagmatisch bis hydrothermale Reduzierung eines primären CO_2-reichen Fluids. Salvi & Williams-Jones (1997) vermuteten den in der chemischen Verfahrenstechnik bekannten Prozess der Fischer-Tropsch-Synthese als Ursache. Auch dafür wird ein CO_2-reiches Fluid benötigt. Beide Erklärungen sind jedoch für die Ilímaussaqintrusion als nicht wahrscheinlich anzusehen, weil die kohlenwasserstoffreichen Fluideinschlüsse, die durch ihre Texturen ganz klar als primär anzusprechen sind, bei fO2-Bedingungen eingeschlossen wurden, bei denen ein CO_2-reiches, also oxidiertes Fluid nicht existiert haben kann. Ein drittes Modell zur Quelle der Kohlenwasserstoffe zieht deren primär-magmatische Herkunft in Betracht (Petersilie & Sørensen, 1970; Konnerup-Madsen & Rose-Hansen, 1982). Dass sich KW bei entsprechenden Bedingungen im oberen Erdmantel aus Karbonatmineralen bilden können, ist hinreichend belegt (Holloway & Jakobsson, 1986; Scott et al., 2004). Beim Aufstieg des Fluides in die Kruste werden höhere KW gegenüber Methan instabil (Kenney et al., 2002). Das ist die Ursache dafür, dass in den primären KW-Einschlüssen im Sodalith nur Methan nachweisbar ist. Für die primäre Herkunft spricht auch die isotopische Zusammensetzung des Kohlenstoffs. Konnerup-Madsen (2001) berechnete für $\delta^{13}C$ einen Wert von -4.5 ± 1.5 ‰ PDB, was in perfekter Übereinstimmung mit typischen Mantelwerten ist (Kyser, 1986). Die höheren KWs, die in sekundären Einschlüssen gefunden wurden, können durch Polymerisierung aus dem primären Methan entstanden sein. Auch dafür liefert die Kohlenstoffisotopie einen Beleg: auf diesem Weg entstandene KWs haben nach Des Marais et al. (1981) geringere Werte im $\delta^{13}C$ als das Methan aus dem sie gebildet wurden. Konnerup-Madsen (2001) konnte das für die in Ilímaussaq vorkommenden höheren KWs zeigen.

Die extensive Sodalithkristallisation beeinflusst das Halogenbudget der Schmelze sehr stark. Neben der Inkorporation von Chlor als Hauptelement nimmt Sodalith auch Brom und Jod auf und sogt dafür, dass die Schmelze an diesen Elementen verarmt. Dagegen passt das leichteste Halogen Fluor aufgrund seiner Größe nicht in das Sodalithgitter und verbleibt in der Schmelze. Die Partitionierung von F von den anderen Halogenen ist bisher nur aus Hydrothermalsystemen durch die Bildung von Fluorit bekannt. Während dort F durch Mineralbildung dem System entzogen wird und die anderen Halogene darin verbleiben, handelt es sich beim Naujait also um den entgegen gesetzten Prozess, der dem System Cl, Br und I entzieht und F übrig lässt. Das Verbleiben von F in der Schmelze stellt zudem möglicherweise die Voraussetzung für die teilweise extreme Anreicherung von HFS Elementen in den Gesteinen aus der dritten Intrusionsphase dar, weil diese Elemente mit Fluor vergleichsweise stabile Spezies bilden (siehe z.B. Salvi & William-Jones, 2006 und Literaturangaben darin).
Eine weitere, mittels Raman-Spektroskopie gemachte Beobachtung ist der Einbau des

Schwefels im Sodalith in Form von Sulfatgruppen, obwohl gemäß den fO_2 Bedingungen in der Schmelze der Schwefel ausschließlich in reduzierter Form als Sulfid vorkommen sollte. Dass zumindest ein Teil des Gesamtschwefels tatsächlich als Sulfid vorlag, zeigt das akzessorische Auftreten von Sphalerit im Naujait. Eine Erklärung hierfür liefert die hohe Peralkalinität der Schmelze. Der sehr hohe Na-Gehalt bei gleichzeitig geringem Al-Gehalt stabilisiert das Auftreten von Sulfat durch die Bildung von Na_2SO_4 – Gruppen in der Schmelze zu niedrigeren fO_2 hin (Baker & Rutherford, 1996, Tsujimura et al., 2004). Da aber fO_2 am Anfang der Sodalithkristallisation selbst für diesen Stabilisierungseffekt zu niedrig ist, wird kaum S in den Sodalith eingebaut. Prinzipiell kann Schwefel zwar auch in reduzierter Form als S^{2-} oder S^{3-} in Sodalith eingebaut werden, allerdings nur in Ca-reichen Gliedern der Sodalithgruppe, also Haüyn und Lazurit (Ostroumov et al., 2002; Di Muro et al., 2004). Da aber die Ca-Komponente im Sodalith von Ilímaussaq völlig fehlt, kann S offenbar nur als Sulfat eingebaut werden. Im oberen Teil des Naujaitprofils ist der S-Gehalt in den früh gebildeten Kernen der Sodalithkristalle sehr gering, im unteren Teil sehr viel höher bei starker Variabilität. Daraus ist zu schlussfolgern, dass fO_2 während der Bildung des oberen Teils noch mehr als 3 log-Einheiten unter dem FMQ-Puffer (Fayalit-Magnetit-Quarz) liegt, der unteren Grenze für den Stabilisierungseffekt durch den hohen Alkaliengehalt in der Schmelze. Die Bildung des unteren Teils des Naujaites und der im CL-Bild sehr hell lumineszierenden Ränder der Sodalithe im gesamten Profil muss dagegen bei höheren fO2 Bedingungen abgelaufen sein, hoch genug, damit S in Form von Sulfat in der Schmelze vorliegt und somit für den Einbau in Sodalith zur Verfügung steht. Dieser generelle Anstieg der Sauerstofffugazität mit fortschreitender Fraktionierung ist in der Literatur schon diskutiert und belegt (Markl et al., 2001). Die Ergebnisse dieser Arbeit erweitern jedoch das Wissen über den genaueren Verlauf der fO_2 Entwicklung während der dritten Intrusionsphase.

Kapitel 3 – Die Bodenkumulate

Der tiefste aufgeschlossene Teil der Ilímaussaq-Intrusion sind die Kakortokite. Er ist heute nur im Südteil der Intrusion zugänglich, weil der Nordteil durch eine Abschiebung versetzt wurde. Man kann aber davon ausgehen, dass sich dieses Gestein über die gesamte Fläche der Intrusion erstreckt. Der Kakortokit ist ein Nephelinsyenit, bestehend aus Alkalifeldspat, Nephelin, Eudialyt, Arfvedsonit und untergeordnet Ägirin, Sodalith und Analcim. Im Gelände auffälligstes Merkmal dieses Gesteins ist seine magmatische Schichtung. Bohse et al. (1971) zählten 29 Einheiten, die sie von unten nach oben mit -11 bis +17 nummerieren. Als Referenzeinheit mit der Nummer 0 diente dabei eine gut aufgeschlossene und über weite Strecken

gut verfolgbare Einheit. Jede Einheit ist wiederum aus drei Lagen aufgebaut. Zuunterst findet sich eine schwarze Lage, die ihre Farbe durch den hohen Anteil an Arfvedsonit erhält. Darauf folgt eine rote Lage, gefärbt durch reichlich Eudialyt, die gelegentlich aber auch fehlt oder nur linsenartig entwickelt ist. Die dritte Lage ist die dickste und verdankt ihre weiße Farbe der Dominanz von Alkalifeldspat und Nephelin. Innerhalb einer Einheit gehen die unterschiedlichen Minerallagen graduell ineinander über. Die Einheiten selbst sind jedoch durch scharfe Kontakte voneinander getrennt. Die Mächtigkeiten der einzelnen Einheiten sind über die gesamte aufgeschlossene Distanz erstaunlich gleichförmig mit einer durchschnittlichen Mächtigkeit von 8 m. Einzige Ausnahme bildet die Einheit +3, in der bis zu 100 m große Xenolithe, die aus dem Dachbereich der Intrusion stammen, eingelagert sind. Diese Xenolithe kompaktierten mehrere darunter liegende Einheiten, und die Einheit 3 verdickt sich zu den Xenolithen hin. Die Einheiten über den Xenolithen formen diese Aufwölbung nach (siehe z.B. Abb. 2a in Schönenberger et al., 2006).

In den untersten Einheiten und nochmals in Einheit +4 finden sich Strukturen wie Kreuzschichtung und Rinnenfüllungen, die auf Ablagerung in einem bewegten Medium hindeuten. Sie sind aber nur nahe des Randes der Intrusion zu finden. (Bohse et al., 1971). Daraus sind ein Wechsel in der Fluiddynamik der Schmelze und ein Unterschied zwischen Kern und Rand ableitbar. Die untersten Einheiten wurden offenbar aus einer stärker bewegten Schmelze abgelagert, wobei die Bewegung am Rand so stark war, dass sich die erwähnten Strukturen ausbilden konnten. Zudem verliert die magmatische Schichtung nahe am Rand an Deutlichkeit und geht schließlich in einen Bereich mit recht unregelmäßigen und viel dünneren Lagen über. Der Hauptteil der Kakortokite jedoch muss unter deutlich ruhigeren Bedingungen entstanden sein. Lediglich in Einheit +4 tauchen wieder Anzeichen von starker Strömung im Magma auf, die wahrscheinlich mit der Einlagerung der großen Xenolithe in Einheit +3 im Zusammenhang stehen.

Die Strukturen in den Einheiten, besonders jene um die großen Xenolithe, lassen nur den Schluss zu, dass es sich bei den Kakortokiten um Kumulate handeln muss. Aus der Schmelze kristallisierte Körner sinken aufgrund ihrer im Vergleich zur Schmelze höheren Dichte auf den Boden der Magmenkammer ab. Daraus lässt sich schließen, dass dies in einem wenig bewegten Medium geschah, denn starke Konvektionsbewegungen in der Schmelze können das Absinken von Mineralkörnern verlangsamen und sogar verhindern. Die Sortierung der Minerale innerhalb jeder Einheit erfolgte gemäß der Mineraldichte. Arfvedsonit mit der höchsten Dichte ist unten angereichert, darauf folgen Eudialyt als Mineral mit der zweitgröß-

ten Dichte und dann Alkalifeldspat und Nephelin, deren Dichte fast gleich ist. Somit kann die Schichtung innerhalb der Einheiten durch die dichtebedingten Unterschiede in der Sinkgeschwindigkeit der Minerale in der Schmelze erklärt werden. Um zu überprüfen, ob die Unterschiede in den Sinkgeschwindigkeiten ausreichend sind, um gut sortierte Lagen der Minerale zu produzieren, wurden die Sinkgeschwindigkeiten berechnet und daraus hypothetische Kumulate erstellt, deren Modalzusammensetzung mit der tatsächlich vorzufindenden verglichen wurde. Für diese Berechnung wurde ein stagnierendes Magma angenommen, was anhand der Strukturen in den Kakortokiten zumindest für einen großen Teil der Abfolge plausibel erscheint. Zudem wurde mit einer fluid-gesättigten Schmelze gerechnet, worauf später noch eingegangen werden soll. Weitere Annahmen sind homogene Nukleation und Kristallwachstum im kristallisierenden Schmelzvolumen. Die Dichte der fluid-gesättigten Schmelze wurde von Larsen & Sørensen (1987) auf 2290 kg*m^{-3} bestimmt. Des Weiteren wurden für die einzelnen Minerale typische Dichtewerte von 2590 (Nephelin), 2600 (Alkalifeldspat), 2950 (Eudialyt) und 3440 kg*m^{-3} (Arfvedsonit) benutzt. Die Viskosität der fluid-gesättigten Schmelze beträgt 139 Pa*s (Larsen & Sørensen, 1987), als Äquivalentradius der absinkenden Kristalle wurde 1.5 mm angenommen, ein typischer Wert für die heute in den Gesteinen zu findende Kristallgröße (Sørensen, 1968). Daraus ergaben sich Sinkgeschwindigkeiten zwischen 0,9 und 3,5 m pro Tag. Allein durch diese differierenden Geschwindigkeiten lassen sich gut sortierte Minerallagen erzeugen. Berechnet man die Modalzusammensetzung einer Kumulatlage, wenn sich ein Mineral rechnerisch komplett abgesetzt hat, so erhält man Werte, sehr gut mit den von Ferguson (1967) und Sørensen (1968) in den Gesteinen bestimmten Werten übereinstimmen.

Um nun zu bestimmen, wie groß das kristallisierende Schmelzvolumen sein muss, um eine durchschnittliche Mächtigkeit der Einheiten von 8 m zu erhalten, kann die Berechnung der kritischen Kristallkonzentration in der Schmelze nach Sparks et al. (1993) benutzt werden. Die kritische Kristallkonzentration gibt an, ab welcher Konzentration neu gebildete Kristalle in der Schmelze absinken können. Aus diesem Anteil kann dann berechnet werden, welches Schmelzvolumen notwendig ist, um eine Kristalllage bestimmter Dicke zu kristallisieren. Dabei muss in Betracht gezogen werden, dass solche Kumuluslagen nicht zu 100 % aus Kumulusmaterial bestehen, sondern auch ein gewisser Anteil aus der Interkumulusschmelze kristallisiert ist. Für die Berechnung der kritischen Kristallkonzentration nach Sparks et al. wurde ein für Schmelzen typischer Wert für den thermischen Expansionskoeffizient benutzt ($5*10^{-5}$ K^{-1}). Außerdem wurde ein relativ großer Temperaturgradient in der Schmelzsäule von 7 K angenommen und die oben schon angegebenen Dichten für Schmelze und Kristal-

le verwendet. Im Ergebnis erhält man kritische Kristallkonzentrationen von 0,3 (Nephelin), 0,29 (Alkalifeldspat), 0,16 (Eudialyt) und 0,1 % (Arfvedsonit). Unter der geologisch plausiblen Annahme, dass 70 % des Materials in den Einheiten Kumulusmaterial ist, ergibt sich aus der Summe der kritischen Kristallkonzentrationen eine Einheitenmächtigkeit von 7,5 m, wenn die Höhe des kristallbildenden Teils der Magmenkammer 600 m beträgt. Auch die Mächtigkeit der einzelnen Minerallagen stimmt dann gut mit der im Gelände beobachteten Mächtigkeit überein. Ob generell Kristallisation in einem derart mächtigen Schmelzhorizont auftreten kann, wird in der Literatur nach wie vor diskutiert. Sparks et al. (1993) und Marsh (1998) beispielsweise lieferten Indizien für eine Kristallisation in mächtigen Schmelzkörpern. Martin et al. (1987) oder Jaupart & Tait (1995) gehen dagegen davon aus, dass Kristallisation in „boundary layern" stattfindet, die nur eine Mächtigkeit von wenigen Metern erreichen können. Anhand der Berechnung kann jedoch mit dem boundary layer – Modell weder die Abfolge der drei Schichten noch die Einheitenmächtigkeit erklärt werden.

Zusammenfassend kann also festgestellt werden, dass die Mächtigkeit der Einheiten, die Dichtesortierung und die Modalzusammensetzung der einzelnen Minerallagen sehr gut erklärt werden können, wenn die Kristallisation in einem stagnierenden oder nur langsam bewegten Medium und die Kristallbildung gleichmäßig in etwa 600 m Magma stattfindet. Das entspricht etwa 75 % der Gesamthöhe der Magmenkammer, die mit 700 bis 800 m aus den heutigen Verhältnissen rekonstruiert werden kann. Die Schmelze in der Magmenkammer war - nach einer anfänglichen, etwas turbulenteren Phase - stagnierend oder höchstens in sehr langsamer Bewegung. Die in einem sehr mächtigen Teil der Magmenkammer gebildeten Mineralkörner konnten in diesem ruhigen Medium quasi ungestört auf den Boden der Kammer absinken. Wie die Petrographie zeigt, kristallisierten dabei alle vier Minerale gleichzeitig aus. Die unterschiedlichen Sinkgeschwindigkeiten der einzelnen Minerale reichen aus, um sie voneinander in ausreichendem Maße zu trennen, dass drei Horizonte entstehen können, die an jeweils einem, bzw. im Falle des weißen zwei, Mineralen angereichert sind. Zu klären bleibt dagegen die Ursache für die regelmäßige Wiederholung der Einheiten.

Die vielfache Wiederkehr der Drei-Lagen-Abfolge im Kakortokit wurde in der Vergangenheit mit verschiedenen Modellen zu erklären versucht. So präsentierte Sørensen (1968) ein Modell, wonach die Liquidustemperatur der Schmelze, ausgelöst durch die Migration von Volatilen und thermischer Energie um die tatsächliche Magmentemperatur herum oszilliert und so Phasen von Kristallbildung und Phasen ohne Kristallisation abwechseln. Larsen & Sørensen (1987) erweiterten dieses Modell um die Idee einer geschichteten Magmenkammer und

präzisierten die die Herkunft und Richtung der Volatil- und Wärmemigration. Danach beginnt die Kristallisation in der untersten Magmenschicht dadurch, dass Wärme und Volatile an die darüber liegende Schicht abgegeben werden. Dadurch wird die Liquidustemperatur des Magmas in der abgebenden Schicht verringert und so die Kristallisation darin ausgelöst. Das Modell erklärt so zwar die Wiederkehr der Lagenabfolge, kann jedoch nicht die sedimentären Strukturen in den Gesteinen erklären. Außerdem reicht, wie oben gezeigt, die Kristallisation eines Magmenhorizontes mit maximal wenigen dutzend Metern Mächtigkeit nicht aus, um die Mächtigkeit der resultierenden Gesteinsschicht zu produzieren. Einen weiteren Vorschlag veröffentlichten Upton (1961) und Bohse et al. (1971), wonach die regelmäßige Wiederkehr durch zyklische konvektive Umwälzung der gesamten Magmenkammer zustande kommt. Dazu steht allerdings im Widerspruch, dass es wahrscheinlich keine Konvektion in der Magmenkammer gab. Angenommen, es hätte Konvektion in der Magmenkammer gegeben, wäre die Anzahl der Konvektionszellen in der Magmenkammer, die wahrscheinlich eine Fläche von 17x8 km bei einer Höhe von lediglich 700-800 m hatte, recht groß gewesen, weil der Durchmesser einer Konvektionszelle üblicherweise dem Doppelten der Höhe der Magmenkammer entspricht. Dass aus diesen zahlreichen Konvektionszellen eine über die gesamte horizontale Erstreckung des Kakortokites gleich bleibende Mächtigkeit der Einheit entstehen kann, ist recht unwahrscheinlich.

Im Lichte der oben diskutierten Eigenschaften der Magmenkammer soll nun ein Modell entwickelt werden, welches sowohl die Strukturen in den Gesteinen als auch die berechneten Magmeneigenschaften mit einbezieht. Da eine Oszillation der Liquidustemperatur, die einen Großteil der Magmenkammer erfasst, kaum durch Wärmeverlust oder Migration von Volatilen erklärt werden kann, bleibt nur eine Variation des Druckes als Erklärung. Tatsächlich wurde die Möglichkeit von eruptiver Aktivität aus der Ilímaussaq-Intrusion von einigen Autoren in Betracht gezogen (Ussing, 1912; Ferguson, 1964), es lassen sich jedoch heutzutage keine Belege mehr davon finden. Zur Erklärung der Zyklizität von Eruptionen bietet sich ein Modell an, welches die Regelmäßigkeit von Geysiren erklärt (White, 1967). Die hydrostatische Auflast verursacht einen ansteigenden Druck im System, wenn aus einem dichteren Medium – im Falle des Geysirs das Wasser, im Falle einer Intrusion die Schmelze – eine Phase mit hohem Volumen und geringer Dichte entweicht. Beim Geysir ist das der Wasserdampf, bei der Intrusion eine volatile Phase. So steigt mit der Zeit im System der Druck an. Wenn der hydrostatische Druck das System schließlich nicht mehr geschlossen halten kann, entweicht die Gasphase bzw. die volatile Phase eruptiv und verursacht so einen plötzlichen Druckabfall im System. Dieser wiederum löst in der Schmelze die Kristallisation aus, weil durch das Entwei-

chen von Volatilen aus der Schmelze die Liquidustemperatur stark erhöht wird. Die Eruption kommt schließlich zum Erliegen, wenn der Überdruck abgebaut ist. Das System wird wieder geschlossen, die hydrostatische Auflast verhindert das weitere Entweichen der Phase mit der geringen Dichte. Der Druck baut sich langsam wieder auf, wodurch die Liquidustemperatur ebenso langsam wieder steigt, bis sie die Magmentemperatur übersteigt und damit die Kristallisation beendet. Schließlich kommt es zur erneuten Eruption, usw.

Dieses Modell ist gut auf den vierten Magmenschub der Ilímaussaq-Intrusion anwendbar, weil diese Schmelze außerordentlich reich an Volatilen war. Neben bis zu 4 % Wasser (Larsen & Sørensen, 1987) enthielt sie auch ein kohlenwasserstoffreiches Fluid (Krumrei et al., 2007) und hohe Gehalte an Halogenen, vor allem Cl und F (Bailey et al., 2001).

Da die Summe der berechneten kritischen Kristallkonzentrationen deutlich unter 1 % liegt, ist die zu erwartende Auswirkung auf die Gesamtchemie der Schmelze gering. In der Tat zeigen sich in der Mineralchemie der Amphibole aus den schwarzen Lagen nur sehr geringe systematische Änderungen. Die Gehalte von Ca und Mg sinken leicht mit der stratigraphischen Höhe, der Gehalt an Li und Na, sowie das Fe^{3+}/Fe^{2+} Verhältnis steigen etwas an. Letzteres ist konsistent mit dem allgemeinen Anstieg der Sauerstoff-Fugazität im Laufe der Fraktionierung (Markl et al., 2001). Die Ausprägung dieser systematischen Änderungen in der Mineralchemie schwankt systematisch mit der Entfernung des Probenprofiles zum Rand der Intrusion. Im Zentrum sind sie deutlich ausgeprägt, am Rand findet sich lediglich der Anstieg von Li und Fe^{3+}/Fe^{2+} Verhältnis. Da Li bevorzugt über die Reaktion $Fe^{3+} + Li = 2Fe^{2+}$ erfolgt, ist diese Koppelung nicht verwunderlich und ist damit lediglich ein Effekt der steigenden Sauerstofffugazität. Während also dieser Anstieg in fO_2 den gesamten Schmelzkörper erfasste, nahm nur der Zentralbereich der Magmenkammer an der chemische Entwicklung im Zuge der Fraktionierung teil. Das kann durch unterschiedliche Bewegungsraten der Schmelze erklärt werden. In Analogversuchen fanden Hort et al. (1999), dass - nach einer anfänglich turbulenten Bewegung - die Konvektion praktisch zum Erliegen kommt, wenn sich die Schmelze an ihrem Liquidus befindet und zwar unabhängig davon, welche Rayleighzahl das Versuchsmedium hatte. Am Rand der Versuchskammer wurde dennoch eine Bewegung registriert, die mit einem Wärmefluss durch die nicht perfekt isolierten Kammerwände erklärt wurde. Dabei handelte es sich jedoch nicht um Konvektion in diskreten Konvektionszellen. Weil das Volumen des sich am Rand bewegenden Fluids im Vergleich zum Gesamtvolumen insignifikant klein ist, verliert sich diese Bewegung in der Gesamtmasse, sobald der Strom den Boden der Kammer erreicht. Mit dieser abwärts gerichteten Strömung von kühlerer, aber an Volatilen

angereicherter Schmelze vom Dachbereich der Magmenkammer lassen sich nicht nur die im Vergleich zu den untersten Proben aus den zentraler gelegenen Profilen etwas weniger primitive Zusammensetzung der Amphibole im randnahen Profil 6 erklären, sondern auch die durch Strömungen entstandenen Strukturen in den Gesteinen, die sich bevorzugt nahe des Intrusionsrandes finden.

Zusammenfassend lässt sich die Entstehung der Kakortokite und deren magmatische Schichtung wie folgt erklären. Die bereits durch Fraktionierung in einer tief liegenden Magmenkammer entwickelte Schmelze mit hohen Gehalten an Volatilen bildete im finalen Intrusionsniveau von etwa 3 km Tiefe eine Magmenkammer von 17x8 km Fläche und einer Mächtigkeit von 700-800 m. Die Bewegungen der Schmelze waren anfänglich noch stark, was durch Strukturen, die typisch für fließende Medien sind, belegt wird. Relativ schnell beruhigte sich diese Bewegung aber und der Hauptteil der Kakortokite wurde in einer stagnierenden oder nur gering bewegten Schmelze gebildet. Ausgelöst durch Druckschwankungen, die mit eruptiver Tätigkeit im Zusammenhang standen, kristallisierten die Kumulusminerale zyklisch wiederkehrend homogen in einem Großteil des Schmelzvolumens. Dabei wurden die verschiedenen Minerale allein aufgrund ihrer dichtebedingt verschiedenen Sinkgeschwindigkeiten in diskreten Horizonten abgelagert. Weil die in jedem Zyklus kristallisierte Menge mit deutlich weniger als 1% recht klein ist, zeigen sich in der stratigraphischen Abfolge kaum bzw. nur schwach ausgeprägte Entwicklungstrends in der Mineralchemie. Wie Andersen et al. (1981) zeigten, ändert sich das, wenn sich die Kristallisationsbedingungen drastisch verändern. Dieser Umschwung wird durch das Verschwinden der magmatischen Schichtung zugunsten von Fließgefügen u.ä. in den über den Kakortokiten in der Stratigraphie folgenden Lujavriten. Außerdem sind diese Gesteine sehr viel feinkörniger und zeigen eine andere Phasenvergesellschaftung.

Literatur

Andersen S., Bailey J.C. and Bohse H. (1981). Zr-Y-U stratigraphy of the kakortokite-lujavrite sequence, southern Ilímaussaq intrusion. Rapp. Grønl. Geol. Unders. 103, 69-76.
Bailey, J.C., 2006. Geochemistry of elemental boron in the Ilímaussaq alkaline complex, South Greenland. Lithos, 91, 301–318.
Bailey, J.C., Gwozdz, R., Rose-Hansen, J. & Sørensen, H., 2001. Geochemical overview of the Ilímaussaq complex, South Greenland. In: Sørensen, H. (Ed.), The Ilímaussaq alkaline complex, South Greenland: status of mineralogical research with new results. Geol. Greenl. Surv. Bull. 190, 35-54.
Baker, L.L. & Rutherford, M.L., 1996. Sulfur diffusion in rhyolite melts. Contrib. Min. Petrol. 123, 335–344.
Begemann, F., Ludwig, K.R., Lugmair, G.W., Min, K., Nyquist, L.E., Patchett, P.J., Renne, P.R., Shih, C.-Y., Villa, I.M. & Walker, R.J., 2001. Call for an improved set of decay constants for geo-

chronological use. Ceochim. Cosmochim. Acta 65, 111-121.

Blaxland, A. B., van Breeman, O. & Steenfelt, A., 1976. Age and origin of agpaitic
magmatism at Ilimaussaq, south Greenland: Rb-Sr study. Lithos 9, 31-38.

Bohse, H., Brooks, C.K., and Kunzendorf, H. (1971) Field observations on the kakortokites of the
Ilímaussaq intrusion, South Greenland, including mapping and analyses by portable X-ray fluore-
scence equipement for zirconium and niobium. Rapp. Grønl. Geol. Unders. 38, 43 pp.

Boily, M. & Williams-Jones, A.E., 1994. The role of magmatic and hydrothermal processes
in the chemical evolution of the Strange Lake plutonic complex, Quebec-Labrador. Contib. Mineral.
Petrol. 118, 33-47.

Dahl, P.S., 1997. A crystal-chemical basis for Pb retention and fission-track annealing
systematics in U-bearing minerals, with implications for geochronology, Earth Planet. Sci. Lett. 150,
270-299.

Di Muro, A., Bonaccorsi, E. & Principe, C., 2004. Complex colour and chemical zonig of sodalite-
group
phases in a haüynophyre lava from Mt. Vulture, Italy. Min. Mag. 68, 591-614.

Escher, A. & Watt, W.S. (1976): Summary of the geology of reenland. In: Escher, A. & Watt, W.S.
(Eds.): Geology of Greenland. Copenhagen, Geological Survey of Greenalnd, 10-16.

Ferguson, J., 1964. Geology of the Ilímaussaq alkaline intrusion, South Greenland. Description of
map
and structure. Bull. Grønl. Geol. Unders. 39, 82pp.

Ferguson, J., 1970. The significance of the kakortokite in the evolution of the Ilímaussaq intrusion,
South Greenland. Bull. Grønl. Geol. Unders. 89, 193 pp.

Hamilton, E.I., 1964. The geochemistry of the northern part of the Ilímaussaq intusion S.W. greenland.
Bull. Grønl. Geol. Unders. 42, 104 pp.

Hort, M., Marsh B.D., Resmini R.G. and Smith M.K. (1999). Convection and crystallization in a liquid
cooled from above: an experimental and theoretical study. J. Petrol. 40, 1271-1300.

Kilinc, I.A. & Burnham, C.W., 1972. Partitioning of chloride between a silicate melt and coexisting
aqueous phase from 2 to 8 kilobars. Econ. Geol. 67, 231-235

Holloway, J.R. & Jakobsson, S., 1986. Volatile solubilities in magmas: transport of volatiles from
mantles to planet surface. J. Geophys. Res. 91 (B4), D505-D508.

Konnerup-Madsen, J., 2001. A review of the composition and evolution of hydrocarbon gases during
the solidification of the Ilímaussaq alkaline complex, South Greenland. In: Sørensen, H. (Ed.), The Ilí-
maussaq alkaline complex, South Greenland: status of mineralogical research with new results. Geol.
Greenl. Surv. Bull. 190, 159-166.

Konnerup-Madsen, J., Larsen, E. & Rose-Hansen, J., 1979. Hydrocarbon-rich fluid inclusions in
minerals from the alkaline Ilímaussaq intrusion, South Greenland. Bull. Mineral. 102, 642-653.

Konnerup-Madsen, J. & Rose-Hansen, J., 1982. Volatiles associated with alkaline igneous rift activity:
fluid inclusions in the Ilimaussaq intrusion and the Gardar granitic complexes (south Greenland).
Chem. Geol. 37, 79-93.

Krumrei, T.V., Villa, I.M., Marks, M. & Markl, G., 2006. A 40Ar/39Ar and U/Pb isotopic study of the
Ilímaussaq complex, South Greenland: implications for the 40K decay constant and for the duration of
magmatic activity in a peralkaline complex. Chem. Geol. 227, 258-273.

Krumrei, T.V., Pernicka, E., Kaliwoda M. & Markl, G., 2007. Volatiles in a peralkaline system:
abiogenic hydrocarbons and F-Cl-Br systematics in the naujaite of the Ilímaussaq intrusion, South
Greenland. Lithos 95, 298-314.

Kuiper K., Hilgen F.J., Krijgsman W. & Wijbrans J., 2004. An astronomiclly dated standard
in 40Ar/39Ar geochronology? Abstract, 32nd Internat. Geol. Congress, Firenze, 812.

Kwon, J., Min, K., Bickel, P. & Renne, P.R., 2002. Statistical methods for jointly estimating
decay constant of 40K and age of a dating standard. Math. Geol. 34, 457-474.

Kyser, T.K., 1986. Stable isotope variation in the mantle. In: Valley, J.W., Taylor, H.P. & O´Neil, J.R.
(eds.): Stable isotopes in high temperature geological processes. Rev. Mineral. 16, 141-164.

Larsen, L.M. & Sørensen, H., 1987. The Ilímaussaq intrusion – progrssive crystallisation and
formation of layering in an agpaitic magma. In: Fitton, J.G. & Upton B.G.J. (Eds.), Alkaline Igneous
Rocks. Geol. Soc. Sp. Publ. 30, London, 473-488.

Markl, G., Marks, M, Schwinn, G. & Sommer, H., 2001a. Phase equilibrium constraints
on intensive crystallization parameters of the Ilimaussaq Complex, South Greenland. J. Petrol. 42,
2231-2258.

Markl, G., Marks, M. & Wirth, R., 2001b. The influence of T, aSiO2, fO2 on exsolution textures in Fe-Mg olivine: an example from augite syenite of the Ilimaussaq Intrusion, South Greenland. Am. Mineral. 86, 36-46.

Marks, M. & Markl, G., 2001. Fractionation and assimilation processes in the alkaline augite syenite unit of the Ilimaussaq Intrusion, South Greenland, as deduced from phase equilibria. J. Petrol. 42, 1947-1969.

Marks, M., Vennemann, T., Siebel, W. & Markl, G., 2004. Nd-, O-, and H-isotopic evidence for complex, closed-system fluid evolution of the peralkaline Ilímaussaq Intrusion, South Greenland. Geochim. Cosmochim. Acta 68, 3379-3395.

Marsh B.D. (1998). On the interpretation of crystals size distributions in magmatic systems. J. Petrol. 39, 553-599.

Martin D., Ross W.G., and Campbell I.H. (1987). Compositional and thermal convection in magma chambers. Contrib. Mineral. Petrol. 96, 465-475.

Min, K., Mundil, R., Renne, P.R. & Ludwig, K.R., 2000. A test for systematic errors in 40Ar/39Ar geochronology through comparision with U/Pb analysis of a 1.1-Ga rhyolite. Geochim. Cosmochim. Acta 64, 73-98.

Nielsen, B.L. & Steenfelt, A., 1979. Intrusive events at Kvanefjeld in the Ilímaussaq igneous Complex. Bull. Geol. Soc. Denmark 27, 143-155.

Ostroumov, M., Fritsch, E., Faulques, E. & Chauvet, O., 2002. Étude spectrometrique de la lazurite du Pamir, Tajikistan. Can. Mineral. 40, 885-893.

Paslick, C. R., Halliday, A. N., Davies, G. R., Mezger, K., & Upton, B. G. J., 1993. Timing of proterozoic magmatism in the Gardar Province, southern Greenland. Bull. Geol. Soc. America 105, 272-278.

Petersilie, I.A. & Sørensen, H., 1970. Hydrocarbon gases and bituminous substances in rocks from the Ilímaussaq alkaline intrusion, South Greenland. Lithos 3, 59-76.

Poulsen, V., 1964. The sandstones of the Precambrian Eriksfjord Formation in South Greenland. Rapp. Grønl. Geol. Unders. 2, 16.

Potter, J., Rankin, A.H. & Treloar, P.J., 2004. Abiogenic Fischer-Tropsch synthesis of hydrocarbons in alkaline igneous rocks; fluid inclusions, textural and isotopic evidence from the Lovozero complex, N.W. Russia. Lithos 75, 311-330.

Renne, P.R., Swisher, C.C., Deino, A.L., Karner, D.B., Owens, T.L. & DePaolo, D.J., 1998. Intercalibration of standards, absolute ages and uncertainties in 40Ar/39Ar dating. Chem. Geol. 145, 117-152.

Rose-Hansen, J., Sørensen, H. & Watt, W.S., 2001. Inventory of the literature on the Ilímaussaq alkaline complex, South Gr eenland. Dan. Grønl. Geol. Unders. Rapp. 2001/102, 38 pp. + CD-ROM

Rose-Hansen, J. & Sørensen, H., 2002. Geology of the lujavrites from the Ilímaussaq alkaline complex, South Greenland, with information from seven bore holes. Med. Grønl. Geosci. 40, 58 pp

Salvi, S. & Williams-Jones, A.E. 1997. Fischer-Tropsch synthesis of hydrocarbons during sub-solidus alteration of the Strange Lake peralkaline granite, Quebec/Labrador, Canada. Geochim. Cosmochim. Acta 61, 83-99.

Salvi, S. & Williams-Jones, A.E., 2006. Alteration, HFSE mineralisation, and hydrocarbon formation in peralkaline igneous systems: Insights from the Strange Lake Pluton, Canada. Lithos , 91, 19-34

Schmitt, A.K., Emmermann, R., Trumbull, R.B., Bühn, B. & Henjes-Kunst, F., 2000. Petrogenesis and 40Ar/39Ar geochronology of the Brandberg Complex, Namibia: evidence for a major mantle contribution in metaluminous and peralkaline granites. J. Petrol. 41, 1207-1239.

Schönenberger J., Marks M., Wagner T., and Markl G. (2006). Fluid–rock interaction in autoliths of agpaitic nepheline syenites in the Ilímaussaq intrusion, South Greenland. Lithos 91, 331 – 351.

Scott, H.P., Hemley, R.J., Mao, H.K., Herschbach, D.R., Fried, L.E. Howard, W.M. & Bastea, S., 2004. Generation of methane in the Earth´s mantle: In situ high pressure-temperature measurements of carbonate reduction. PNAS 101, 14023-14026.

Sharp, Z.D., Helffrich, G.R., Bohlen, S.R. & Essene, E.J., 1989. The stability of sodalite in the system NaAlSiO4-NaCl. Geochim. Cosmochim. Acta 53, 1943-1954.

Sørensen, H., 1966. On the magmatic evolution of the alkaline igneous province of South Greenland. Rapp. Grønl. Geol. Unders. 7, 1-19.

Sørensen H. (1968). Rhythmic igneous layering in peralkaline intrusions. An essay review on Ilímaussaq (Greenland) and Lovozero (Kola, USSR). Lithos 2, 261-283.

Sørensen, H., Bohse, H. & Bailey, J.C. (2006). The origin and mode of emplacement of lujavrites in

the Ilímaussaq alkaline complex, South Greenland. Lithos, 91, 286-300.

Sparks R.S., Huppert H.E., Koyaguchi T., and Hallworth M.A. (1993). Origin of modal and rhythmic igneous layering by sedimentation in a convecting magma chamber. Nature 361, 246-249.

Steiger, R.H. & Jäger, E., 1977. Subcommision on Geochronology: Convention on the use of decay constants in geo- and cosmochronology. Earth Planet. Sci. Lett. 36, 359-362.

Stevenson, R., Upton, B.G.J. & Steenfelt, A., 1997. Crust-mantle interaction in the evolution of the Ilímaussaq Complex, South Greenland: Nd isotopic studies. Lithos 40, 189-202.

Tsujimura, T., Xue, X., Kanzaki, M. & Walter, M.J., 2004. Sulfur speciation and network structural changes in sodium silicate glasses: Constraints from NMR and Raman spectroscopy. Geochim. cosmochim. acta 68, 5081 - 5101.

Upton B.G.J. (1961). Textural features of some contrasted igneous cumulates from South Greenland. Bull. Grønl. Geol. Unders. 29.

Upton, B.G.J., Emeleus, C.H., Heaman, L.M., Goodenough, K.M. & Finch, A.A., 2003. Magmatism of the mid-Proterozoic Gardar Province, South Greenland: chronology, petrogenesis and geological setting. Lithos 68, 43-65.

Ussing, N.V., 1912. Geology of the country around Julianehaab, Greenland. Meddelelser om Grønland 38, 376 pp.

Villa, I.M., 1998. Isotopic closure. Terra Nova 10, 42-47.

Villa, I.M. & Renne, P.R., 2005. Decay constants in geochronology. Episodes 28, 50-51.

White D.E. (1967). Some priciples of geyser activity, mainly from Steamboat Springs, Nevada. Am. J. Sci. 265, 641-684.

A ^{40}Ar/^{39}Ar and U/Pb isotopic study of the Ilimaussaq complex, South Greenland: implications for the ^{40}K decay constant and for the duration of magmatic activity in a peralkaline complex

Thomas V. Krumrei, Igor M. Villa, Michael A.W. Marks & Gregor Markl

Thomas V. Krumrei, Gregor Markl, Michael A.W. Marks

Eberhard Karls Universität Tübingen,

Institut für Geowissenschaften, Wilhelmstr. 56,

D-72074 Tübingen, Germany

Igor M. Villa

University of Bern, Institut für Geologie, Baltzerstrasse 1,

3012 Bern, Switzerland;

Università di Milano Bicocca, Dipartimento di Scienze Geologiche e Geotecnologie,

20126 Milano, Italy

Abstract

Magmatism in the Gardar Province, South Greenland, is related to two main rifting events at 1280 Ma and 1180 to 1140 Ma. Little is known about the duration of the magmatic activity in a specific complex. The Ilímaussaq intrusion belongs to the second period of rifting and comprises an extraordinary diversity of granitic and syenitic rock types, which intruded and fractionated in three successive magmatic events. As the intrusion contains some of the most evolved, incompatible element-rich rocks on Earth, it was chosen for a detailed geochronological study to quantify the duration of melt production, intrusion, fractionation and cooling. Amphiboles, which are abundant in all rock types, including pegmatites and late magmatic veins, were dated using the $^{40}Ar/^{39}Ar$ technique. Since the solidus temperature of the most evolved melts is below the closure temperature of amphibole, and no later heating event occurred, the $^{40}Ar/^{39}Ar$ ages reflect the magmatic crystallisation and can be used to determine the duration of igneous differentiation. The $^{40}Ar/^{39}Ar$ plateau ages range between 1142.6 ± 2.2 Ma and 1152.3 ± 3.7 Ma using the Steiger & Jäger (1977) 40K decay constant. These ages are younger than an U-Pb age of 1160 ± 5 Ma on baddeleyite from the first magma batch. Our results indicate that the 40K decay constant of Steiger & Jäger may be too high; a lambda similar to that proposed by Kwon et al. (2002) is required to make the 40Ar/39Ar match the U-Pb age.

Introduction

The Mesoproterozoic Ilímaussaq igneous complex is one of ten alkaline intrusive bodies in the Gardar Province, South Greenland. Since the first detailed description by Ussing (1912) who introduced the term agpaitic nepheline syenites for peralkaline rocks containing complex Zr-Ti silicates like eudialyte and rinkite, numerous papers dealing with the Ilímaussaq complex have been published (e.g. Sørensen & Larsen, 1987; Rose-Hansen et al., 2001; Markl et al., 2001a+b; Marks & Markl, 2001). The detailed chronology of the complex, however, and the time needed to evolve to the most fractionated rocks, are still a matter of debate. Investigations from other alkaline provinces (e.g. Namibia, East African rift system) suggest that the formation of evolved and non-evolved rocks may be contemporaneous (Heaman & Machado, 1992; Harris et al., 1999; Mingram et al., 2000; Schmitt et al., 2000). Geochronological studies of the alkaline rocks from the Kola Peninsula (Kramm et al., 1993; Kramm & Kogarko, 1994; Arzamastsev et al., 2000) do not have the necessary resolution to judge the formation history of single complexes, but it appears that there is no hiatus in the development within the single complexes. Evidence from peralkaline rocks (e.g. Azores, Kenya) indicate very short timescales of fractionation, i.e. only tens of thousands of years (Widom et al., 1992;

Bourdon et al., 1994; Rogers et al., 2004). In non-peralkaline magmatic provinces, the diffe-rentiation from andesitic to rhyolitic rocks needs a few hundred thousand years depending on the Si-content of the melts (Christensen & DePaolo, 1993; Reid et al., 1997; Hawkesworth et al., 2000; Reagan et al., 2003).

The Ilímaussaq complex is specifically suited for studying the duration of processes of mag-ma evolution and the quantification of such processes because the complex is made up of three distinct magma batches that are successively more evolved and which include some of the most fractionated rocks on Earth. Additionally, the rocks are well exposed, easy to distin-guish in the field and their petrography, petrology and geochemistry are very well known (e.g. Ferguson, 1964; Sørensen & Larsen, 1987; Bailey et al., 2001; Markl et al., 2001a, Marks et al., 2004). The intrusion level was shallow and no metamorphic overprint is recorded since the time of intrusion (Upton et al., 2003).

The Ilímaussaq complex is also suited for a comparison and examination of dating methods using isotopic systems because it has been dated by different independent methods. Blax-land et al. (1976) presented Rb-Sr data, from which they calculated a whole rock isochron of 1168 ± 21 Ma (MSWD = 3.6). Paslick et al. (1993) obtained 1130 ± 50 Ma (MSWD = 0.08) from a Sm-Nd whole rock – mineral isochron whereas Marks et al. (2004) calculated 1160 ± 30 Ma (MSWD = 3.7) from their Sm-Nd data. More precise results are given by a U-Pb radio-metric date of the second magma pulse (alkali granite, 1166 ± 9 Ma, Heaman & Upton, cited in Upton et al., 2003) and by a Rb-Sr age of a late agpaitic rock of 1160.1 ± 2.3 Ma (Waight et al., 2002). In this paper we present a detailed dating study including ^{40}Ar/^{39}Ar ages of amphi-boles from the major rock types and late stage pegmatites and a new U-Pb age of baddeley-ite from the earliest magma pulse (augite syenite).

Geology

Magmatism in the Gardar Province, South Greenland, is closely related to rifting between 1350 and 1140 Ma. Based on U-Pb chronology, two main periods of magmatic activity around 1280 Ma and between 1180 and 1140 Ma, respectively, can be separated (Upton et al., 2003). During these time spans, several alkaline to peralkaline plutonic complexes and a lar-ge number of dykes with variable compositions intruded the Ketilidian (1.7 - 1.8 Ga) granitic basement rocks (Julianehåb granite). The Ilímaussaq intrusion belongs to the second period (Blaxland et al., 1976) and consists of alkaline, peralkaline and agpaitic (i.e. (Na+K)/Al > 1.2, Ussing, 1912) rocks. Controlled by early fault systems (Sørensen, 1966), the complex intru-

ded at the contact between the Julianehåb granite and the late-Gardar Eriksfjord formation that consists mainly of basalts and sandstones (Poulsen, 1964).
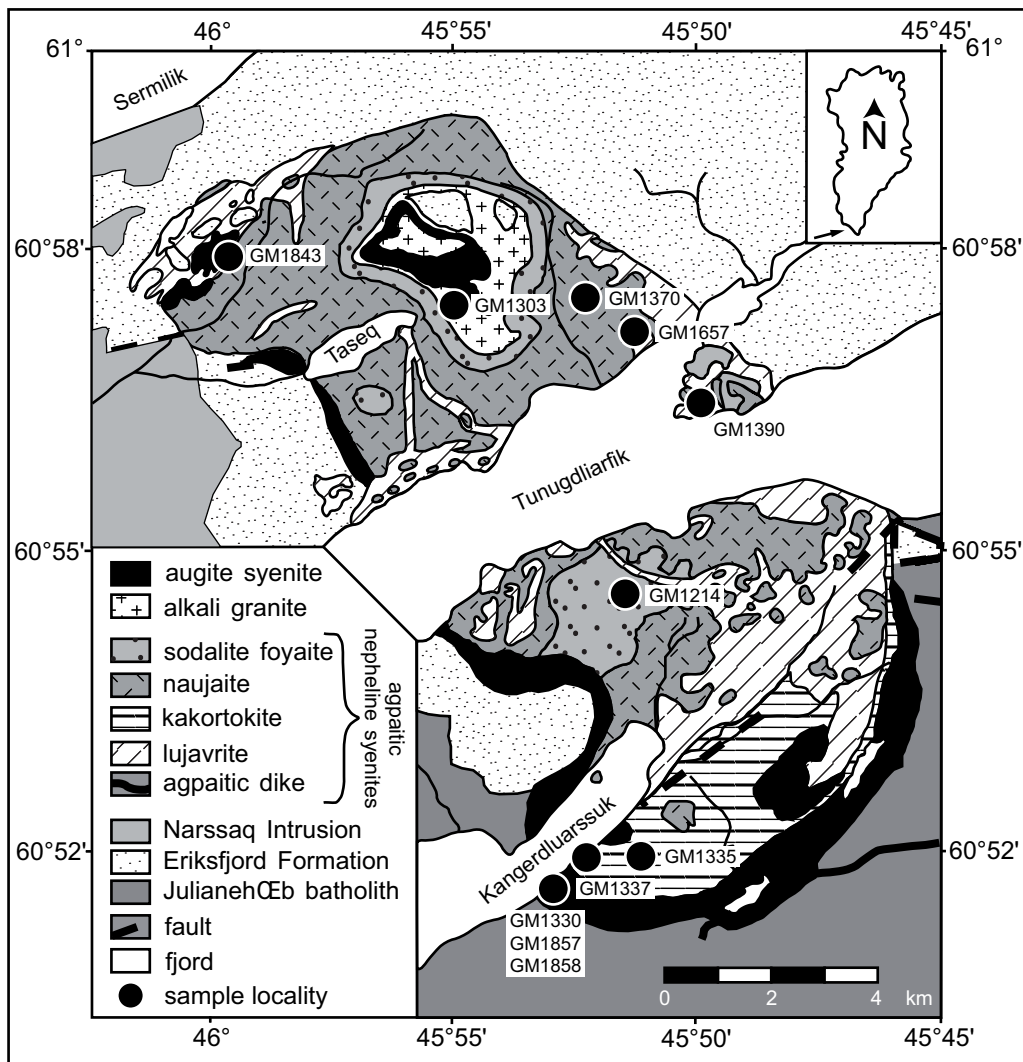
Fig. 1
Geological map of Ilímaussaq with sample localities, modified after Ferguson (1964).

Three pulses of magma intruded successively to 3 - 4 km depth (Larsen & Sørensen, 1987). The first one produced a silica-saturated to slightly under-saturated augite syenite, which is now found as the outer shell of the intrusion. Subsequently, a sheet of a peralkaline granite (in the literature on Ilímaussaq called alkali granite) intruded the augite syenite. According to Marks et al. (2004), this represents a more evolved and crustally contaminated equivalent of the augite syenite that possibly assimilated 10 to 15 % of siliceous Archeaen lower crustal rocks. In a third stage, various agpaitic nepheline syenites (pulaskite, sodalite foyaite, naujaite, kakortokite and lujavrite) were formed by low-pressure in situ fractionation of a broadly phonolitic melt. They contain nepheline, eudialyte, sodalite, alkali feldspar, aegirine and arfvedsonite in various proportions as well as rare minerals like rinkite, aenigmatite, neptunite and others. These agpaites make up the major part of the complex (Fig. 1). The pulaskite, the sodalite foyaite and the naujaite are cumulates formed at the roof of the magma chamber by

flotation of minerals less dense than the melt, whereas the strongly layered kakortokites are interpreted as cumulates on the bottom of the magma chamber. The lujavrites form intrusive contacts to the other rocks and are interpreted as the residual melts between the roof and bottom cumulates intruding along fractures into the earlier solidified cumulates. Numerous pegmatites and late-magmatic to hydrothermal veins occur all over the intrusion.

We are aware of the problems in using non-recommended rock names. However, the alternative of using only recommended nomenclature would mean that all rocks would be lumped together as "nepheline syenite" despite their striking differences. Since the names for these exotic rocks are well established in the literature, we use them to discriminate our samples and make possible their attribution to the different subunits of the Ilímaussaq complex. Fig. 2 provides a survey of rock types, their stratigraphic position, the position of the samples and types of amphiboles.

	sample	amphiboles
augite syenite	GM1330, GM1857, GM1858	ferropargasite
alkali granite	GM1303	arfvedsonite
sodalite foyaite	GM1214	arfvedsonite/ferric-ferronyböite
naujaite	GM1370	arfvedsonite
lujavrite	GM1843	arfvedsonite
kakortokite	GM1335	arfvedsonite/ferric-ferronyböite
	GM1337	arfvedsonite

agpaitic nepheline syenites

Fig. 2
Schematic profile of the Ilímaussaq complex summarising the geology, the stratigraphic position of the samples and amphibole types.

Several publications mainly dealing with the isotopic composition of the rocks show that the different magma batches, starting with the augite syenite and ending with the lujavrites, originated from a single sou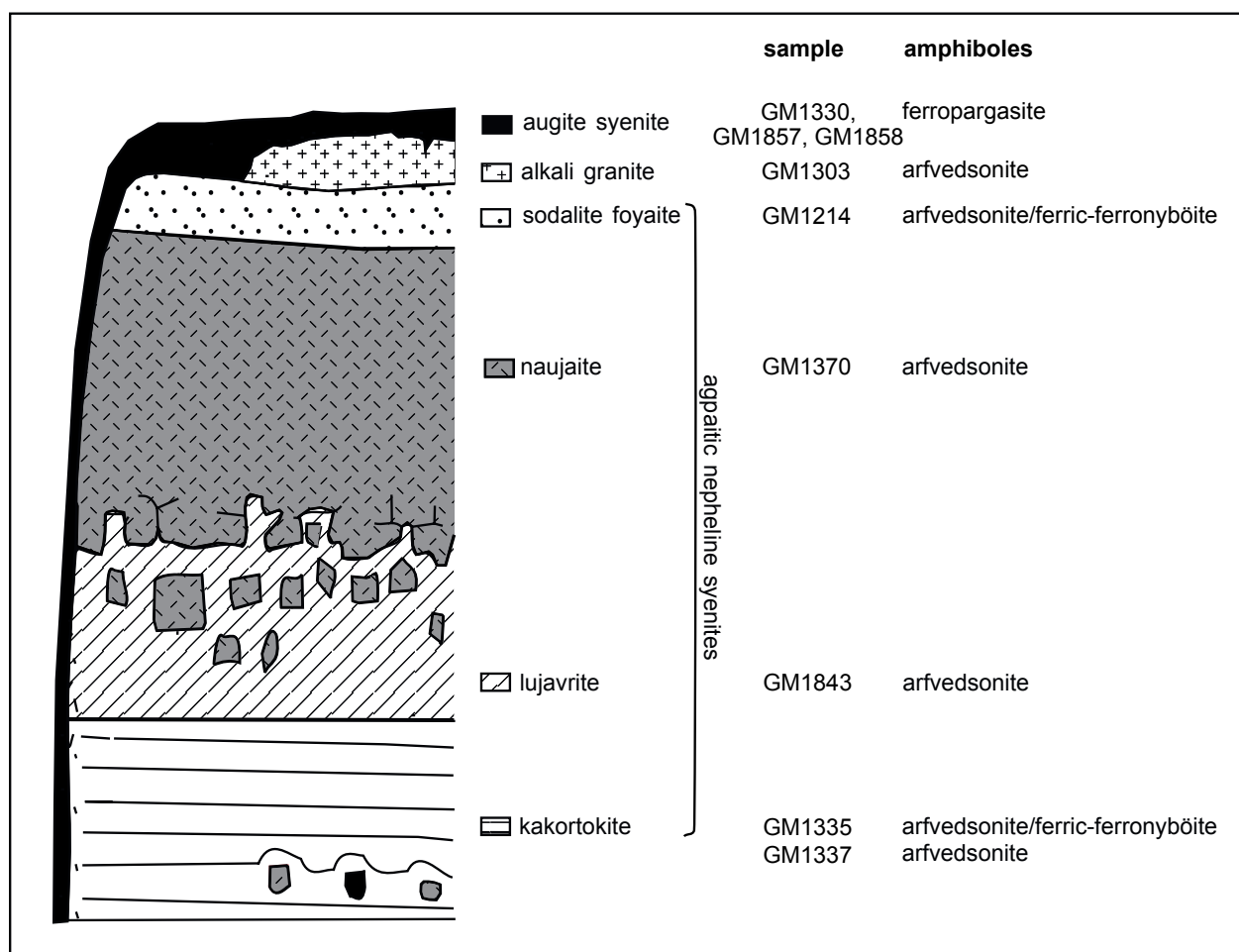rce (Nielsen & Steenfelt, 1979; Larsen & Sørensen, 1987; Stevenson et al., 1997; Marks et al., 2004). The extreme fractionation trend found in the Ilímaussaq complex appears to be governed by low water activity, low SiO_2 activity and low oxygen fugacity in the parental melt (Larsen, 1976, 1977, 1981; Markl et al., 2001a+b; Marks & Markl, 2001).

Petrography and mineral chemistry

The petrography of the Ilímaussaq rocks is reported in many publications (e.g. Ferguson, 1964; Sørensen, 2001). Amphibole occurs in all rock types of the complex. Most of the samples used in this study are described in Marks et al. (2004) with a focus on amphibole and aegirine textures. Chemical analyses of the amphiboles and pictures of amphibole textures are also presented therein. Microprobe analyses of amphiboles from the three samples GM1335, GM1390 and GM1657 not published in Marks et al. (2004) are given in Tab. 1. The early augite syenite contains Ca-rich amphiboles (ferro-edenite, ferro-pargasite). In this rock, amphibole occurs in two generations, as a magmatic phase and as later overgrowths on olivine. The latter was excluded during hand picking. Amphibole in the alkali granite is an early magmatic phase. In the more evolved rocks, amphiboles are also of clearly magmatic origin. In some samples they form euhedral crystals (black kakortokite, lujavrite), in others they occur interstitially (sodalite foyaite, naujaite, red kakortokite). The only sample not described texturally in Marks et al. (2004), the pegmatitic sample GM1657, is similar to sample GM1390 but the size of the crystals is still larger, up to half a meter. All amphiboles from the agpaitic rocks show enrichments in Na (nyböite, arfvedsonite) and contain elevated amounts of Li (up to 2500 ppm), Zn (5600 ppm) and Zr (5000 ppm). In the augite syenite, the lujavrite and in the naujaite, the amphiboles show a chemical zonation. Since all amphiboles contain at least 1.5 % K_2O, they are well suited for dating with the $^{40}Ar/^{39}Ar$ technique. Numerous studies showed that the Ilímaussaq intrusion as well as the whole Gardar province did not experience any metamorphic overprint after the end of magmatic activity (Markl, 2001; Markl et al., 2001b; Sørensen, 2001, Upton et al., 2003)

Baddeleyite is an early phase in the augite syenite as indicated by the occurrence as inclusions in olivine, clinopyroxene, feldspar and Fe-Ti-oxide minerals. The crystals are euhedral but in most cases smaller than 0.5 mm. A BSE image of a baddeleyite texture can be found in Marks & Markl (2001). The textures show that baddeleyite is clearly a primary phase crystallised from the augite syenite magma. Neither BSE images nor CL images indicate zona-

tions or other chemical variations within the baddeleyite crystals. Inheritance from the country rocks of the Ilímaussaq intrusion can be excluded because of the lack of baddeleyite in these rocks.

Two samples of the augite syenite were chosen for the extraction of baddeleyite (GM1857 and GM1858). GM 1857 is a fine-grained variety taken close to the contact to the country rocks. The locality of the coarse-grained augite syenite GM1858 is close to the inner contact to the agpaites. Both sample localities have a distance to the respective contact of approximately 20m.

Table 1
Selected microprobe analyses of amphibole from samples GM1335, GM1390 and GM1657 not published in Marks et al. (2004). n.a. = not analysed, b.d. = below detection limit.

sample	GM1335		GM1390		GM1657	
rock type	kakortokite (red)		agpaitic pegmatite		agpaitic pegmatite	
SiO_2	45,48	43,45	47,74	49,6	47,61	47,81
TiO_2	0,75	0,69	0,74	0,64	0,57	0,42
Al_2O_3	1,23	2,59	0,93	0,89	2,41	2,01
FeO	34,67	35,15	32,75	32,9	34,61	34,25
MnO	0,93	0,79	1,12	1,24	0,44	0,41
MgO	0,53	0,86	0,1	0,19	0,19	0,11
CaO	0,69	2,67	0,29	0,22	1,43	1,56
Na_2O	8,1	7,61	8,41	8,3	8,1	8,56
K_2O	2,6	1,62	2,57	3,03	1,8	1,61
ZrO_2	0,08	0,43	b.d.	0,07	n.a.	0,34
Cl	n.a.	n.a.	b.d.	b.d.	b.d.	0,01
F	0,84	0,71	0,12	b.d.	0,91	0,84
Total	95,9	96,57	94,77	97,08	98,07	97,93
	Formulae based on 16 cations and 23 oxygens					
Si	7,435	7,075	7,812	7,920	7,617	7,639
Al	0,237	0,497	0,179	0,167	0,454	0,379
Ti	0,092	0,085	0,091	0,077	0,069	0,050
Fe^{3+}	1,805	1,855	1,219	1,015	1,055	1,169
Mg	0,129	0,209	0,024	0,045	0,045	0,026
Fe^{2+}	2,936	2,932	3,263	3,378	3,576	3,407
Mn	0,129	0,109	0,155	0,168	0,060	0,055
Ca	0,121	0,466	0,051	0,038	0,245	0,267
Na	2,568	2,403	2,668	2,570	2,512	2,652
K	0,542	0,337	0,537	0,617	0,367	0,328
Zr	0,006	0,034		0,005		0,026
Cl						0,003
F	0,434	0,366	0,062		0,460	0,424
Sum	16,000	16,000	16,000	16,000	16,000	16,000

Analytical techniques

40Ar/39Ar technique

The rock samples were crushed and sieved. Amphiboles were enriched by gravimetric and magnetic means and finally handpicked from the 250 – 180 m grain size fraction to ensure visual purity. The samples were irradiated at the McMaster reactor, Ontario, Canada including the MMhb standard (McClure Mountain hornblende) with an age of 523.1 Ma (Renne et al., 1998). The analyses of the Ar isotopes were performed at the University of Bern and the analytical procedure of stepwise heating is described in Villa et al. (2000).

U-Pb technique

Baddeleyite was concentrated by gravimetric means and finally handpicked. It was analysed using conventional U-Pb analytical techniques. Separated and washed grains were spiked with a mixed $^{205}Pb/^{235}U$ tracer and digested in 22N HF at 200°C for one week in a Parr bomb. Chemical separation of U and Pb was made using ion exchange techniques similar to those described by Chen et al. (2000) for zircon analyses. Uranium and lead were isotopically analysed on a Finnigan MAT 262 mass spectrometer at the University of Tübingen. Initial common Pb remaining after correction for tracer and blank was corrected using values from the Stacey & Kramers (1975) model. U-Pb data were calculated and plotted with software from Ludwig (1988, 2003).

Results

40Ar/39Ar dating

Amphibole releases its Ar by a dehydration reaction to pyroxene and feldspar and by a melting reaction, respectively (Wartho et al., 1991; Lee, 1993). Therefore, the release pattern of an unzoned amphibole displays two maxima with the first maximum being dominant. The temperature of these reactions depends on the chemical composition (Villa et al., 2000). Ca- and Mg-rich amphiboles (magnesiohastingsite, actinolite) degas at higher temperatures than Na-rich amphiboles (riebeckite). Our Na-dominated amphiboles (mainly arfvedsonite) have their first maximum of degassing at temperatures between 680 and 800 °C, which extends the range of degassing rates of various amphibole compositions given in Fig. 3a in Villa et al. (2000) to lower temperatures. In contrast, sample GM1330 from the augite shows a first degassing peak at 980°C in accordance with its Ca-dominated composition. One sample (GM1214, the sodalite foyaite) degasses continuously over a wide temperature range between 700 and 1200 °C (see Fig. A1 in the Electronic Supplement). In contrast to the chemical zonation of some of the amphiboles, systematic variations in Ca/K or Cl/K ratios during stepwise heating were found only in sample GM1303 where the age correlates with Cl/K.

This means that zones of different composition do not degas in well-separated breakdown intervals.

The isotopic composition of the released Ar is listed in Tab. 2 and shown graphically in Fig. 3 in terms of age spectra. The step ages in Tab. 2 were calculated with the decay constant of Steiger & Jäger (1977) and age monitor calibrations of Renne et al. (1998). The young ages of the first few heating steps not shown in the age spectra (Fig. 3) are the result of gas release from minor alteration products that contribute only a few percent to the total 39Ar. The gas-rich steps have more uniform step ages, mostly in the range 1145 – 1155 Ma. A statistical analysis of step ages often gives an acceptable low dispersion with MSWD values ranging between 2.0 and 5.4. The steps used to calculate the weighted average age are marked by asterisks in Tab. 2.

Table 2
Isotopic composition of the released Ar. All Ar concentrations are in picolitres per gram (pl/g), the calculated ages are in million years, the integrated K2O and CaO values are in wt-%. The step ages, the plateau ages and the total gas ages are calculated with the Steiger & Jäger (1977) decay constant and age monitor calibrations by Renne et al. (1998). b.d. = below detection limit. Steps used for the calculation of the plateau ages are marked by asterisks.

step	T (°C)	$^{40}Ar_{tot}$	^{39}Ar	^{38}Ar	^{37}Ar	^{36}Ar	Age ± 1 σ
GM1330		10.0mg; J=3.825*10^{-3}; K$_2$O = 1.60; CaO = 9.61; plateau age = 1150.2 ± 4.2; MSWD = 5.4 % ^{39}Ar in plateau = 50.7					
1	586	233.25 ± 0.00	0.962 ± 0.017	b.d.	1.761 ± 0.072	0.282 ± 0.010	845.2 ± 18.0
2	656	519.57 ± 0.01	2.021 ± 0.019	0.145 ± 0.017	1.751 ± 0.055	0.459 ± 0.016	985.8 ± 12.0
3	786	1384.27 ± 0.16	5.645 ± 0.017	0.245 ± 0.013	1.505 ± 0.031	0.337 ± 0.017	1130.0 ± 4.2
4*	913	2376.65 ± 0.28	9.883 ± 0.017	1.056 ± 0.004	9.977 ± 0.089	0.292 ± 0.020	1145.9 ± 2.6
5*	975	17761.20 ± 2.60	75.786 ± 0.072	22.574 ± 0.042	212.075 ± 0.605	0.397 ± 0.019	1151.3 ± 0.9
6*	997	13495.80 ± 2.40	57.688 ± 0.056	17.428 ± 0.038	168.227 ± 0.489	0.222 ± 0.011	1151.4 ± 0.9
7*	1014	5443.33 ± 0.69	23.250 ± 0.030	6.921 ± 0.027	67.715 ± 0.209	0.231 ± 0.022	1145.4 ± 1.5
8	1028	6161.59 ± 1.00	26.047 ± 0.042	7.849 ± 0.021	77.250 ± 0.247	0.522 ± 0.012	1143.5 ± 1.5
9	1064	2428.27 ± 0.16	10.324 ± 0.019	2.949 ± 0.031	32.018 ± 0.118	0.150 ± 0.013	1144.6 ± 2.0
10	1085	913.03 ± 0.08	3.646 ± 0.033	1.131 ± 0.023	14.501 ± 0.153	0.248 ± 0.015	1143.2 ± 8.9
11	1118	1856.12 ± 0.23	7.863 ± 0.030	2.397 ± 0.037	32.619 ± 0.169	0.242 ± 0.021	1130.9 ± 4.3
12	1154	1415.39 ± 0.17	5.996 ± 0.047	1.749 ± 0.026	34.893 ± 0.299	0.156 ± 0.016	1137.5 ± 7.2
13	1203	1194.36 ± 0.24	5.044 ± 0.017	1.508 ± 0.015	52.465 ± 0.230	0.188 ± 0.020	1131.8 ± 4.9
14	1449	22106.40 ± 1.20	94.585 ± 0.092	28.199 ± 0.052	368.223 ± 1.038	0.362 ± 0.018	1151.4 ± 0.8
GM1214		9.7mg; J = 3.830*10^{-3}; K$_2$O = 1.86; CaO = 2.60; plateau age = 1142.6 ± 2.2; MSWD = 2.2 % ^{39}Ar in plateau = 43.8					
1	584	225.59 ± 0.25	1.052 ± 0.015	0.250 ± 0.011	1.029 ± 0.074	0.287 ± 0.012	747.8 ± 19.0
2	648	1305.89 ± 0.00	5.877 ± 0.024	0.153 ± 0.023	2.036 ± 0.035	0.455 ± 0.019	1023.6 ± 4.8
3	697	8363.73 ± 0.79	36.162 ± 0.042	0.706 ± 0.021	15.381 ± 0.070	0.541 ± 0.011	1128.5 ± 1.0
4	742	11849.07 ± 0.78	50.836 ± 0.052	1.200 ± 0.011	28.489 ± 0.125	0.515 ± 0.019	1140.6 ± 0.9
5*	781	13305.77 ± 1.13	57.156 ± 0.056	1.212 ± 0.019	39.686 ± 0.123	0.391 ± 0.008	1143.2 ± 0.9
6*	819	11726.60 ± 0.98	50.468 ± 0.053	1.183 ± 0.019	48.059 ± 0.149	0.288 ± 0.024	1143.0 ± 1.0
7*	877	14212.78 ± 1.13	61.066 ± 0.059	1.123 ± 0.023	37.600 ± 0.119	0.383 ± 0.013	1143.5 ± 0.9
8	932	14012.78 ± 1.13	60.014 ± 0.057	1.301 ± 0.022	44.087 ± 0.132	0.232 ± 0.012	1149.0 ± 0.8
9	1039	13811.13 ± 0.43	59.298 ± 0.058	1.581 ± 0.033	73.094 ± 0.216	0.436 ± 0.016	1143.5 ± 0.9
10	1454	798.11 ± 0.14	2.975 ± 0.011	0.122 ± 0.008	3.691 ± 0.039	0.463 ± 0.009	1112.4 ± 4.6

Tab. 2 continued.

step	T (°C)	$^{40}Ar_{tot}$	^{39}Ar	^{38}Ar	^{37}Ar	^{36}Ar	Age ± 1 σ
GM1303		9.5mg; J = 3.861*10^{-3}; K$_2$O = 1.51; CaO = 1.06; plateau age = 1152.3 ± 3.7; MSWD = 5.1 % ^{39}Ar in plateau = 71.2					
1	586	323.13 ± 0.56	2.013 ± 0.031	0.272 ± 0.031	1.682 ± 0.052	0.227 ± 0.019	720.9 ± 16.0
2	634	662.70 ± 0.06	3.124 ± 0.025	0.337 ± 0.022	2.692 ± 0.066	0.331 ± 0.017	955.4 ± 9.0
3	713	10253.36 ± 0.80	44.032 ± 0.052	3.778 ± 0.028	15.555 ± 0.108	0.494 ± 0.015	1145.0 ± 1.1
4*	792	25265.16 ± 0.75	107.877 ± 0.102	9.666 ± 0.039	36.907 ± 0.119	0.858 ± 0.021	1153.5 ± 0.8
5*	824	4773.71 ± 0.22	20.290 ± 0.028	1.823 ± 0.023	7.626 ± 0.095	0.265 ± 0.032	1151.9 ± 2.1
6*	866	10379.20 ± 0.27	44.479 ± 0.043	3.790 ± 0.031	14.144 ± 0.096	0.390 ± 0.013	1149.4 ± 0.9
7*	912	11856.95 ± 0.59	50.664 ± 0.049	4.697 ± 0.032	19.383 ± 0.096	0.347 ± 0.032	1154.1 ± 1.1
8	955	4854.21 ± 0.22	20.615 ± 0.034	1.968 ± 0.015	10.037 ± 0.082	0.196 ± 0.017	1156.5 ± 1.6
9	994	2718.83 ± 0.21	11.763 ± 0.025	0.893 ± 0.018	5.925 ± 0.076	0.216 ± 0.017	1130.8 ± 2.4
10	1034	1153.09 ± 0.20	5.019 ± 0.045	0.427 ± 0.033	2.941 ± 0.065	0.223 ± 0.015	1096.7 ± 8.1
11	1450	883.14 ± 0.14	3.672 ± 0.021	0.229 ± 0.041	2.330 ± 0.079	0.440 ± 0.021	1052.4 ± 8.0
GM1335		9.8mg; J = 3.865*10^{-3}; K$_2$O = 1.69; CaO = 1.43; plateau age = 1152.3 ± 1.8; MSWD = 2.6 % ^{39}Ar in plateau = 81.5					
1	583	678.71 ± 0.41	3.595 ± 0.034	0.402 ± 0.032	2.107 ± 0.077	0.468 ± 0.017	826.7 ± 8.8
2	680	7434.04 ± 0.43	32.124 ± 0.042	1.389 ± 0.024	12.019 ± 0.111	0.393 ± 0.023	1139.4 ± 1.4
3*	724	22421.84 ± 1.73	95.707 ± 0.088	2.855 ± 0.029	39.386 ± 0.134	0.695 ± 0.018	1155.4 ± 0.8
4*	762	7795.94 ± 0.28	33.303 ± 0.039	0.799 ± 0.020	15.096 ± 0.067	0.254 ± 0.022	1154.3 ± 1.2
5*	814	4893.16 ± 0.19	20.961 ± 0.029	0.558 ± 0.021	9.993 ± 0.064	0.154 ± 0.030	1152.3 ± 1.9
6*	846	7855.78 ± 0.18	33.715 ± 0.038	1.011 ± 0.030	14.411 ± 0.071	0.257 ± 0.027	1150.3 ± 1.3
7*	885	13539.29 ± 0.31	58.070 ± 0.060	1.683 ± 0.018	25.632 ± 0.104	0.352 ± 0.017	1152.6 ± 0.9
8*	926	10697.55 ± 0.47	45.656 ± 0.048	1.930 ± 0.028	25.636 ± 0.082	0.415 ± 0.011	1153.6 ± 0.9
9	981	3975.28 ± 0.23	17.071 ± 0.029	0.861 ± 0.024	10.464 ± 0.055	0.223 ± 0.019	1144.0 ± 1.9
10	1031	1239.02 ± 0.10	5.305 ± 0.013	0.137 ± 0.018	2.852 ± 0.045	0.146 ± 0.015	1130.5 ± 3.8
11	1451	1623.61 ± 0.29	6.830 ± 0.028	0.318 ± 0.022	3.543 ± 0.079	0.268 ± 0.016	1133.2 ± 4.3
GM1337		8.6mg; J = 3.820*10^{-3}; K$_2$O = 1.92; CaO = 1.56; total gas age = 1134.2					
1	584	323.34 ± 0.56	1.760 ± 0.049	0.922 ± 0.029	1.282 ± 0.077	0.414 ± 0.012	653.5 ± 18.0
2	651	779.08 ± 0.20	3.029 ± 0.026	1.583 ± 0.020	2.052 ± 0.059	0.810 ± 0.020	936.8 ± 10.0
3	681	4491.93 ± 0.47	19.109 ± 0.028	2.101 ± 0.027	7.366 ± 0.083	0.760 ± 0.016	1112.9 ± 1.6
4	712	7064.73 ± 1.08	29.748 ± 0.035	1.723 ± 0.019	11.576 ± 0.094	0.763 ± 0.016	1137.3 ± 1.2
5	743	10439.24 ± 1.86	44.560 ± 0.058	1.926 ± 0.023	17.177 ± 0.107	0.584 ± 0.024	1139.1 ± 1.3
6	765	11425.45 ± 3.02	48.672 ± 0.051	1.589 ± 0.027	19.352 ± 0.083	0.652 ± 0.010	1140.5 ± 1.0
7	790	7973.21 ± 0.60	33.937 ± 0.037	0.989 ± 0.031	14.027 ± 0.063	0.439 ± 0.015	1141.8 ± 1.1
8	850	8397.65 ± 0.67	35.991 ± 0.048	1.369 ± 0.024	16.475 ± 0.070	0.466 ± 0.016	1135.8 ± 1.2
9	897	15511.98 ± 0.92	66.343 ± 0.069	2.604 ± 0.045	27.967 ± 0.129	0.497 ± 0.027	1143.5 ± 1.0
10	938	13827.44 ± 0.57	59.140 ± 0.059	2.176 ± 0.029	26.621 ± 0.089	0.633 ± 0.022	1140.0 ± 0.9
11	988	8275.45 ± 0.35	35.674 ± 0.041	1.533 ± 0.013	21.704 ± 0.075	0.427 ± 0.015	1132.0 ± 1.1
12	1036	3331.77 ± 0.34	14.329 ± 0.023	0.573 ± 0.017	7.938 ± 0.064	0.332 ± 0.021	1121.7 ± 2.1
13	1458	777.29 ± 0.23	2.726 ± 0.026	0.098 ± 0.016	1.130 ± 0.069	0.556 ± 0.021	1118.9 ± 11.0
GM1370		9.9mg; J = 3.845*10^{-3}; K$_2$O = 2.09; CaO = 2.61; total gas age = 1165.0					
1	583	767.07 ± 0.09	3.438 ± 0.017	1.599 ± 0.014	1.852 ± 0.060	0.426 ± 0.017	975.7 ± 7.1
2	652	8653.19 ± 1.01	37.426 ± 0.042	3.840 ± 0.015	21.236 ± 0.107	0.716 ± 0.008	1127.1 ± 1.0
3	683	28966.67 ± 2.93	122.225 ± 0.111	6.069 ± 0.022	66.361 ± 0.195	1.093 ± 0.014	1159.5 ± 0.8
4	711	9420.75 ± 0.31	39.798 ± 0.042	1.944 ± 0.016	27.298 ± 0.090	0.530 ± 0.018	1153.8 ± 1.0
5	738	7597.06 ± 0.32	32.385 ± 0.035	1.716 ± 0.020	25.967 ± 0.107	0.270 ± 0.011	1151.5 ± 1.0
6	785	9100.86 ± 0.22	38.544 ± 0.038	2.376 ± 0.017	35.632 ± 0.108	0.251 ± 0.021	1159.2 ± 1.0
7	837	8206.00 ± 0.31	33.885 ± 0.037	2.548 ± 0.020	25.056 ± 0.080	0.470 ± 0.015	1173.1 ± 1.0
8	883	12325.25 ± 0.64	49.706 ± 0.048	3.475 ± 0.012	27.327 ± 0.092	0.573 ± 0.016	1196.3 ± 0.9
9	928	10484.24 ± 0.57	41.794 ± 0.044	3.415 ± 0.023	31.223 ± 0.117	0.634 ± 0.017	1203.0 ± 1.0
10	979	5486.80 ± 0.27	22.314 ± 0.023	2.028 ± 0.021	22.071 ± 0.072	0.334 ± 0.017	1185.6 ± 1.2
11	1030	1532.72 ± 0.17	6.304 ± 0.023	0.636 ± 0.017	5.340 ± 0.066	0.234 ± 0.015	1151.8 ± 4.1
12	1449	1205.88 ± 0.00	4.778 ± 0.023	0.297 ± 0.015	3.700 ± 0.055	0.311 ± 0.016	1155.3 ± 5.6

Tab. 2 continued.

| step	T (°C)	$^{40}Ar_{tot}$	^{39}Ar	^{38}Ar	^{37}Ar	^{36}Ar	Age ± 1 σ
GM1657		9.4mg; J = 3.835*10^{-3}; K$_2$O = 1.92; CaO = 1.30; plateau age = 1145.5 ± 1.7; MSWD = 2.0 % ^{39}Ar in plateau = 59.7					
1	586	572.99 ± 0.01	2.291 ± 0.021	0.213 ± 0.026	1.526 ± 0.065	0.433 ± 0.017	1005.1 ± 11.0
2	651	4720.64 ± 0.46	20.017 ± 0.026	0.605 ± 0.019	6.992 ± 0.050	0.372 ± 0.017	1142.4 ± 1.4
3	696	18728.51 ± 1.60	80.208 ± 0.073	1.396 ± 0.022	28.455 ± 0.096	0.665 ± 0.023	1145.0 ± 0.8
4	738	11332.45 ± 1.60	48.798 ± 0.056	0.888 ± 0.011	18.436 ± 0.105	0.385 ± 0.014	1140.8 ± 1.0
5*	765	5220.19 ± 0.30	22.434 ± 0.032	0.259 ± 0.016	8.319 ± 0.087	0.142 ± 0.014	1144.2 ± 1.4
6*	791	4326.51 ± 1.06	18.531 ± 0.028	0.193 ± 0.015	6.717 ± 0.057	0.184 ± 0.008	1143.1 ± 1.4
7*	828	8297.00 ± 0.78	35.792 ± 0.040	0.787 ± 0.011	12.859 ± 0.054	0.097 ± 0.011	1144.9 ± 1.0
8*	863	16594.26 ± 0.65	71.361 ± 0.073	1.157 ± 0.022	25.949 ± 0.093	0.199 ± 0.024	1147.4 ± 1.0
9*	909	17099.47 ± 1.49	73.646 ± 0.080	1.287 ± 0.024	27.803 ± 0.103	0.262 ± 0.020	1145.3 ± 1.0
10*	952	3566.13 ± 0.67	14.989 ± 0.022	0.106 ± 0.015	5.886 ± 0.050	0.307 ± 0.015	1148.0 ± 1.7
11	1031	1092.50 ± 0.16	4.546 ± 0.018	0.163 ± 0.024	1.946 ± 0.048	0.237 ± 0.011	1122.3 ± 4.3
12	1446	1018.55 ± 0.38	4.139 ± 0.015	0.159 ± 0.017	1.303 ± 0.033	0.365 ± 0.011	1104.2 ± 4.1
GM1843		10.0mg; J = 3.853*10^{-3}; K$_2$O = 3.24; CaO = 0.19; total gas age = 1138.7					
1	586	1197.25 ± 0.13	5.949 ± 0.012	0.155 ± 0.022	1.157 ± 0.042	0.482 ± 0.015	939.4 ± 3.3
2	652	27309.30 ± 0.52	117.361 ± 0.110	1.554 ± 0.029	3.581 ± 0.036	0.863 ± 0.019	1146.7 ± 0.8
3	674	43977.65 ± 0.38	191.426 ± 0.035	2.939 ± 0.029	6.787 ± 0.055	0.680 ± 0.015	1141.1 ± 1.2
4	697	20154.40 ± 1.70	87.697 ± 0.083	1.308 ± 0.026	2.620 ± 0.070	0.260 ± 0.019	1140.9 ± 0.8
5	727	4935.66 ± 0.33	21.985 ± 0.030	0.154 ± 0.030	0.585 ± 0.052	0.212 ± 0.018	1113.8 ± 1.4
6	768	8925.51 ± 1.30	39.166 ± 0.044	0.483 ± 0.016	1.120 ± 0.069	0.099 ± 0.015	1134.3 ± 1.0
7	818	20532.60 ± 0.77	89.351 ± 0.083	1.158 ± 0.029	2.954 ± 0.094	0.160 ± 0.018	1142.1 ± 0.8
8	866	21807.70 ± 0.98	94.979 ± 0.092	1.204 ± 0.024	3.364 ± 0.071	0.000 ± 0.014	1143.8 ± 0.8
9	911	3937.32 ± 0.20	17.485 ± 0.025	0.379 ± 0.023	0.600 ± 0.049	0.120 ± 0.015	1119.4 ± 1.5
10	952	1744.40 ± 0.17	7.515 ± 0.021	0.067 ± 0.020	0.259 ± 0.049	0.030 ± 0.011	1148.3 ± 2.9
11	1033	1169.91 ± 0.20	4.833 ± 0.019	0.049 ± 0.028	0.366 ± 0.077	0.054 ± 0.013	1176.8 ± 4.5
12	1454	730.49 ± 0.01	3.060 ± 0.019	0.027 ± 0.014	0.215 ± 0.075	0.145 ± 0.009	1125.3 ± 6.1
GM1390		10.4mg; J = 3.840*10^{-3}; K$_2$O = 2.85; CaO = 0.29; total gas age = 1148.6					
1	586	400.06 ± 0.16	1.724 ± 0.017	0.104 ± 0.016	1.037 ± 0.021	0.532 ± 0.017	780.1 ± 14.0
2	652	6583.85 ± 0.85	27.943 ± 0.042	0.612 ± 0.044	1.886 ± 0.063	0.817 ± 0.028	1130.8 ± 1.7
3	698	31546.73 ± 0.84	134.986 ± 0.125	2.153 ± 0.022	6.897 ± 0.064	0.941 ± 0.016	1148.0 ± 0.8
4	749	50780.50 ± 0.30	216.015 ± 0.221	2.566 ± 0.007	11.349 ± 0.078	0.856 ± 0.032	1156.3 ± 0.9
5	791	11547.40 ± 1.63	48.899 ± 0.053	0.925 ± 0.026	2.303 ± 0.032	0.950 ± 0.019	1143.5 ± 1.0
6	844	11246.92 ± 1.54	47.896 ± 0.048	0.932 ± 0.009	2.619 ± 0.038	0.624 ± 0.020	1145.5 ± 1.0
7	892	7781.25 ± 1.15	32.952 ± 0.037	0.547 ± 0.020	2.127 ± 0.040	0.564 ± 0.020	1145.9 ± 1.2
8	933	8630.54 ± 0.24	36.655 ± 0.040	0.449 ± 0.022	2.096 ± 0.026	0.332 ± 0.019	1152.1 ± 1.1
9	1036	9027.99 ± 2.31	38.628 ± 0.046	0.630 ± 0.019	2.084 ± 0.035	0.429 ± 0.021	1143.5 ± 1.2
10	1458	637.22 ± 0.09	1.993 ± 0.031	b.d.	b.d.	0.584 ± 0.015	1153.4 ± 16.0
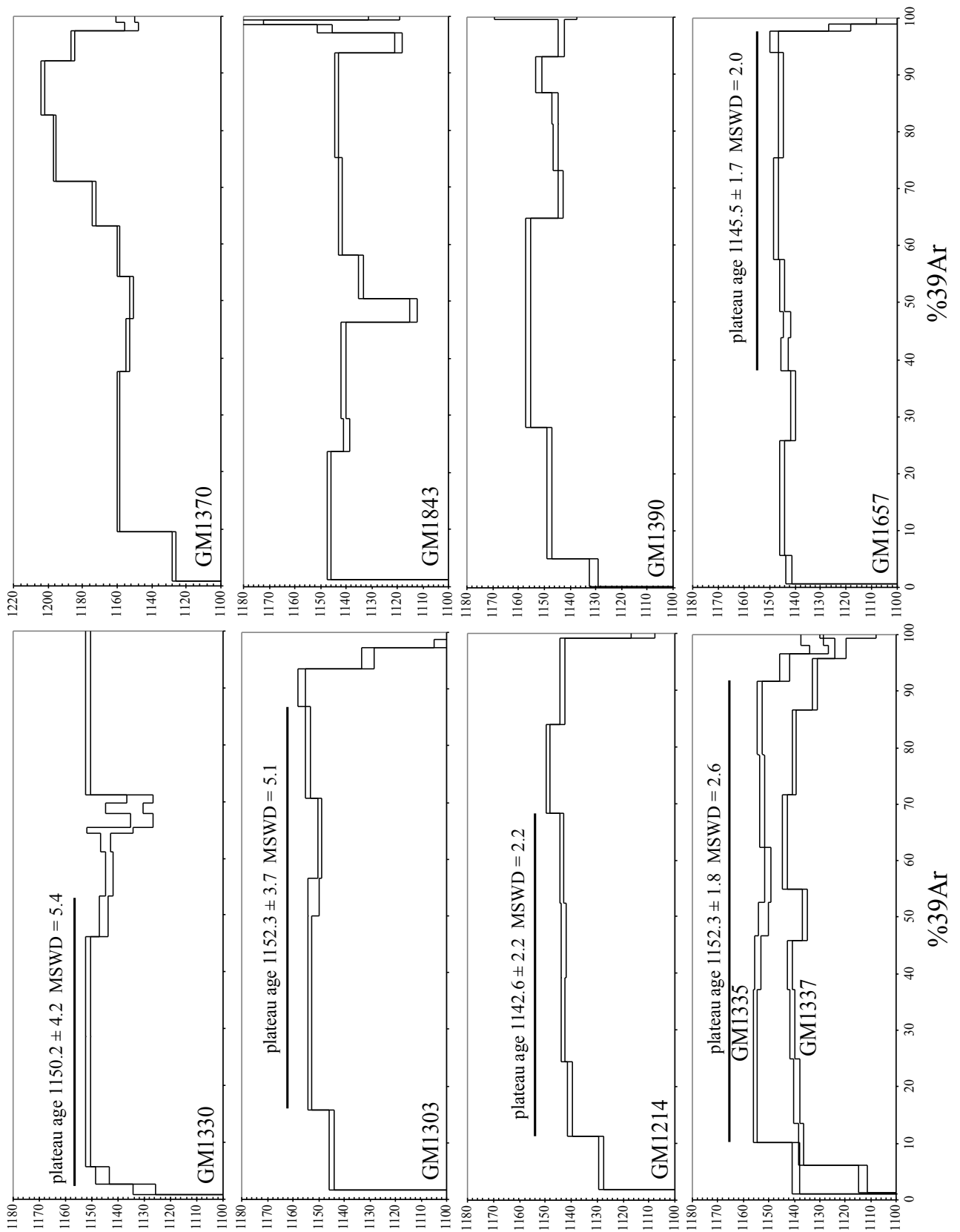
Fig. 3
Age spectra from 40Ar/39Ar stepwise heating experiments with the calculated plateau ages. Note the different ages of the two kakortokite samples and the different age scale of sample GM1370. All ages are calculated using the Steiger & Jäger (1977) values for the 40K decay constant and the age monitor calibration by Renne et al. (1998).

Some of the age spectra show well-defined plateaus, others do not. The weighted average ages of those samples with a plateau scatter around 1150 Ma. The age spectrum of the naujaite (GM1370) is problematic because of the poorly developed plateau (Fig. 3) and hence no plateau age was calculated. In this sample, the Ca content of the amphiboles measured with the microprobe is about twice as high as that calculated from the Ar-isotope analyses (Tab. 3). A discrepancy of the Ca content is also found in sample GM1303, the alkali granite. The $^{37}Ar/^{39}Ar$ ratios vary by a factor of 2 at most during stepwise heating of the samples (Tab. 2). This indicates that the analysed amphiboles were not severely contaminated by inclusions capable of distorting the Ca/K ratios. During the irradiation of the samples in the nuclear reactor, ^{37}Ar is produced from ^{40}Ca. If the discrepancy were a result of Ca rich mineral inclusions, the $^{37}Ar/^{39}Ar$ ratios would not be as constant as they are because of the different degassing behaviour of the different minerals. The work on fluid inclusions in the alkali granite by Konnerup-Madsen & Rose-Hansen (1984) showed that, in contrast to the agpaitic rocks, the alkali granite contains mainly aqueous inclusions with highly variable salinities ranging from almost zero to more than 60 % NaCl-eq. The chemical composition of the entrapped fluid is not known exactly but components other than NaCl are indicated by the occasional occurrence of sylvite and other minerals as daughter crystals in the inclusions (Konnerup-Madsen & Rose-Hansen 1984). The composition of the fluid inclusions explains the one order of magnitude higher Cl/K of sample GM1303 (calculated from the Ar isotopes) and may be the reason for the difference in the Ca content derived from the microprobe and the Ar isotopes, respectively.

The slightly different 40Ar/39Ar step ages of the two kakortokite varieties (GM1335, GM1337) are possibly due to excess Ar in sample GM1335. The samples originate from different layers of the strongly layered sequence. The red variety (GM1335) comes from a higher level (layer +10, following the numeration of Bohse et al., 1971) than the black one (GM1337, layer +5). Hence, the latter must have formed later when the residual melt was more evolved. With further fractionation the magma became richer in incompatible elements. Villa (1983) showed that cumulates incorporate incompatible elements from the magma including excess Ar. Additionally, the amphiboles in the black variety are euhedral and, hence, an early magmatic phase whereas the amphiboles in the red variety occur interstitially. Therefore, the sample from a higher stratigraphic level could contain higher amounts of incompatible elements including excess Ar and display an older age. The well-developed plateau of sample GM1335 does not argue against excess Ar (Von Blanckenburg & Villa, 1988). The naujaite, the corresponding flotation cumulate on the roof of the magma chamber, exhibits an apparent age that is still older than that of the red kakortokite. In this rock, the amphiboles occur interstitially, similar to

the red kakortokite. Additionally, no plateau is developed in the age spectrum of this sample. Konnerup-Madsen et al. (1981) showed that fluid inclusions in amphiboles from the naujaite do contain small quantities of Ar. We therefore cannot rule out fluid inclusions as carriers of excess Ar, which could have decrepitated during step-wise heating between 785 and 980 °C. Isochron treatment of the stepheating data is often used to diagnose the presence of excess Ar, in so far as the intercept on the axis representing trapped Ar may have a different value from atmospheric Ar. However, it is important to point out that the regression must be made only on isochronous reservoirs; from the Ca/Cl/K signature (cf. Villa, 2001) it is straightforward to exclude extraneous phases and restrict the calculation to steps having isochemical Ca/K and Cl/K ratios. If this is done, it can be seen that none of our samples defines an „isochemical isochron" with a trapped Ar significantly different from atmospheric Ar.

Table 3
Comparison of Ca and K contents of the amphiboles measured by the microprobe with those calculated from the released Ar. Except samples GM1390, GM1335 and GM1657, the analyses are already published in Marks et al. (2004). The CaO and K2O values derived from the microprobe are mean values to ensure comparableness with the values calculated from the released Ar.

sample	GM1330	GM1303	GM1214	GM1370	GM1335	GM1337	GM1390	GM1657	GM1843
rock type	augite syenite	alkali granite	sodalite foyaite	naujaite	kakortokite (red)	kakortokite (black)	agpaitic pegmatite	agpaitic pegmatite	lujavrite
wt%									
microprobe analyses									
CaO	10.89	0.35	2.11	1.47	1.19	1.91	0.31	1.45	0.16
K$_2$O	1.58	1.4	1.82	2.26	2.13	1.83	2.68	1.71	3.13
CaO/K$_2$O	6.87	0.25	1.16	0.65	0.56	1.04	0.12	0.85	0.05
calculated from the Ar-isotopes									
CaO	9.61	1.06	2.6	2.61	1.43	1.56	0.29	1.3	0.16
K$_2$O	1.59	1.51	1.87	2.09	1.69	1.92	2.85	1.92	2.5
CaO/K$_2$O	6.04	0.70	1.39	1.25	0.85	0.81	0.10	0.68	0.06

U-Pb radiometric age

Four fractions of baddeleyite from samples GM1857 and GM1858 each consisting of four single grains were chosen for dating with the U-Pb method. The results are shown in Tab. 4 and in a concordia diagram (Fig. 4). Two fractions are concordant and the other two slightly discordant, whereas one lies above the concordia. This is possibly due to loss of U during the analysis of that particular sample. Another explanation is meteoric leaching of U under oxi-

dising conditions indicated by the lower intercept of the discordia at zero, within uncertainty. Excess ^{207}Pb caused by initial ^{231}Pa in the melt as found by Anczkiewicz et al. (2001) in zircons from an alkali granite dyke would move the point only to higher ^{207}Pb/^{235}U ratios but not to both, higher ^{207}Pb/^{235}U and higher ^{206}Pb/^{238}U values, as observed in the inverse discordant sample. The four data points together define a discordia that intersects the concordia exactly where the two concordant data points lie. An intercept age of 1160 ± 5 Ma with a MSWD of 0.55 was calculated.

Table 4
Isotopic data for baddeleyite from the augite syenite.

sample	weight[1] (µg)	$\frac{^{206}Pb[2]}{^{204}Pb}$	U[1] ppm	Pb[1] ppm	Th/U[3]	$\frac{^{206}Pb}{^{238}U}$	±	$\frac{^{207}Pb}{^{235}U}$	±	$\frac{^{207}Pb}{^{206}Pb}$	±
						isotopic ratios[4]					
GM1858A	8	16.9	106	19	1.7	0.1956	20	2.116	22	0.078437	68
GM1858B	10	18.7	37	7	5.0	0.2108	22	2.287	24	0.078691	176
GM1857C	15	16.9	986	180	0.19	0.1962	20	2.123	22	0.078492	40
GM1857D	10	16.9	374	66	0.50	0.1881	29	2.035	31	0.078487	95

sample	calculated ages (Ma) $\frac{^{206}Pb}{^{238}U}$	$\frac{^{207}Pb}{^{235}U}$	$\frac{^{207}Pb}{^{206}Pb}$
GM1858A	1151.9	1154.0	1158.0
GM1858B	1232.9	1208.2	1164.4
GM1857C	1154.8	1156.4	1159.3
GM1857D	1111.0	1127.4	1159.2

[1]Weight and concentration error better than 20%
[2]Measured ratio corrected for mass discrimination and spike contribution
[3]Th/U model ratio calculated from ^{208}Pb/^{206}Pb ratio and age of the sample
[4]Corrected for blank Pb, U, and initial common Pb based on the Stacey & Kramers (1975) model, errors are 2σ

Discussion

Peralkaline to agpaitic rocks have an unusually long crystallisation interval between 950 and ~ 450 °C since the volatiles are retained in the melt during most of the crystallisation history (Boily & Williams-Jones, 1994; Markl et al., 2001a). The solidus of the agpaitic melt lies at temperatures well below the closure temperature of the amphiboles. While the re-evaluated closure temperature of hornblende sensu stricto is about 600 °C for a cooling rate > 10 °C/Ma (Villa, 1998), it is necessary to take into account the ionic porosity (Dahl, 1997) of the alkali amphiboles to estimate their Ar retentivity. This results in a lower closure temperature of approximately 500 to 550 °C. Hence, the geochronological watch started to tick while the amphiboles in the agpaitic rocks were still surrounded by melt. Consequently, the 40Ar/39Ar ages of the agpaitic rocks clearly reflect magmatic processes.
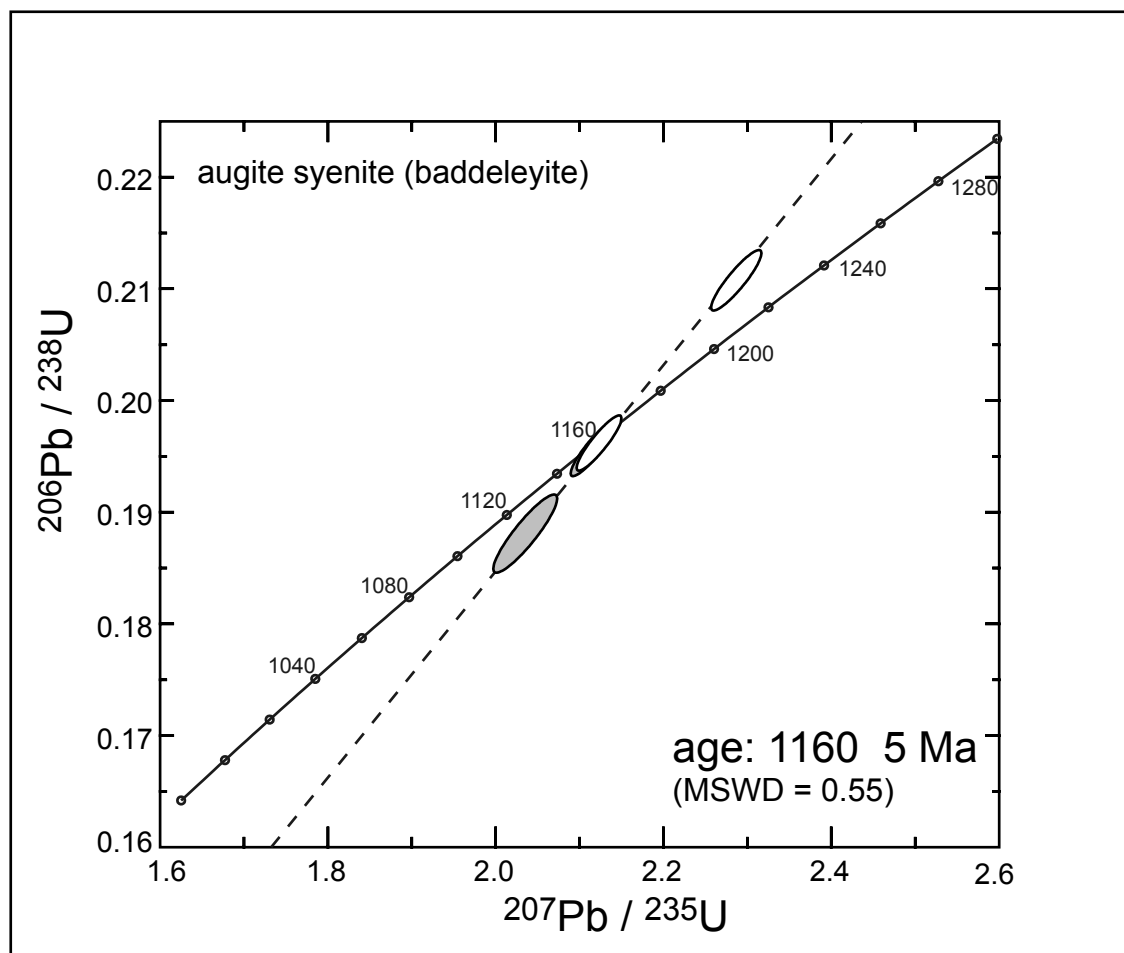
Fig. 4
Concordia diagram of samples GM1857 (grey) and GM1858 (white) from the augite syenite.

Rb-Sr ages

The Rb-Sr age for the kakortokite by Waight et al. (2002) recalculated with the ^{87}Rb decay constant given by Begemann et al. (2001) is 1175 Ma and, hence, not in agreement with the U-Pb data. Following the field relationships of the Ilímaussaq rocks, the agpaites including the kakortokites developed from the youngest magma batch. The Rb-Sr age by Waight et al. (2002) is based on a two point isochron using eudialyte and alkali feldspar. The whole rock is not included but they assumed the whole rock point to be zero. Bailey et al. (2001) showed that the kakortokites contain up to 540 ppm Rb. Consequently, the whole rock point would not be zero as assumed by Waight et al. (2002). Parsons et al. (1988) demonstrated that alkali feldspars in plutons are likely to have structural damages in terms of micropores. This also may have affected the Rb-Sr system. We therefore conclude that the recalculated Rb-Sr age of Waight et al. (2002) is not reliable.

Blaxland et al. (1976) presented Rb-Sr data, from which they calculated a whole rock iso-chron of 1168 ± 21 Ma. From the data in their Tables 1 and 2 we recalculated the isochrons, both using the 87Rb decay constant used by them (1.39 x 10^{-11} a^{-1}) and a revised one of

1.402 x 10^{-11} a^{-1} as summarised by Begemann et al. (2001). The former indeed gives 1168 ± 24 Ma, but the MSWD is 53 rather than 3.6; this very high scatter suggests that the whole-rock system may not represent a suitable chronometer. In any case, the apparent age formally calculated with the revised 87Rb decay constant is 1158 ± 24 Ma which agrees with the U-Pb baddeleyite age.

40K decay constant

The decay constant of ^{40}K currently used in geochronology is 5.543 x 10^{-10} a^{-1} and was recommended by the IUGS Subcommission on Geochronology (Steiger & Jäger, 1977). In recent times it has been suggested that the uncertainties in the radioactive decay constants can be a source of systematic error (Begemann et al., 2001). The ^{40}K decay constant is still a matter of debate and several workers re-examined the values (Min et al., 2000; Kwon et al., 2002; Villa & Renne, 2005). A peculiarity of the K-Ar system, which further complicates the attainment of reliable age estimates, is the difficulty of performing a precise and accurate determination of absolute volumes of radiogenic Ar, and the consequent widespread use of "age monitors" to indirectly calibrate the ages of unknown samples. The age monitors themselves have been dated with finite precision and accuracy. The review paper by Renne et al. (1998) proposes an intercalibration of several age monitors, including MMhb1 used in the present study, relative to each other. For historical reasons, the Fish Canyon Tuff sanidine monitor (FCT) is used as a pivot for the other monitors. The FCT age was estimated at 28.02 ± 0.16 Ma by Renne et al. (1998).

Our samples are germane to the problem of assessing the various estimates of the ^{40}K decay constant from the literature. For the discussion's sake, we can assume either (i) that most samples do not contain excess Ar, or (ii) that most of them do, neglecting, for the time being, our argument in the previous section. In case (i), the calculation with the constant of Steiger & Jäger (1977) results in ages around 1145 Ma, significantly younger than the U-Pb ages of 1160 Ma (Fig. 5a). To explain this large age difference, one has to postulate either an intrusion history with a gap of 15 Ma between the younger agpaitic series and the older augite syenite and alkali granite, or a prolonged history of isotopically open behaviour. In the first case, the intrusion of the agpaites has to reset the amphiboles of the earlier rocks completely. Additionally, the deep-seated magma chamber is required to be stable over 15 Ma. As pointed out by Marks et al. (2004), all Ilímaussaq rocks have a single source. Fractionation in a deep-seated magma chamber from the augite syenite to the agpaitic rocks would have to last those 15 Ma, which is unreasonable according to work by several authors who have shown

that differentiation is a much faster process (e.g. Christensen & DePaolo, 1993; Reid et al., 1997; Hawkesworth et al., 2000; Reagan et al., 2003). The possibility that the amphiboles record delayed "cooling ages" can, as explained in the Appendix, also be ruled out. All independent arguments request that the amphiboles be 1160 Ma old. Based on this geological, petrological and isotopical argumentation, we conclude that using the Steiger & Jäger (1977) ^{40}K decay constant and the FCT age of 28.02 Ma results in inaccurate $^{40}Ar/^{39}Ar$ ages. In case (ii), we should consider the age of the youngest sample, GM 1337, as the least affected by excess Ar. The „true age" of the amphiboles would thus become 1138 Ma. This requires a much larger correction to the decay constant and/or the FCT age than case (i). Seeing as in a preceding paragraph we argued that excess Ar was unlikely to have affected more than a few outliers, we believe that case (i) requiring the smaller correction is the more conservative and realistic one.
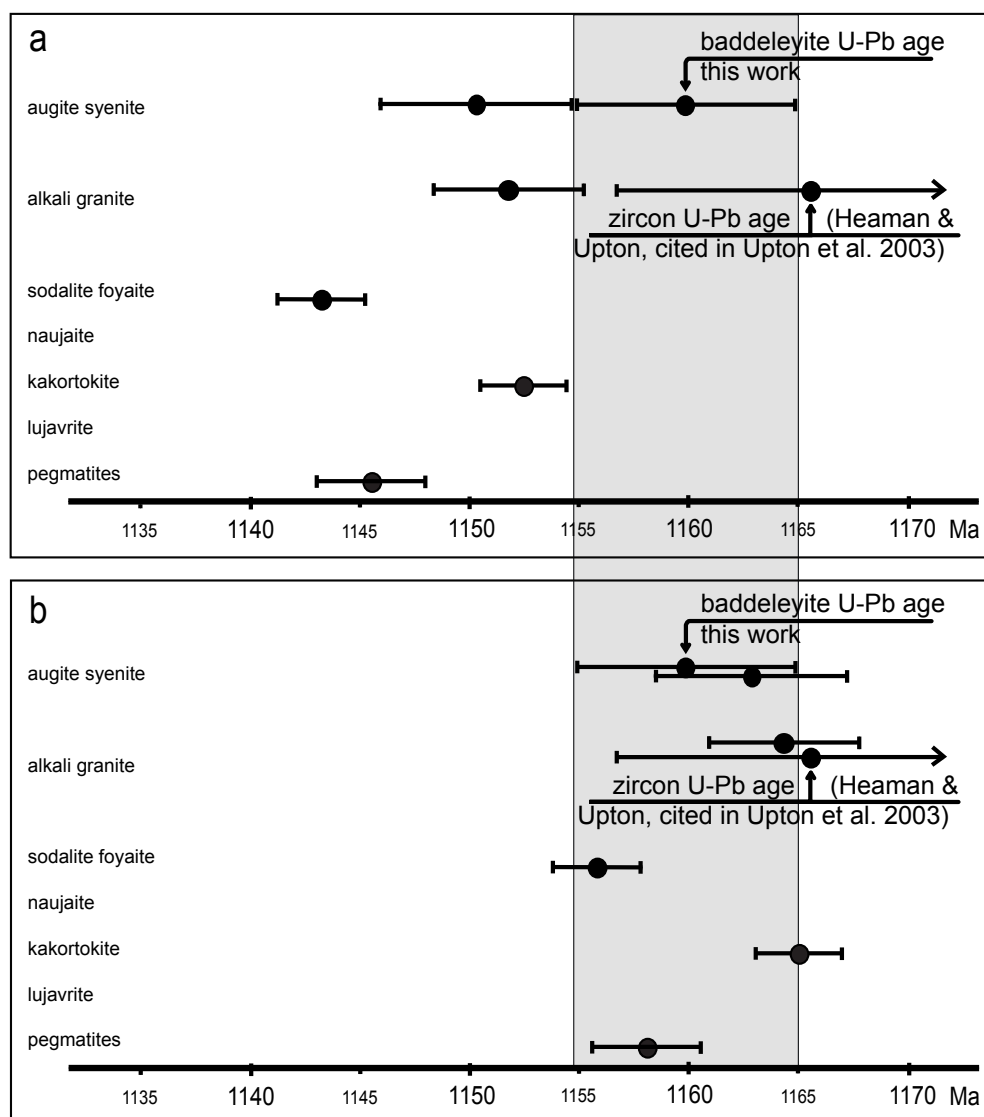

Fig. 5
Diagram comparing the amphibole 40Ar/39Ar ages (unlabeled points), the baddeleyite U/Pb age and ages published elsewhere. The grey box indicates the proposed age of intrusion, given by our U-Pb age. a. 40Ar/39Ar ages calculated using the 40K decay constant of Steiger & Jäger (1977) and age monitor calibration by Renne et al. (1998). b. 40Ar/39Ar ages calculated using revised values. Note the conformity of the different dating methods.

In order to reduce the 15 Ma age gap between the U-Pb and K-Ar systems to zero, one can modify (a) the decay constant, but not the FCT age, (b) modify the FCT age, but not the decay constant, (c) modify both simultaneously. Approach (c) has been followed by Kwon et al. (2002) who proposed a decay constant for ^{40}K of $(5.476 \pm 0.034) \times 10^{-10}$ a^{-1} and an FCT age of 28.27 ± 0.13 Ma. For our amphiboles, these values produce ages around 1170 Ma under assumption (i). Approach (b) has been followed by Kuiper et al. (2004) who compared cyclostratigraphic ages with interbedded tephras and derived an FCT age of 28.24 ± 0.01 Ma all while keeping the Steiger & Jäger (1977) decay constant. In our case, this results in amphibole ages around 1155 Ma under assumption (i). Finally, approach (a) is not represented in the recent literature. Clearly, our single data-set is not capable of simultaneously solving for three unknowns (FCT age, decay constant, and possible concentration of excess Ar), but still can provide constraints on the magnitude of the changes to either of the former two parameter.

Summary and Conclusions

Both amphiboles and baddeleyite recorded the intrusion of the Ilímaussaq complex. After their intrusion, the rocks were not affected by any metamorphic overprint. Therefore, we can use these magmatic rocks as a "point-like geological event" sensu Begemann et al. (2001) to provide constraints on the intercalibration of the K-Ar and U-Pb clocks. Comparing the U-Pb ages from the augite syenite (this work) and the alkali granite (Heaman & Upton, cited in Upton et al., 2003) with our apparent ^{40}Ar- ^{39}Ar ages on amphiboles strongly suggests that the K-Ar system suffers from a systematic bias when calculated using the Steiger & Jäger (1977) decay constants in conjunction with an FCT monitor age of 28.02 Ma. Furthermore, the recalculated Rb-Sr age of Blaxland et al. (1976) and the Sm-Nd ages by Paslick et al (1993) and by Marks et al. (2004) give also ages around 1160 Ma even though these ages are loaded with a much larger error. The geology, the petrology, the isotopic composition and the thermal modelling argue for the use of a new ^{40}K decay constant close to that published by Kwon et al. (2002).

The time of formation of the Ilímaussaq complex can be fixed at 1160 ± 5 Ma (Fig. 5). The development of the complex is characterised by a short-lived fractionation history in a deep-seated magma chamber from the parental phonolitic melt to an agpaitic one. From this magma chamber, two early magma batches (augite syenite and alkali granite) and one late batch (agpaitic nepheline syenites) were injected into the upper crust. The last batch underwent further fractionation at the final level of intrusion forming cumulates both on the roof and on

the bottom of the upper crustal magma chamber. The time span needed for this fractionation is limited by the Ar results to a maximum of 5 million years, presumably much shorter on the order of 500 ka to 800 ka as indicated by the thermal modelling and the conformity of the results from all dating methods.

Acknowledgements

This is Contribution to the mineralogy of Ilímaussaq No. 124.

References

Anczkiewicz, R., Oberli, F., Burg, J. P., Villa, I. M., Günther, D. & Meier, M., 2001. Timing of normal faulting along the Indus Suture in Pakistan Himalaya and a case of major 231Pa/235U initial disequilibrium in zircon. Earth Planet. Sci. Lett. 191, 101-114

Andersen, T., 1997. Age and petrogenesis of the Qassiarsuk carbonatite-alkaline silicate volcanic complex in the Gardar rift, South Greenland. Min. Mag. 61, 499-513.

Arzamastsev, A.A., Belyatsky, B.V. & Arzamastseva, L.V., 2000. Agpaitic magmatism in the northeastern Baltic Shield: a study of the Niva intrusion, Kola Peninsula, Russia. Lithos 51, 27-46.

Bailey, J.C., Gwozdz, R., Rose-Hansen, J. & Sørensen, H., 2001. Geochemical overview of the Ilímaussaq complex, South Greenland. In: Sørensen, H. (Ed.), The Ilímaussaq alkaline complex, South Greenland: status of mineralogical research with new results. Geol. Greenl. Surv. Bull. 190, 35-54.

Begemann, F., Ludwig, K.R., Lugmair, G.W., Min, K., Nyquist, L.E., Patchett, P.J., Renne, P.R., Shih, C.-Y., Villa, I.M. & Walker, R.J., 2001. Call for an improved set of decay constants for geochronological use. Ceochim. Cosmochim. Acta 65, 111-121.

Blaxland, A. B., van Breeman, O. & Steenfelt, A., 1976. Age and origin of agpaitic magmatism at Ilimaussaq, south Greenland: Rb-Sr study. Lithos 9, 31-38.

Blundell, D.J., 1978. A gravity survey across the Gardar Igneous Province, SW Greenland. J. geol. Soc. London 135, 545-554.

Bohse, H., Brooks, C.K. & Kunzendorf, H., 1971. Field observations on the kakortikites of the Ilímaussaq intrusion, South Greenland, including mapping and analyses by portable X-ray fluorescence equipment for zirconium and niobium. Rapp. Grønl. Geol. Unders. 38, 43 pp.

Boily, M. & Williams-Jones, A.E., 1994. The role of magmatic and hydrothermal processes in the chemical evolution of the Strange Lake plutonic complex, Quebec-Labrador. Contib. Mineral. Petrol. 118, 33-47.

Bourdon, B., Zindler, A. & Wörner, G., 1994. Evolution of the Laacher See magma chamber: evidence from SIMS and TIMS measurements of U-Th diequilibria in minerals and glasses. Earth Planet. Sci. Lett. 126, 75-90.

Chen, F., Hegner, E. & Todt, W., 2000. Zircon ages and Nd isotopic and chemical compositions of orthogneisses from the Black forest, Germany: evidence for a Cambrian magmatic arc. Int. J. Earth Sci. 88, 791-802.

Christensen, J.N. & DePaolo, D.J., 1993. Time scales of large volume silicic magma systems; Sr isotopic systematics of phenocrysts and glass from the Bishop Tuff, Long Valley, California. Contrib. Min. Petrol. 113, 100-114.

Dahl, P.S., 1997. A crystal-chemical basis for Pb retention and fission-track annealing systematics in U-bearing minerals, with implications for geochronology, Earth Planet. Sci. Lett. 150, 270-299.

Delaney, P.T., 1984. Heating of a fully saturated Darcian half-space: Pressure generation, fluid expulsion and phase change. Int. J. Heat Mass Transf. 27, 1327-1335.

Ferguson, J., 1964. Geology of the Ilimaussaq alkaline intrusion, South Greenland. Bull. Grønl. Geol. Unders. 39, 82.

Forsberg, R. & Rasmussen, K.L., 1978. Gravity and rock densities in the Ilímaussaq area, South Greenland. Rapp. Grønl. Geol. Unders. 90, 81-84.

Furlong, K.P., Hnason, R.B. & Bowers, J.R., 1991. Modeling thermal regimes. In Contact metamorphism (ed. D.M. Kerrick), Rev. Mineral. 26, 437-497.

Halama, R., Wenzel, T., Upton, B.G.J., Siebel, W. & Markl, G., 2003. A geochemical and Sr-Nd-O isotopic study of the Proterozoic Eriksfjord Basalts, Gardar Province, South Greenland: Reconstruction of an OIB signature in crustally contaminated rift-related basalts. Min. Mag. 67, 831-853.

Harris C, Marsh, J.S. & Milner, S.C., 1999. Petrology of the alkaline core of the Messum igneous complex, Namibia: evidence for the progressively decreasing effect of crustal contamination. J. Petrol. 40, 1377-1397.

Hawkesworth, C.J., Blake, S., Evans, P., Hughes, R., Macdonald, R., Thomas, L.E., Turner, S.P. & Zellmer, G., 2000. Time scales of crystal fractionation in magma chamber – integrating physical, isotopic and geochemical perspectives. J. Petrol. 41, 991 – 1006.

Heaman, L.M. & Machado, N., 1992. Timing and origin of midcontient rift alkaline magmatism, North America: evidence from the Coldwell Complex. Contrib. Mineral. Petrol. 110, 289-303.

Konnerup-Madsen, J. & Rose-Hansen, J., 1984. Composition and significance of fluid inclusions in the Ilímaussaq peralkaline granite, South Greenland. Bull. Mineral. 107, 317-326.

Konnerup-Madsen, J., Rose-Hansen, J. & Larsen, E., 1981. Hydrocarbon gases associated with alkaline igneous activity: evidence from compositions of fluid inclusions. Rapp. Grønl. Geol. Unders. 103, 99-108.

Kramm, U., Kogarko, L.N., Kononova, V.A. & Vartiainen, H., 1993. The Kola Alkaline Province of the CIS and Finland: precise Rb-Sr age define 380-360 Ma age range for all magmatism. Lithos 30, 33-44.

Kramm, U. & Kogarko, L.N., 1994. Nd and Sr isotope signatures of the Khibina and Lovozero agpaitic centres, Kola Alkaline Province, Russia. Lithos 32, 225-242.

Kuiper K., Hilgen F.J., Krijgsman W. & Wijbrans J., 2004. An astronomiclly dated standard in 40Ar/39Ar geochronology? Abstract, 32nd Internat. Geol. Congress, Firenze, 812.

Kwon, J., Min, K., Bickel, P. & Renne, P.R., 2002. Statistical methods for jointly estimating decay constant of 40K and age of a dating standard. Math. Geol. 34, 457-474.

Larsen, L. M., 1976. Clinopyroxenes and coexisting mafic minerals from the alkaline Ilimaussaq intrusion, south Greenland. J. Petrol. 17, 258-290.

Larsen, L. M., 1977. Aenigmatites from the Ilimaussaq intrusion, south Greenland: Chemistry and petrological implications. Lithos 10, 257-270.

Larsen, L. M., 1981. Chemistry of feldspars in the Ilímaussaq augite syenite with additional data on some other minerals. Rapp. Grønl. Geol. Unders. 103, 31-37.

Larsen, L.M. & Sørensen, H., 1987. The Ilímaussaq intrusion – progrssive crystallisation and formation of layering in an agpaitic magma. In: Fitton, J.G. & Upton B.G.J. (Eds.), Alkaline Igneous Rocks. Geol. Soc. Sp. Publ. 30, London, 473-488.

Lee, J.K.W., 1993. The argon release mechanisms of hornblende in vacuo. Chem. Geol. 106, 133-170.

Ludwig, K.R., 1988. PBDAT for MS-DOS: a computer program for IBM-PC compatibles for processing raw Pb-U-Th isotope data. U.S. Geological Survey Open-File Report. 88-0542.

Ludwig, K.R., 2003. Isoplot 3.00 - a geochronological toolkit for Microsoft Excel: Berkeley Geochronology Center, Spec Publ. No. 4.

Markl, G., 2001. Stability of Na-Be minerals in late-magmatic fluids of the Ilímaussaq alkaline complex, South Greenland. In: Sørensen, H. (Ed.), The Ilímaussaq alkaline complex, South Greenland: status of mineralogical research with new results. Geol. Greenl. Surv. Bull. 190, 145-158.

Markl, G., Marks, M, Schwinn, G. & Sommer, H., 2001a. Phase equilibrium constraints

on intensive crystallization parameters of the Ilimaussaq Complex, South Greenland. J. Petrol. 42, 2231-2258.

Markl, G., Marks, M. & Wirth, R., 2001b. The influence of T, aSiO2, fO2 on exsolution textures in Fe-Mg olivine: an example from augite syenite of the Ilimaussaq Intrusion, South Greenland. Am. Mineral. 86, 36-46.

Marks, M. & Markl, G., 2001. Fractionation and assimilation processes in the alkaline augite syenite unit of the Ilimaussaq Intrusion, South Greenland, as deduced from phase equilibria. J. Petrol. 42, 1947-1969.

Marks, M., Vennemann, T., Siebel, W. & Markl, G., 2004. Nd-, O-, and H-isotopic evidence for complex, closed-system fluid evolution of the peralkaline Ilímaussaq Intrusion, South Greenland. Geochim. Cosmochim. Acta 68, 3379-3395.

Min, K., Mundil, R., Renne, P.R. & Ludwig, K.R., 2000. A test for systematic errors in 40Ar/39Ar geochronology through comparision with U/Pb analysis of a 1.1-Ga rhyolite. Geochim. Cosmochim. Acta 64, 73-98.

Mingram, B, Trumbull, R.B., Littman, S. & Gerstenberger, H., 2000. A petrogenetic study of anorogenic felsic magmatism in the Cretaceous Paresis ring complex, Namibia, evidence for mixing of crust and mantle-derived components. Lithos 54, 1-22.

Nielsen, B.L. & Steenfelt, A., 1979. Intrusive events at Kvanefjeld in the Ilímaussaq igneous Complex. Bull. Geol. Soc. Denmark 27, 143-155.

Parsons, I., Rex, D.C., Guise, P. & Halliday, A.N., 1988. Argon-loss by alkali feldspars. Geochim. Cosmochim. Acta 52, 1097-1112.

Paslick, C. R., Halliday, A. N., Davies, G. R., Mezger, K., & Upton, B. G. J., 1993. Timing of proterozoic magmatism in the Gardar Province, southern Greenland. Bull. Geol. Soc. America 105, 272-278.

Piper, J.D.A., Thomas, D.N., Share, S. & Zhang Qi Rui, 1999. The palaeomagnetism of (Mesoproterozoic) Eriksfjord Group red beds, South Greenland: multi-phase remagnetization during the Gardar and Grenville episodes. Geophys. J. Int. 136, 739-756.

Poulsen, V., 1964. The sandstones of the Precambrian Eriksfjord Formation in South Greenland. Rapp. Grønl. Geol. Unders. 2, 16.

Reagan, M.K., Sims, K.W.W., Erich, J. Thomas, R.B., Cheng, H., Edwards, R.L., Layne, G. & Ball, L., 2003. Time-scales of differentiation from mafic parents to rhyolite in North American Continental Arcs. J. Petrol. 44, 1703-1726.

Reid, M.R., Coath, C.D., Harrison, T.M. & McKeegan, K.D., 1997. Prolonged residence times for the youngest rhyolites associated with Long Valley Caldera; 230Th-238U ion microprobe dating of young zircons. Earth Planet. Sci. Lett. 150, 27-39.

Renne, P.R., Swisher, C.C., Deino, A.L., Karner, D.B., Owens, T.L. & DePaolo, D.J., 1998. Intercalibration of standards, absolute ages and uncertainties in 40Ar/39Ar dating. Chem. Geol. 145, 117-152.

Rogers, N.W., Evans, P.J., Blake, S., Scott, S.C. & Hawkesworth, C.J., 2004. Rates and timescales of fractional crystallisation from 238U-230Th-226Ra disequilibria in trachyte lavas from Longonot volcano, Kenya. J. Petrol. 45, 1747-1776.

Rose-Hansen, J., Sørensen, H. & Watt, W.S., 2001. Inventory of the literature on the Ilímaussaq alkaline comlex, South Greenland. Dan. Grønl. Geol. Unders. Rapp. 2000/57, 38 pp. + CD-ROM.

Schmitt, A.K., Emmermann, R., Trumbull, R.B., Bühn, B. & Henjes-Kunst, F., 2000. Petrogenesis and 40Ar/39Ar geochronology of the Brandberg Complex, Namibia: evidence for a major mantle contribution in metaluminous and peralkaline granites. J. Petrol. 41, 1207-1239.

Shaw, H.R., Hamilton, M.S. & Peck, O.L., 1977. Numerical analysis of lava lake cooling model. I. description of model. Am. J. Sci. 277, 384-414.

Sørensen, H., 1966. On the magmatic evolution of tha alkaline igneous province of South Greenland. Rapp. Grønl. Geol. Unders. 7, 1-19.

Sørensen, H., 2001. Brief introduction to the geology of the Ilímaussaq alkaline complex, South Greenland, and its exploration history. In: Sørensen, H. (Ed.), The Ilímaussaq alkaline complex, South Greenland: status of mineralogical research with new results. Geol. Greenl. Surv. Bull. 190, 7-24.

Sørensen, H. & Larsen, L.M., 1987. The Ilimaussaq Intrusion; progressive crystallization and formation of layering in an agpaitic magma. In: Fitton, J.G. & Upton, B.G.J. (Eds.), Alkaline ig-

neous rocks. Geol. Soc. Spec. Publ. 30, 473-488.

Stacey, J.S. & Kramers, J.D., 1975. Approximation of terrestrial lead isotope evolution by a two stage model. Earth Planet Sci Lett 127, 30-45.

Steenken, A., Siegesmund, S., Heinrichs, T. & Fügenschuh, B., 2002. Cooling and exhumation of the Rieserferner pluton (Eastern Alps, Italy/Austria). Int. J. Earth Sci. 91, 799-817.

Steiger, R.H. & Jäger, E., 1977. Subcommision on Geochronology: Convention on the use of decay constants in geo- and cosmochronology. Earth Planet. Sci. Lett. 36, 359-362.

Stevenson, R., Upton, B.G.J. & Steenfelt, A., 1997. Crust-mantle interaction in the evolution of the Ilímaussaq Complex, South Greenland: Nd isotopic studies. Lithos 40, 189-202.

Upton, B.G.J., Emeleus, C.H., Heaman, L.M., Goodenough, K.M. & Finch, A.A., 2003. Magmatism of the mid-Proterozoic Gardar Province, South Greenland: chronology, petrogenesis and geological setting. Lithos 68, 43-65.

Ussing, N.V., 1912. Geology of the country around Julianehaab, Greenland. Medd. Grønl. 38, 426.

Villa, I.M., 1983. 40Ar/39Ar chronology of the Adamello gabbros, southern Alps. Memorie della Societa Geologica Italiana, 26,1, 309-318.

Villa, I.M., 1998. Isotopic closure. Terra Nova 10, 42-47.

Villa I.M., 2001. Radiogenic isotopes in fluid inclusions. Lithos 55, 115-124.

Villa, I.M., Hermann, J., Müntener, O. & Trommelsdorf, V., 2000. 39Ar-40Ar dating of multiply zoned amphibole generations (Malenco, Italian Alps). Contib. Min. Petr. 140, 363-381.

Villa, I.M. & Renne, P.R., 2005. Decay constants in geochronology. Episodes 28, 50-51.

von Blanckenburg, F & Villa, I.M., 1988. Argon retentivity and argon excess in amphiboles from the graben schists of the Western Tauern Window, Eastern Alps. Contrib. Mineral. Petrol. 100, 1-11.

Waight, T., Baker, J. & Willigers, B., 2002. Rb isotope dilution analyses by MC-ICPMS using Zr to correct for mass fractionation: towards improved Rb-Sr geochronology? Chem. Geol. 186, 99-116.

Wartho, J.A., Dodson, M.H., Rex, D.C. & Guise, P.G., 1991. Mechanisms of Ar release from Himalayan metamorphic hornblende. Am. Mineral. 76, 1446-1448.

Widom, E., Schmincke, H.U. & Gill, J.B., 1992. Process and timescales in the evolution of a chemically zoned trachyte: Fogo A, Sao Miguel, Azores. Contrib. Mineral. Petrol. 111, 311-328

Wohletz, K. & Heiken, G., 1992. Volcanology and Geothermal Energy. University of California Press, Berkeley, 432 pp.

Appendix

Cooling model

In order to test independently the validity of our geochronological results, we modelled the thermal evolution of the Ilímaussaq complex after its intrusion.

The geometry of the intrusion (Sørensen, 2001), the physical properties of the intrusives and the host rocks (Forsberg & Rasmussen, 1978) and the intrusion level of 3-4 km (e.g. Larsen & Sørensen, 1987) are well known. Mafic cumulates at depth are indicated by a positive gravity anomaly beneath the complex (Blundell, 1978; Forsberg & Rasmussen, 1978). However, Blundell (1978) related the anomaly to a gabbroic body and interpreted the Narssaq intrusion as its surface expression. Based on field observations, the Narssaq intrusion predates the Ilímaussaq complex. Therefore, the gravity anomaly may not be caused by basal cumulates of the Ilímaussaq magmas.

Several processes influence the cooling history. As pointed out by Furlong et al. (1991), circulation of a fluid phase through the pluton would enhance cooling. However, the Ilímaussaq intrusion can be regarded as a closed system (Marks et al., 2004) even during late stage hydrothermal activity (Markl et al., 2001a). Accordingly, no fluid phase from the surrounding had access to the intrusive body or escaped from it and the heat transport to the host rocks must have been dominated by conduction. Cooling can be enhanced by vaporisation of fluid in the host rocks close to a pluton (Shaw et al., 1977; Delaney, 1984). Another fact that accelerates the cooling especially of shallow intrusions is a high thermal gradient between host rock and magma body. This is expected to be the most important feature with regards to the cooling of the Ilímaussaq complex.

Some assumptions concerning the starting conditions of the model had to be made. The geothermal gradient was assumed to be higher than normal because of the large amount of magma penetrating the crust and forming the alkaline intrusions and the basalts of the Eriksfjord formation in an extensional rift setting. Accordingly, the calculations were carried out with a geothermal gradient of 50°/km. However, tests during modelling showed that this higher geothermal gradient extends the cooling of the pluton below the closure temperature of the amphiboles only in that way that it has no consequence for the interpretation. Another assumption is the way of transporting the heat. As pointed out above, we believe that heat conduction at least close to the pluton is the favourable mechanism. Formation of a convection cell in the host rocks is especially likely in the subaerial to submarine (Poulsen, 1964) and hence fluid-

saturated basalts and sandstones of the Eriksfjord formation. It is still not clear, whether the Eriksfjord formation is partly contemporaneous with the Ilímaussaq intrusion or not (Halama et al., 2003; Upton et al., 2003). Based on field observations, the Ilímaussaq rocks clearly intruded the basaltic lava flows, which can be found as xenoliths especially in the upper part of the intrusion. Several dating studies using both isotopes and paleomagnetics were carried out resulting in ages between 1.17 and 1.35 Ga (Paslick et al., 1993; Andersen, 1997; Piper et al., 1999). The youngest age of 1170 ± 30 Ma published by Paslick et al. (1993) from the second of three volcanic groups indicates the possibility that the upper parts of the Eriksfjord basalts are contemporaneous with the Ilímaussaq rocks or even post-date them providing a heat source above the pluton. The effect on the duration of the cooling is, however, minor and can be disregarded. The volumes of the two earlier magma batches, especially that of the alkali granite, are small. They should have cooled down very fast. From field observation it is known that the two earlier rocks were solidified when the agpaites intruded. Therefore, we decided to create a simple model without magma rejuvenation.

For thermal modelling, we used the latest version of the freely available HEAT 3D software. A former version of the software is described in Wohletz & Heiken (1992). Models were calculated using the 3D mode of the HEAT 3D software with different starting conditions considering the problems mentioned above. The results are surprisingly uniform. The intrusion cooled to 500°C within at most 800 ka (Fig. A2).

Figures in the Electronic Supplement
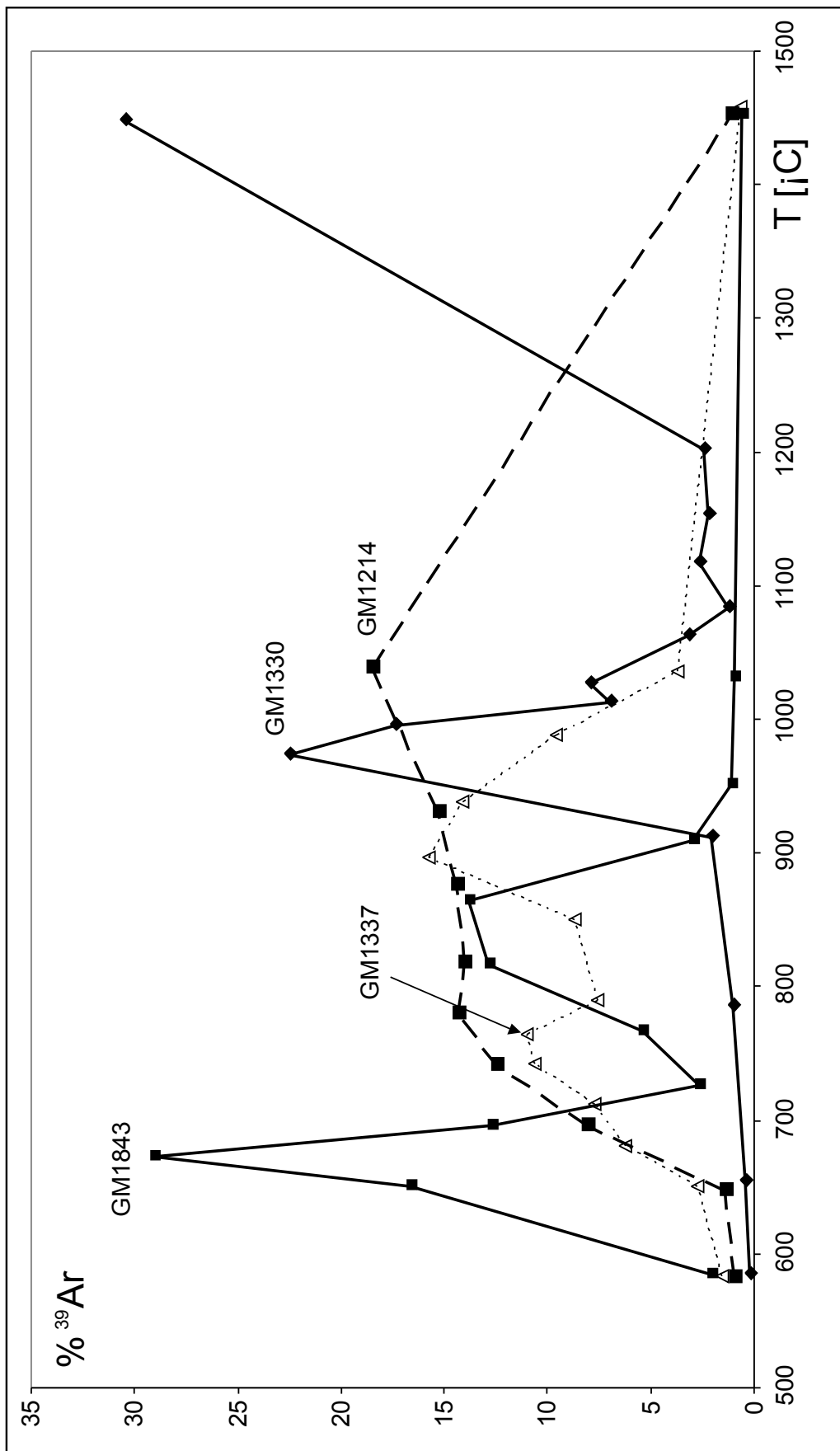
Fig. A1
Temperature dependence of the degassing of amphiboles during stepwise heating experiments. Samples GM1370, GM1390, GM1335, GM1657 and GM1303 not shown in the diagram exhibit similar degassing patterns as sample GM1843.
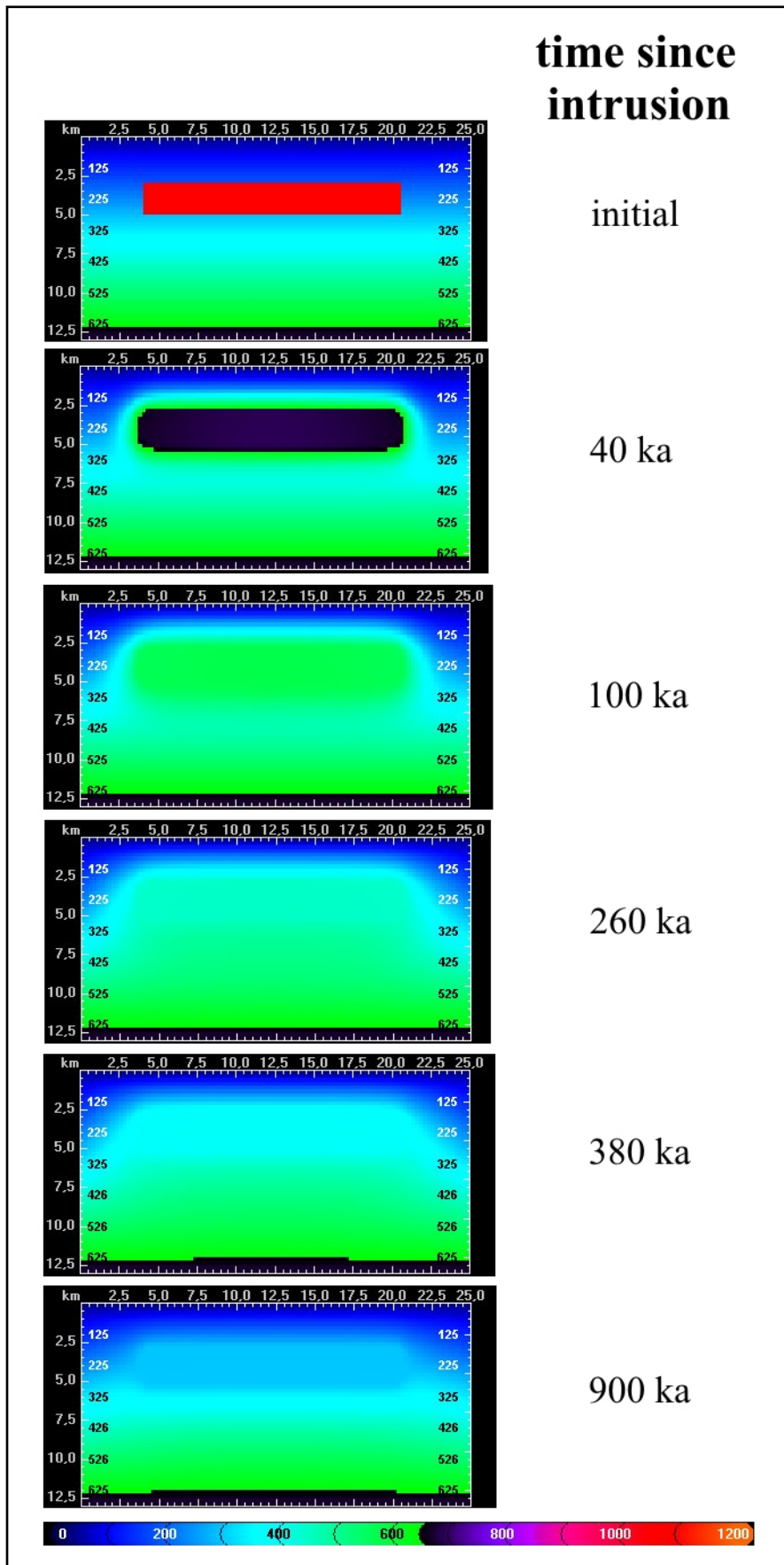
Fig. A2
Cooling model for the Ilímaussaq intrusion calculated as detailed in the text. Temperatures of the scale and in the model pictures are in °C.

Volatiles in a peralkaline system: abiogenic hydrocarbons and F-Cl-Br systematics in the naujaite of the Ilímaussaq intrusion, South Greenland.*

Thomas V. Krumrei, Ernst Pernicka, Melanie Kaliwoda and Gregor Markl

Thomas V. Krumrei, Melanie Kaliwoda, Gregor Markl

Eberhard Karls Universität Tübingen,

Institut für Geowissenschaften, Wilhelmstr. 56,

D-72074 Tübingen, Germany

Ernst Pernicka

Eberhard Karls Universität Tübingen,

Institut für Ur- und Frühgeschichte, Schloss Hohentübingen

D- 72070 Tübingen, Germany

Abstract

Agpaitic rocks comprise most of the exposed part of the 1.16 Ga old, 8x17 km large and about 1700 m thick Ilímaussaq intrusion in South Greenland. Within these, a more than 600 m thick sequence of sodalite-rich „naujaites" (mainly sodalite + arfvedsonite + alkali feldspar + nepheline + eudialyte + aenigmatite) is interpreted as a sodalite flotation cumulate. Sodalites show two to three different zones in cathodoluminescence (CL) and at least two zones in thin sections. The CL zones can be related to chemical differences detectable by electron microprobe, whereas relations with optical zonations are less obvious. Compositional trends in sodalite reflect trends in the evolution of volatile contents in the melt. The sodalite at Ilímaussaq is almost free of Ca and closely corresponds to the pure Na-Cl sodalite endmember with about 7 wt.% of Cl; S contents reach up to 0.9 wt.%. Cl/Br ratios range from 500 to 1700. Raman spectroscopy shows that S is present as SO_4^{2-} in sodalite, although sphalerite (ZnS) is a stable phase in naujaites. Peralkalinity and fO2 conditions allow S^{2-} and SO_4^{2-} to be present contemporaneously.

The whole naujaite sequence is divided into two parts, an upper part with low, homogeneous S contents and Cl/Br ratios in the sodalite cores, and a lower part with strongly variable and higher S contents and with Cl/Br ratios, which are decreasing downwards. The details of the S content and the Cl/Br ratio evolution show that sodalite strongly influences the halogen contents of the melt by scavenging Cl and Br.

The naujaites were formed from a highly reduced, halogen-rich magma in equilibrium with magmatic methane at about 800°C, which, upon ascent, cooling and fractionation, exsolved an aqueous fluid phase. Both fluids were trapped in separate inclusions indicating their immiscibility.

Micrometer-sized aegirine crystals and primary hydrocarbon-bearing inclusions are abundant in the crystal cores. The inclusions were trapped at pressures up to 4 kbar, although the emplacement pressure of the intrusion is about 1 kbar. This indicates growth of the sodalite during melt ascent and a very effective mechanism of trace element scavenging during sodalite growth. Sodalite rims are devoid of aegirine or primary hydrocarbon inclusions and probably reflect the emplacement stage.

Keywords: halogen systematics, sodalite, hydrocarbon-bearing fluid inclusions, Ilímaussaq

Introduction

The Mesoproterozoic Ilímaussaq igneous complex is one of ten alkaline intrusive bodies in the Gardar igneous province, South Greenland. Since the first detailed description by Ussing (1912), numerous papers dealing with the Ilímaussaq complex have been published (e.g. Sørensen & Larsen, 1987; Rose-Hansen et al., 2001; Markl et al., 2001a+b; Marks & Markl, 2001). Thus, the petrography, petrology and geochemistry of the Ilímaussaq complex are relatively well known (e.g. Ferguson, 1964; Sørensen & Larsen, 1987; Bailey et al., 2001; Markl et al., 2001a, Marks et al., 2004b) and it can serve as a textbook example for the evolution of a peralkaline magma chamber.

Phase relationships, fluid evolution and element enrichment processes in the course of the crystallisation of silicate melts in general, and of agpaitic specifically, are strongly influenced by their volatile content and speciation (e.g. Lowenstern, 1994; Carroll & Webster, 1994; Metrich & Clocchiatti, 1996; Greenough et al., 1999; Moretti et al., 2003; Kravchuk et al., 2004). Therefore, understanding the type, stability relations and evolution of the fluid phases in igneous systems, and particularly of halogens (e.g. Marr et al., 1998; Webster & De Vivo, 2002; Schmitt et al., 2002; Carroll, 2005), is of prime importance. This, together with the fact that many Ilímaussaq rocks are strongly enriched in halogens (Bailey et al., 2001) and that methane and higher hydrocarbons of abiogenic origin occur in most of them (Petersilie & Sørensen, 1970; Konnerup-Madsen, 2001), makes the intrusion an ideal place to study the details of halogen partitioning and fluid evolution in peralkaline melts.

Hydrocarbon-bearing fluids are a typical feature of peralkaline and agpaitic rocks (Konnerup-Madsen, 2001; Potter & Konnerup-Madsen, 2003; Beeskow et al., in press; Salvi & Williams-Jones, in press; Ryabchikov & Kogarko, in press), but their origin is still a matter of debate. An abiogenic origin is nowadays widely accepted (e.g. Konnerup-Madsen, 2001; Beeskow, in press). Konnerup-Madsen & Rose-Hansen (1982) explained the hydrocarbons in the Ilímaussaq rocks by a late-magmatic reduction of a primary CO_2-H_2O fluid. Another hypothesis invokes a Fischer-Tropsch-type reaction under post-magmatic conditions, for which again a CO_2-rich fluid is needed (e.g. Salvi & Williams-Jones, 1997). Extended reviews of these models can be found in Potter & Konnerup-Madsen (2003) and Beeskow et al. (in press). A main point of criticism of both models is the requirement of a primary fluid containing CO_2. Such a fluid is unlikely to have existed given the low fO_2 conditions recorded for the Ilímaussaq magmas (Markl et al., 2001a; Ryabchikov & Kogarko, in press) and no fluid inclusion study at Ilímaussaq has ever reported high-temperature CO_2 fluid inclusions. Experimental and theoretical studies show that hydrocarbons form a stable fluid phase at high temperatures and high pressures when the oxygen fugacity is sufficiently low (Kenney et al., 2002). Indeed,

they can form at fO_2 values close to the wüstite-magnetite buffer and P-T conditions of the upper mantle from any carbonate species (Scott et al., 2004). Our data renew the model of the primary origin of the hydrocarbons in the Ilímaussaq rocks (Petersilie & Sørensen, 1970; Konnerup-Madsen & Rose-Hansen, 1982). We will show that the hydrocarbons are of primary magmatic origin and no CO_2 –rich fluid is needed to explain their occurrence.

Geology

Magmatism in the Gardar Province, South Greenland, is closely related to rifting between 1350 and 1140 Ma. Based on U-Pb chronology, two main periods of magmatic activity around 1280 Ma and between 1180 and 1140 Ma, respectively, can be separated (Upton et al., 2003). During these time spans, several alkaline to peralkaline plutonic complexes and a large number of dykes with variable compositions intruded the Ketilidian (1.7 - 1.8 Ga) granitic basement rocks (Julianehåb granite). The Ilímaussaq intrusion belongs to the second of these periods (Blaxland et al., 1976). Krumrei et al. (2006) dated the complex at 1161 ± 5 Ma using the Ar-Ar technique on amphiboles. It consists of alkaline to peralkaline, mostly agpaitic rocks. Controlled by early fault systems (Sørensen, 1966), the complex intruded at the contact between the Julianehåb granite and the late-Gardar Eriksfjord basalts and sandstones (Poulsen, 1964). The intrusion level was shallow and no metamorphic overprint at all has changed the mineralogy of the rocks (Upton et al., 2003).

Three pulses of magma intruded successively to 3 - 4 km depth (Larsen & Sørensen, 1987). The first one produced a silica-saturated to slightly under-saturated augite syenite, which is now found in parts of the intrusion as the outer shell and as xenoliths within the agpaitic rocks. Subsequently, a sheet of a peralkaline granite (called alkali granite in the literature on Ilímaussaq) intruded the augite syenite. According to Marks et al. (2004b), it represents a more evolved and crustally contaminated equivalent of the augite syenite that possibly assimilated 10 to 15 % of Archeaen lower crustal rocks. In a third stage, various nepheline syenites (pulaskite, foyaite, sodalite foyaite, naujaite, kakortokite and lujavrite) were formed mostly by low-pressure in situ fractionation of a broadly phonolitic melt. They contain nepheline, eudialyte, sodalite, alkali feldspar, aegirine and arfvedsonite in various proportions as well as rare minerals like rinkite, aenigmatite, neptunite and others. These agpaites make up the major part of the complex (Fig. 1) and can be subdivided into a roof series (pulaskite, foyaite, sodalite foyaite and naujaite, from the roof downwards), a bottom series (kakortokites), the most evolved rocks (lujavrites) in between and an unexposed part below the kakortokites. The current interpretation is that the roof and the bottom series are cumulates. The first formed by downward crystallisation and flotation of minerals less dense than the melt and

the latter by gravitational separation after the solidification of the roof series. That the residual melts intruded the roof cumulates along fractures (Larsen & Sørensen, 1987). Recently, however, Sørensen et al. (in press) provided evidence for the idea that the bottom cumulate and the lujavrites were formed from a separate magma batch. Numerous pegmatites and late-magmatic to hydrothermal veins occur in all parts of the intrusion.
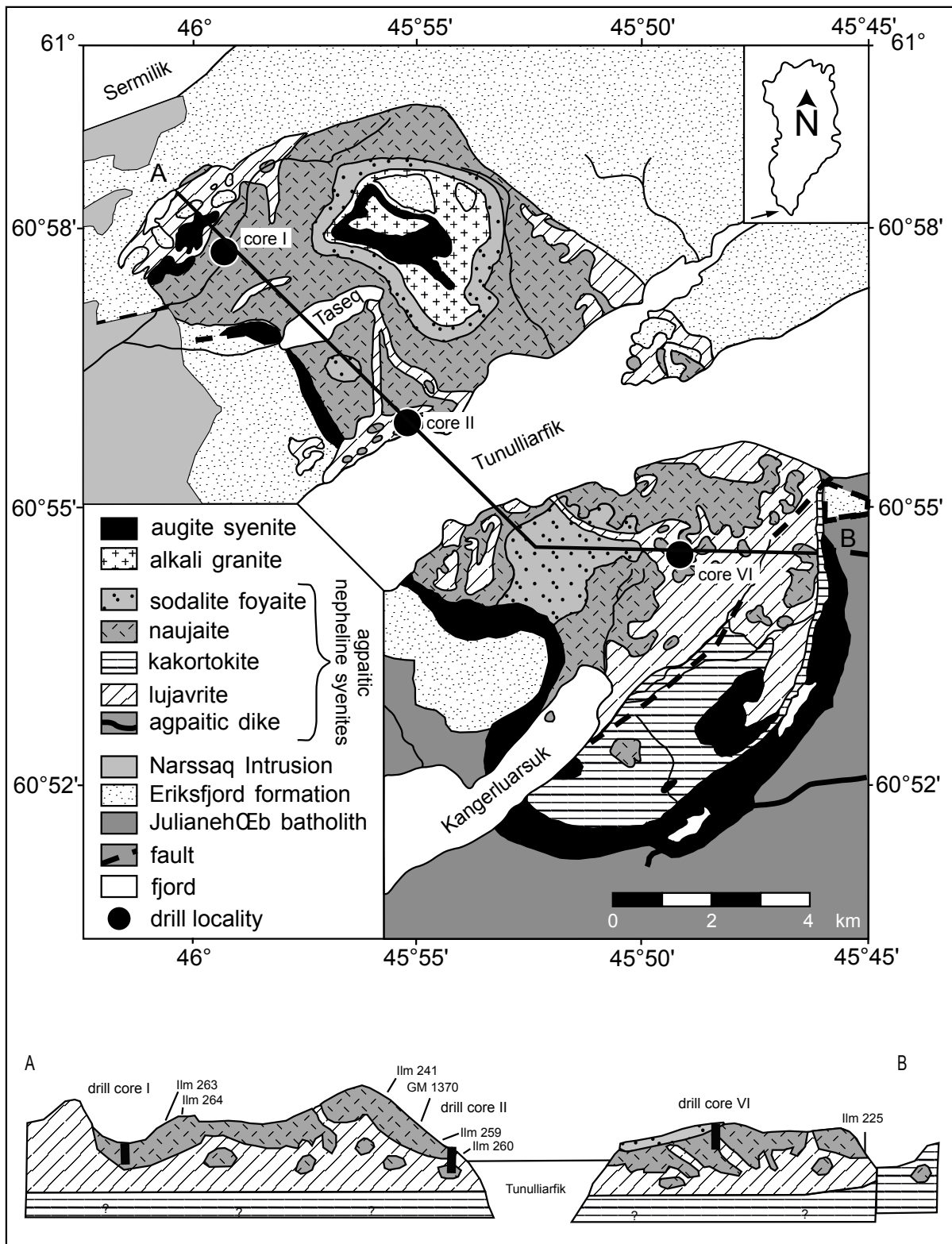
Fig. 1
Geological map of the Ilímaussaq intrusion with a schematic cross section (after Rose-Hansen & Sørensen, 2002). The drill locations are marked on the map and the sample locations of the surface samples are given in the cross section.

One of the agpaitic syenites, the naujaite, is a more than 600 m thick and slightly layered body that represents approximately 40% of the exposed volume of the complex (Rose-Hansen & Sørensen, 2002). Large naujaite xenoliths occur in the rocks below it (kakortokite and lujavrite). Therefore, Sørensen et al. (in press) argue for an originally even thicker naujaite horizon that was reduced to the present dimensions by piecemeal stoping. To explain the enormous amount of sodalite, the magma volume from which the sodalite crystallised must have been several times larger than today's volume of the complex. Bailey et al. (2001) and Bailey (in press) provide geochemical evidence for two naujaite generations formed from two slightly different magma compositions based on differences in the contents of B, Br, S and Be in the sodalites and two different Zr-U regression lines in whole rock analyses.

Several publications mainly dealing with the isotopic composition of the rocks show that the different magma batches, starting with the augite syenite and ending with the evolved nepheline syenites, originated from a single source (Nielsen & Steenfelt, 1979; Larsen & Sørensen, 1987; Stevenson et al., 1997; Marks et al., 2004b). The extreme fractionation trend found in the Ilímaussaq complex appears to be governed by low water activity, low SiO_2 activity and low oxygen fugacity in the parental melt (Larsen, 1976, 1977, 1981; Markl et al., 2001a+b; Marks & Markl, 2001).
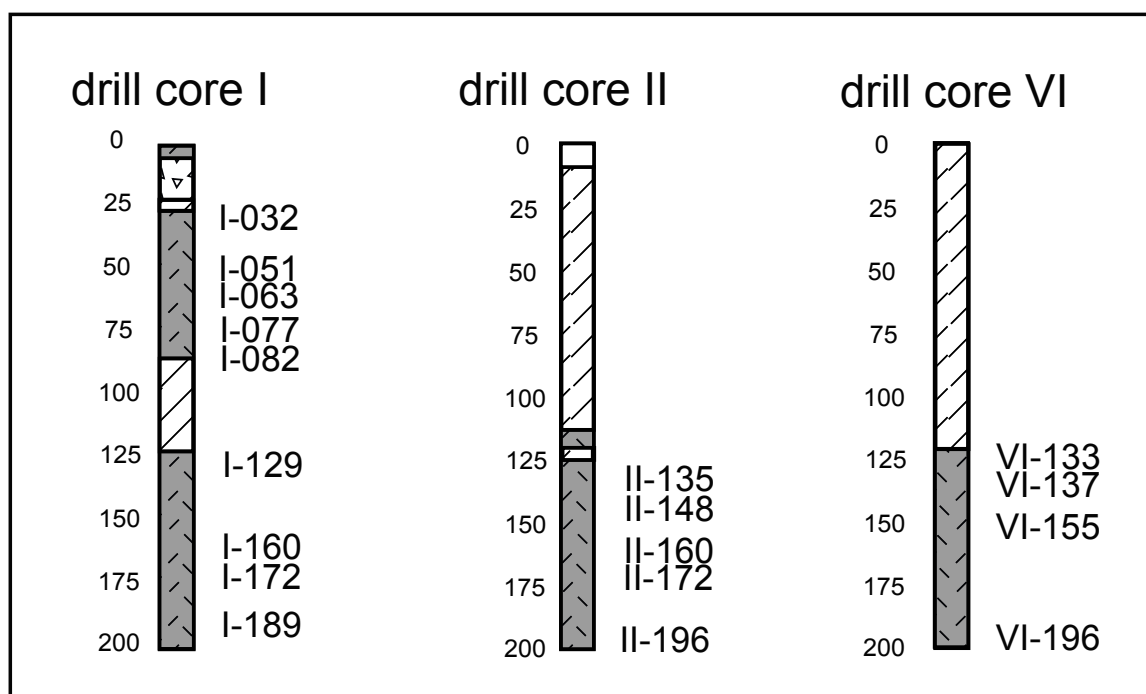
Fig. 2
Lithologies of the three naujaite-bearing drill cores and the samples taken from them. Modified after Rose-Hansen & Sørensen (2002), same lithologies as in Fig. 1. The numbers to the left of the cores refer to the depth (m) below the surface at the drilling location.

Petrography of the naujaite and fluid inclusions therein

The petrography of the Ilímaussaq rocks is reported in many publications (e.g. Ussing, 1912; Ferguson, 1964; Sørensen, 2001). The naujaite is a roof cumulate formed by flotation of minerals less dense than the melt, mainly sodalite. The sodalite crystals are euhedral and show areas with oriented inclusions of aegirine needles. Sodalites from the lower part of the naujaite sequence have aegirine-free rims or even lack aegirine inclusions at all. Large crystals of aegirine, arfvedsonite, eudialyte, and alkali feldspar enclose the sodalites poikilitically. Accessory minerals are fluorite, villiaumite, sphalerite, apatite, aenigmatite and others.
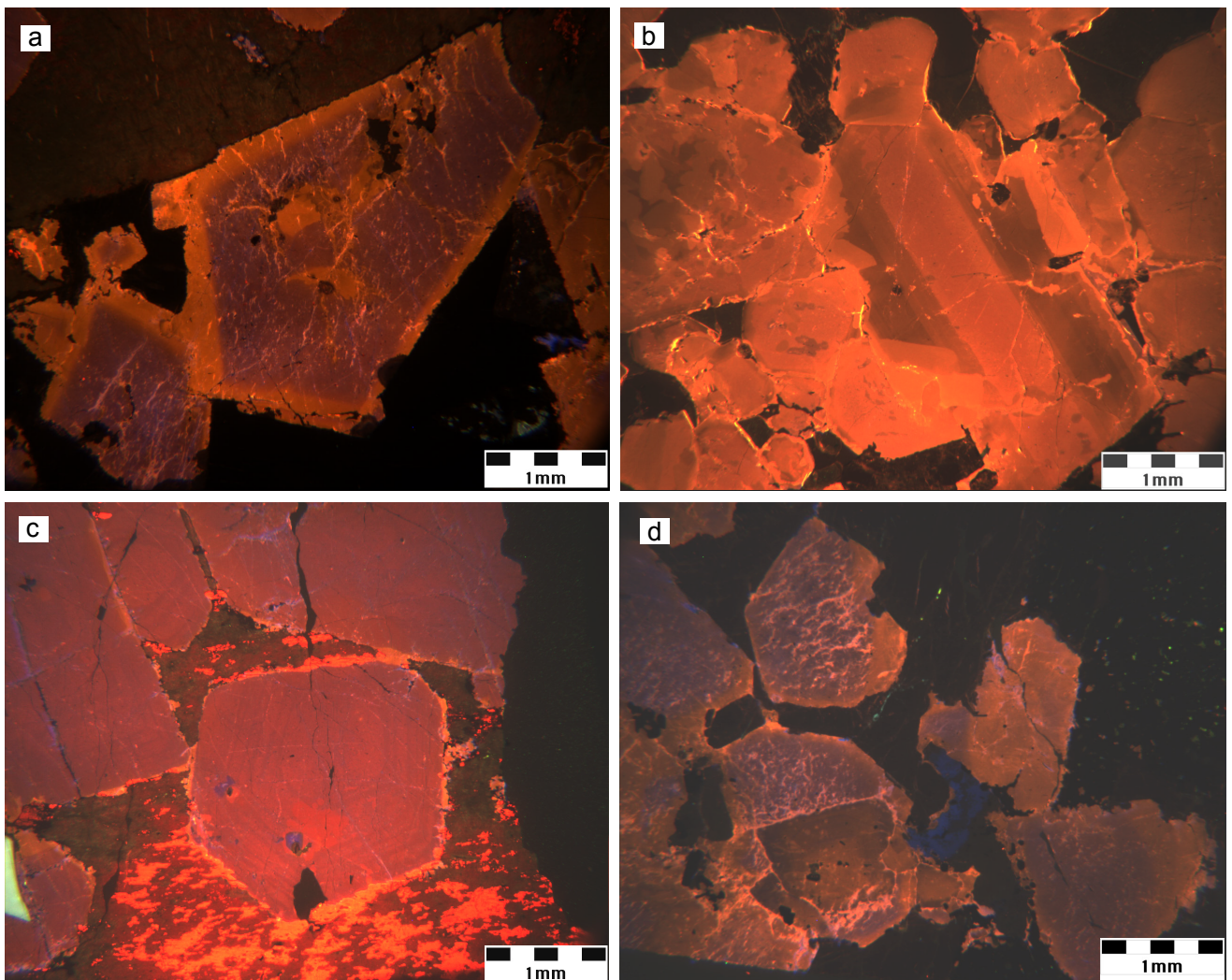
Fig. 3
CL-photomicrographs of sodalite. a) Sodalite with two CL-zones. b) Sodalite showing three CL-zones starting with light orange colours in the core, turning to a more brownish zone; the rims show light orange colours again. c) Concentrically zoned sodalite with an oscillating zonation of narrow purple and reddish zones. d) Sodalite crystals with two-zone zonation and additional dark coloured old cores.

The samples of this study mainly come from three naujaite-bearing drill cores (cores I, II and VI) described by Rose-Hansen & Sørensen (2002) (see also our Fig. 2). The drilling locations are marked in Fig. 1. These drill core samples were supplemented by samples collected from the surface. Together, they were arranged in a stratigraphic order using Fig. 13 in Rose-

Hansen & Sørensen (2002). In this order, we present our results in the following Tables and Figures. We note that the stratigraphic position of the naujaite mass in drill cores II and VI may be unclear because these are most probably xenoliths. However, the density contrast between solid naujaite and the lujavrite melt is very small (Sørensen et al., in press, and references therein). Therefore, the naujaite masses in drill cores II and VI are most probbaly not far below their original position.

Under the cathodoluminescence microscope (CL), the sodalite grains show a strong zonation with up to three zones of light orange to brownish and purple colours (Fig. 3). The zonation starts with a purple zone in the core in the case of two-zone crystals (Fig. 3a) and with a light orange zone in the case of three zones changing to brownish colours towards the rim (Fig. 3b). In most samples, the euhedral crystals are overgrown by more or less irregular rims of a younger sodalite generation with brightly orange colours. Some grains are concentrically zoned (Fig. 3c), others seem to have old cores (Fig. 3d). These cores have darker orange luminesence colours than the overgrowths. There is no clear correlation between the aegirine content of the sodalites or the stratigraphic position of the sample in the naujaite sequence and the CL zonations.

Two types of fluid inclusions can be found in the sodalites; those dominated by hydrocarbons (HC) and those dominated by aqueous high-salinity fluids. The aqueous inclusions are located only in those parts of the sodalites that are free of aegirine needles, whereas inclusions with hydrocarbons occur in both the aegirine-bearing and the aegirine-free parts (Fig. 4a). Aqueous inclusions are always of secondary origin. They are aligned along inclusion trails or they form clusters (Fig. 4b). Aqueous inclusions occur accumulated in those samples that were taken close to lujavrite. With increasing distance to lujavrite, the amount of aqueous inclusions decreases.

Based on their textures, HC-bearing inclusions are partly primary, partly secondary. The primary inclusions often exhibit negative crystal shapes (Fig. 4c). They are disseminated randomly in the sodalite cores between aegirine needles but are, in most cases, not attached to them. Secondary HC-bearing inclusions form trails (Fig. 4d). The lack of clear age relationships at intersections of hydrous with hydrocarbon inclusion trails suggests that the two types of trails were formed contemporaneously. Very rarely, Konnerup-Madsen et al. (1979) found inclusions in chkalovite from a hydrothermal vein and in nepheline from the naujaite that trapped both fluid types. This proves that both fluids existed from the magmatic naujaite phase to the hydrothermal phase of the intrusion.
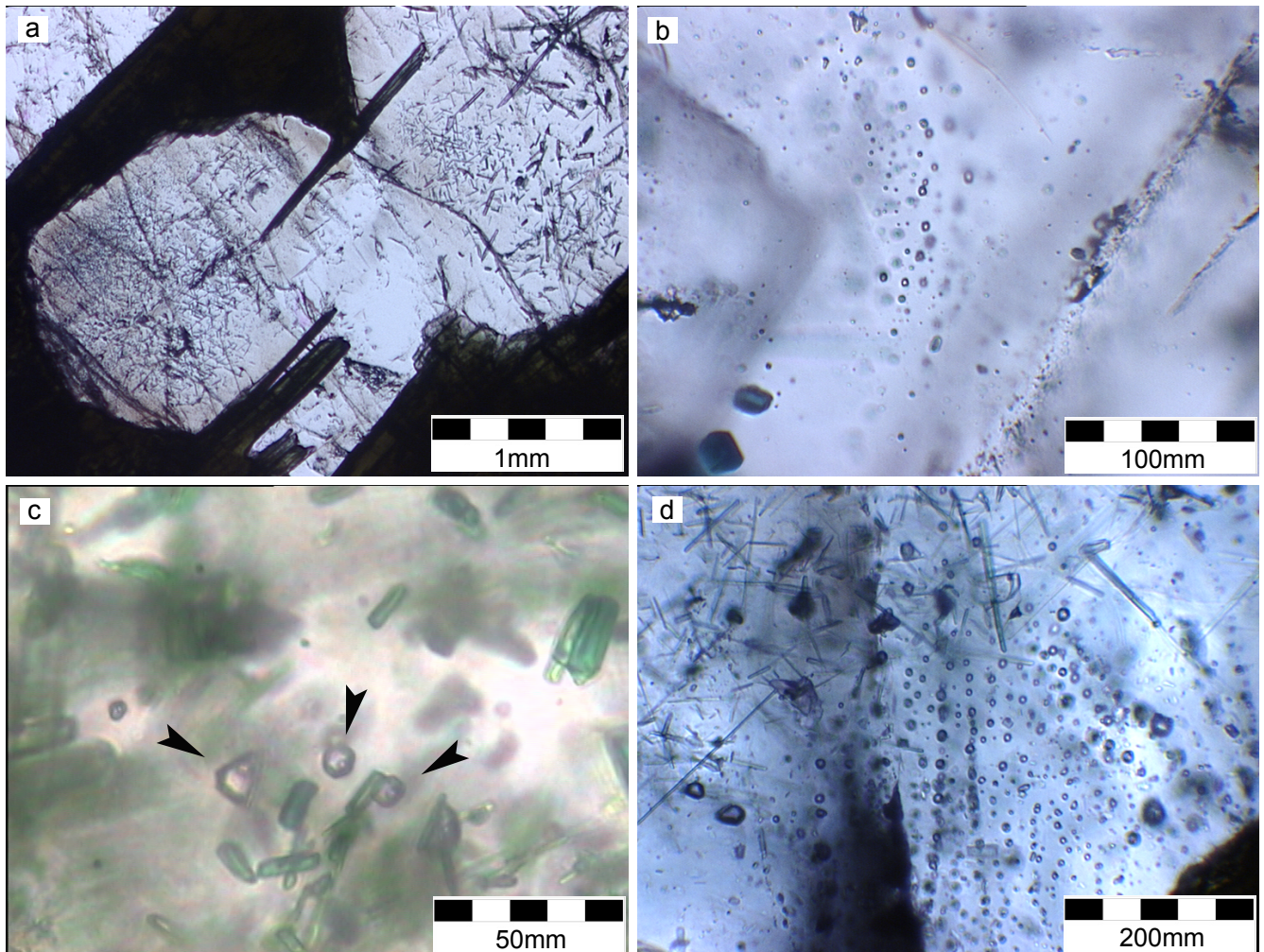
Fig. 4
Photomicrographs of sodalite. a) Distribution of aegirine needles in sodalite showing areas with abundant and oriented aegirine needles in the cores and aegirine-free areas at the rims. b) Trail of aqueous inclusions (~5 μm in diameter) in an aegirine-free part of sodalite. c) Primary hydrocarbon-bearing inclusions marked by the black arrows between green aegirines. They are approximately 10 μm in diameter and show negative crystal shapes. They exhibit a gas bubble because they are pictured at -100 °C before homogenisation (at –96.1 °C). d) Large trail of secondary hydrocarbon-bearing inclusions cutting through an aegirine-free part of sodalite. Note, that the trail does not proceed into the aegirine-bearing part on top.

Methods

Cathodoluminescence (CL)

For the CL analyses, we used a Technocyn 8200 Mk 4 Luminoscope fitted with an Alcatel Vacuum Pump at the Universität Tübingen. The chamber is mounted on a Zeiss Microscope of which the normal stage was replaced by the CL chamber. Acceleration voltage and beam current of the electron gun were set to 14.5 kV and 300 μA, respectively. Pictures were taken with a digital camera (DVC 1310-FW) mounted on the third ocular of the microscope. Typical exposure times were 3 to 6 seconds.

Electron Microprobe

Major element compositions of sodalite were determined using a JEOL 8900 electron micro-probe at the Institut für Geowissenschaften, Universität Tübingen, Germany. For calibration,

Tab. 1

Mean values of sodalite chemistry analysed by EMP

		n	Al$_2$O$_3$	Na$_2$O	K$_2$O	Cl	SiO$_2$	CaO	SO$_3$	FeO	total
sodalite rim	llm241	10	31.17	24.16	0.01	6.72	37.25	0.01	0.49	0.22	100.02
	llm264	20	31.31	23.76	0.02	6.66	37.43	0.01	0.60	0.33	100.12
	GM1370	11	31.11	25.13	0.02	6.85	36.93	0.01	0.30	0.14	100.48
	I-032	2	31.68	24.77	0.01	6.75	37.08	0.01	0.56	0.03	100.87
	I-077	8	31.29	24.74	0.02	6.63	37.07	0.01	0.80	0.17	100.73
	llm260	8	31.27	25.01	0.03	6.71	37.04	0.01	0.54	0.22	100.82
	llm225	4	31.13	24.43	0.01	6.56	36.86	0.01	0.76	0.24	99.99
	I-143	2	31.46	24.93	0.01	6.82	37.04	0.01	0.49	b.d.	100.75
	I-160	12	31.13	23.19	0.05	6.44	37.13	0.01	1.00	0.16	99.10
	I-189	8	31.03	23.96	0.02	6.75	36.91	0.01	0.63	0.20	99.50
	II-142	6	31.30	24.28	0.01	6.77	37.32	0.01	0.37	0.28	100.34
	II-199	4	30.84	23.7	0.01	6.82	36.85	0.01	0.44	0.13	98.80
sodalite core	llm241	10	31.15	23.99	0.01	6.93	37.20	0.01	0.15	0.06	99.51
	llm264	18	31.36	23.84	0.01	6.98	37.52	0.01	0.09	0.09	99.89
	GM1370	8	30.95	24.96	0.03	6.87	37.03	0.11	0.12	0.27	100.33
	I-003	1	31.45	25.11	0.02	6.85	37.05	b.d.	0.33	0.09	100.90
	I-032	2	31.60	24.89	0.01	6.82	36.95	0.01	0.32	0.08	100.66
	I-077	6	31.30	24.87	0.01	6.76	37.13	0.01	0.46	0.12	100.66
	llm260	10	31.35	24.73	0.02	6.93	37.50	0.02	0.16	0.11	100.82
	llm225	4	31.06	25.11	0.02	6.94	36.93	0.01	0.17	0.29	100.52
	I-160	10	31.16	23.95	0.02	6.50	36.93	0.01	0.88	0.16	99.61
	I-189	10	31.01	23.71	0.02	6.60	36.97	b.d.	0.88	0.13	99.32
	II-142	4	31.43	24.44	0.01	6.73	37.37	0.01	0.54	0.17	100.69
	II-199	8	31.00	24.08	0.02	6.16	36.74	0.01	1.73	0.13	99.86
old cores	llm264	3	31.25	23.49	0.01	6.89	37.48	0.01	0.14	0.07	99.34
	GM1370	15	31.21	25.22	0.02	6.83	36.71	0.01	0.22	0.07	100.29
	I-003	5	31.21	25.37	0.01	6.69	36.80	0.01	0.71	0.08	100.87
	I-032	8	31.22	25.16	0.02	6.73	37.27	0.01	0.51	0.06	100.96
	I-077	2	31.37	24.52	0.02	6.38	37.20	0.01	1.18	0.05	100.73
	llm225	2	30.94	24.82	0.02	6.91	37.11	b.d.	0.17	0.32	100.28
	I-143	6	31.52	24.94	0.01	6.42	36.88	0.01	1.13	0.05	100.94
	I-160	2	31.22	23.13	0.02	6.12	36.72	0.01	1.76	0.12	99.09
	I-189	2	31.26	24.32	0.02	6.40	36.87	0.01	1.15	0.15	100.16

n = number of analyses; b.d. = below detection limit

both natural and synthetic standards were used. The beam current was 15 nA and the acceleration voltage was 15 kV. The counting time on the peak was 16 s for major elements, and 30-60 s for minor elements. Background counting times were half of the peak counting times. To avoid Na migration under the electron beam, sodalite was analyzed using a defocused beam of 20 μm diameter. Data reduction was performed using the internal $\phi\rho Z$ procedures of JEOL (Armstrong, 1991). Mean values of sodalite composition are presented in Tab. 1.

Neutron Activation Analysis (NAA)

For the determination of bromine, hand-picked sodalite mineral separates were used. 100 to 150 mg of each sample were weighed into small polyethylene containers with caps that were welded to the containers with a hot glass rod in order to make them water tight. A standard solution of 0.2 mg/ml was prepared by dissolving a weighed amount of KBr in distilled water in a volumetric flask. Aliquots of 50 μl of this solution were pipetted onto filter paper in the same polyethylene containers as used for the samples. Four of these flux monitors were irradiated together with each batch of 10 samples in the TRIGA research reactor of the Institut für Kernchemie, University of Mainz, for four hours at a flux of 2 x 10^{12} neutrons*cm^{-2}*s^{-1}. In addition, two aliquots of a standard clay (TONY) that was calibrated against several international geological reference materials (Kuleff & Pernicka, 2002) were also irradiated with the samples. The major aim was the determination of the bromine concentration so that the measuring scheme was optimised for this purpose. Since the samples contain very high concentrations of sodium, which produces ^{24}Na with a half-life of 15.0 h and emits high-energy gamma rays causing a high background, the samples were allowed to decay for two weeks. Bromine was determined by measuring the 559 keV gamma signal of ^{82}Br which decays with a half life of 35.3 h using a hyperpure germanium detector with an energy resolution of 1.9 keV at 1.33 MeV. The longer than usual decay period reduced the sensitivity of the bromine determination somewhat, but was sufficient for the concentration range encountered in the samples. In addition to bromine, 22 other elements were analysed whose concentrations are reported in Tab. 2. The analytical errors given represent only counting errors comprising background and signal. They are given in percent of the concentration value.

Fluid inclusion studies

The microthermometric measurements were carried out at the Universität Tübingen fluid inclusion laboratory. Microthermometric determinations were made on doubly polished wafers (about 500 μm thick), using a Leica microscope equipped with a Linkam THM600/S heating-freezing stage. Accuracy of the measurements was ensured by calibration against the melting point of pure CO_2 (-56.6 °C), pure H_2O (0.0 °C) and the critical total homogenisation tem

Tab. 2
Trace element contents of sodalite analysed by NAA.

	Ilm241	± [%]	Ilm264	± [%]	Ilm263	± [%]	I-032	± [%]	I-051	± [%]	I-063	± [%]	I-077	± [%]	VI-155	± [%]	Ilm259	± [%]
Sc	0.08	5.7	0.06	5.5	0.13	4.6	0.16	3.6	0.09	5.2	0.07	6.8	0.09	4.8	0.16	3.8	0.05	7.3
Cr	5.19	18	4.62	11	5.06	11	3.58	11	4.69	11	6.29	10	5.14	10	4.58	15	4.34	11
Co	0.31	15	0.13	25	0.09	54	0.07	34	0.07	41	0.13	32	0.07	38	0.38	9.6	0.09	30
Zn	189	5.2	84.5	5.1	92.2	5.7	48.9	5.5	59.1	6.2	55.6	6.1	63.6	5.5	177	4.7	151	4.8
Br	67.1	4.0	141	3.0	60.2	4.0	65.4	4.0	69.1	4.0	87.6	4.0	85.6	3.0	80.3	4.0	110	4.0
Rb	497	5.5	186	5.4	66.9	7.6	22.9	8.8	44.4	8.6	221	5.3	61.2	6.6	150	5.1	146	5.6
Zr	b.d.		341	41	b.d.		b.d.		b.d.		b.d.		40.9	57	155	30	b.d.	
Sb	0.28	29	0.15	45	0.10	43	0.15	43	0.12	50	0.11	41	b.d.		0.80	14	0.15	28
Cs	21.7	3.7	4.84	3.9	0.93	8.3	0.09	36	0.27	20	5.24	4.1	0.39	11	1.93	4.8	1.46	6.5
Ba	b.d.		b.d.		b.d.		98	lim	b.d.		b.d.		b.d.		b.d.		b.d.	
La	31.9	3.9	11.9	5.0	1.29	10	11.8	4.5	4.18	8.7	1.49	10	8.99	5.4	37.3	3.1	5.00	3.4
Ce	58.4	3.1	22.5	3.1	16.2	4.3	27.8	3.1	9.33	5.5	3.57	13	16.7	4.1	59.1	2.9	7.83	7.2
Nd	25.9	54	11.9	47	7.5	78	18.1	42	8.45	74	7.43	59	5.13	72	12.7	45	b.d.	
Sm	3.15	2.8	1.12	3.3	0.17	6.5	1.40	3.4	0.58	4.5	0.21	6.5	1.00	3.5	2.50	2.8	0.25	4.8
Eu	0.30	8.9	0.18	9.8	0.16	12	0.22	8.4	0.16	17	0.13	17	0.18	14	0.28	8.0	0.09	17
Tb	0.42	12	0.49	9.4	0.25	15	0.21	13.1	0.10	26	0.14	42	0.12	20	0.89	7.9	0.35	18
Yb	0.29	lim	0.32	7.1	b.d.		0.29	lim	0.37	36	b.d.		0.29	47	2.03	12	0.22	40
Lu	0.06	39	b.d.		0.07	lim	0.04	lim	0.06	52	b.d.		0.04	59	0.27	21	0.09	24
Hf	0.21	24	0.63	8.6	0.47	12	2.54	6.1	1.30	8.4	0.14	28	0.85	8.1	6.42	6.1	0.23	15
Ta	0.25	19	0.25	16	1.0	10	1.21	7.4	0.42	13	0.19	28	0.44	11	1.38	7.8	0.14	24
Th	6.36	3.0	12.1	2.7	5.2	3.2	1.35	3.5	1.45	3.9	0.79	6.8	1.48	4.2	24.6	2.7	7.23	2.8
U	0.66	53	2.17	29	0.54	48	0.75	51	b.d.		0.53	43	0.54	45	3.40	18	0.81	22

Tab. 2 continued

	llm260	± [%]	VI-196	± [%]	llm225	± [%]	I-160	± [%]	I-172	± [%]	II-148	± [%]	II-172	± [%]	II-196	± [%]
Sc	0.09	4.7	0.35	3.2	0.10	4.5	0.06	6.0	0.32	3.0	0.07	6.2	2.11	2.6	0.07	5.6
Cr	4.60	10	5.13	15	4.17	11	5.45	9.2	4.16	11	4.81	15	7.82	11	4.86	10
Co	0.10	35	0.16	27	0.08	38	0.10	27	0.22	20	0.17	24	0.07	77	0.10	29
Zn	218	4.6	203	4.7	55.6	5.4	86.4	5.6	37.6	6.9	166	4.6	94.7	5.7	87.5	4.8
Br	100	4.0	134	3.0	40.6	5.0	40.1	5.0	47.3	4.0	67.5	4.0	95.2	4.0	54.7	4.0
Rb	50.4	6.8	140	5.8	424	4.8	8.76	19	20.1	11	21.5	13	31	14	33.8	8.9
Zr	b.d.		b.d.		b.d.		b.d.		124	27	b.d.		3588	50	b.d.	
Sb	0.20	37	0.34	27.1	0.21	34	0.17	43	0.15	10	0.23	24	0.29	31	0.12	43
Cs	0.55	8.7	5.02	4.0	0.98	6.5	0.70	9.4	1.43	5.3	5.46	3.9	1.21	9.4	3.34	4.0
Ba	b.d.		120		b.d.		b.d.		b.d.		b.d.		152	32	b.d.	
La	25.8	3.5	17.6	4.0	15.7	3.7	127	3.3	52.6	3.2	2.44	9.6	179	2.9	6.77	4.8
Ce	50.4	2.9	40.3	3.2	23.4	3.5	211	2.8	108	2.8	4.73	7.4	371	2.7	10.7	4.5
Nd	29.7	36	24.8	43	7.50	49	67.5	41	51.5	41	b.d.		159	45	7.63	88
Sm	3.15	2.7	2.47	2.9	1.15	3.1	3.47	2.8	6.63	2.6	0.15	14	21.9	2.6	1.03	2.3
Eu	0.42	6.9	0.31	8.4	0.21	9.0	0.30	8.1	0.75	5.8	0.10	18	2.53	4.7	0.14	11
Tb	0.61	8.8	0.59	9.8	0.35	11	0.26	14	0.64	9.5	0.05	56	2.79	7.0	0.12	19
Yb	0.34	7.1	0.36	lim	1.06	16	0.32	7.7	1.96	14	0.09	73	21.1	9.9	0.25	57
Lu	0.13	34	0.13	39	0.14	27	0.05	11	0.24	21	0.03	9.2	2.55	11	0.07	46
Hf	1.30	6.8	0.86	8.4	2.40	6.5	0.36	12	4.85	6.6	0.11	43	74.1	6.0	0.76	9.4
Ta	0.61	10	3.19	6.8	0.61	10	0.27	24	2.86	8.2	0.08	44	17.9	6.2	0.22	23
Th	9.28	2.7	12.8	2.7	8.10	2.8	5.56	3.0	2.10	3.3	0.90	5.3	7.20	3.1	1.78	3.5
U	1.48	27	2.47	22	1.76	22	1.51	36	4.95	34	b.d.		10.5	20	0.90	33

b.d. = below detection limit;
lim = very large error because of element content close to detection limit

perature of pure H_2O (374.1 °C) in synthetic fluid inclusion standards. The reproducibility of melting temperatures is 0.1-0.2 °C, of homogenisation temperatures around 2-3 °C. Apparent salinities in the aqueous inclusions are expressed as weight percent (wt.-%) NaCl equivalent, calculated using data from Bodnar (1993) based on the final ice melting temperature for two-phase inclusions

Fig. 5
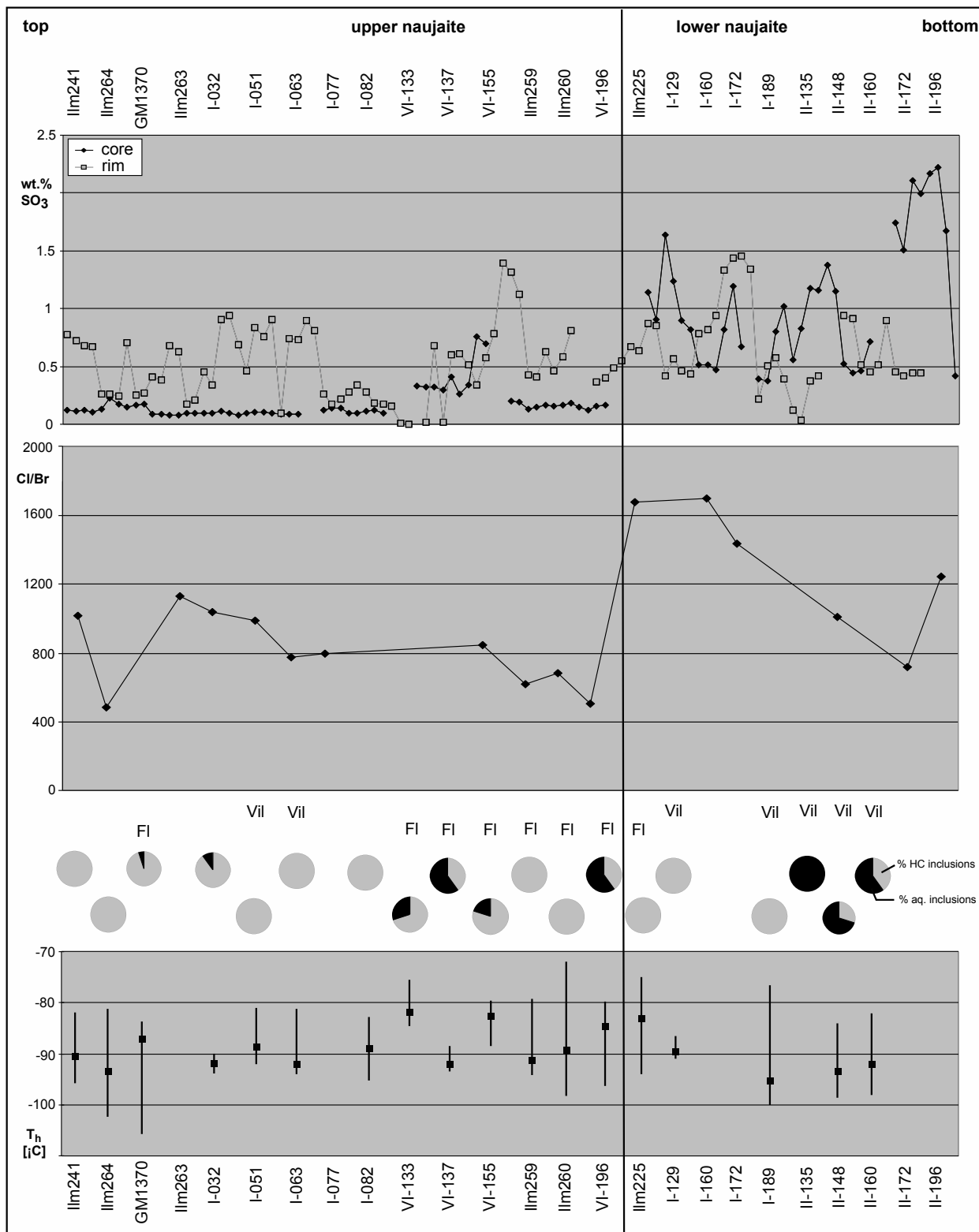Stratigraphic arrangement of S analyses in sodalite cores and rims, Cl/Br ratios, the fluoride mineral found in the samples, the fluid inclusion inventory of the samples and the homogenisation temperatures of the primary hydrocarbon-bearing inclusions. Note that the fluid inclusion data and the type of fluoride mineral is not correlated to the systematics in the sodalite mineral chemistry.

Raman Spectroscopy

The composition of the fluid inclusions was determined qualitatively by a confocal laser Raman microprobe Dilor LABRAM 2 equipped with a Peltier cooled CCD detector at the Universität Tübingen. We used an Argon laser with a wavelength of 514.5 nm. The system was calibrated against silicon and diamond standards. Since sodalite has a strong fluorescence, only qualitative analyses were possible. Especially wavenumbers above 3500 cm^{-1} are totally obscured by this fluorescence.
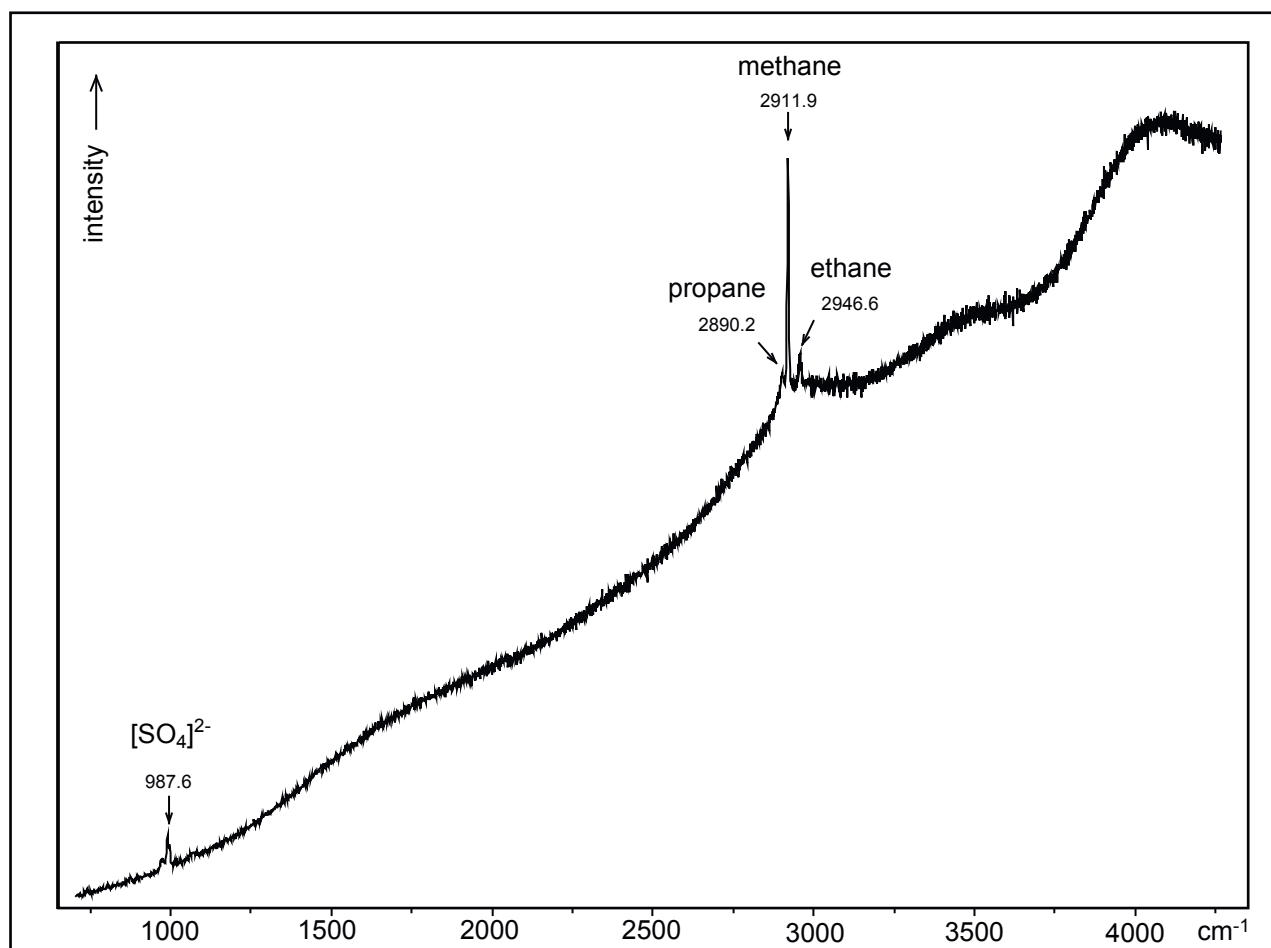
Fig. 6
Raman spectrum of HC-bearing inclusions from the inclusion trail in Fig. 4d showing the wavenumbers typical of methane, ethane and propane and the sulphate frequency of the host sodalite. The strong increase of the background with increasing wavenumbers is due to the strong fluorescence of sodalite.

Sodalite mineral chemistry

Selected microprobe analyses of sodalite from various stratigraphic levels are presented in Tab. 1. The sample spots and profiles were selected according to the CL-zonations to investigate the relation between major and minor element compositions and these zonations. In general, the sodalites from the naujaite contain only very minor amounts of Ca and K. From the top of the naujaite downwards, the SO_3 content in the sodalite cores with relatively dark CL colours remains stable at ~0.15 wt.% for approximately two thirds of the sequence.

Then, it increases strongly with depth to values above 2 wt.% (Fig. 5). Cl in the cores shows an inverse behaviour. The brighter luminescing rims exhibit a wide scatter in SO3 along the entire profile. Based on the data summarised by Ostroumov et al. (2002), which show that the wavenumber of 990 cm^{-1} is indicative for the sulphate ion (see Tab. 1 therein), our Raman measurements show clearly that the sulphur species in the sodalites is $[SO4]^{2-}$ (Fig. 6). This frequency appears in all our Raman spectra, while frequencies indicative for other sulphur species are absent.

Bromine exhibits a stratigraphic behaviour similar to that of sulphur. It increases from the up-permost naujaites downwards, from 60 ppm to ~140 ppm, then dropping to values below the initial and increasing again. Cl/Br values range from 500 to 1700 (Fig. 5). The upper naujaite exhibits homogeneous and slightly decreasing Cl/Br ratios whereas the lower naujaite starts with high Cl/Br values that decrease downwards.

Most of the sodalites show zonations in their Fe content; the rims have higher contents than the cores (Fig. 7). Some crystals show a more complex zonation with a maximum in the core, then a decrease outwards and a final increase at the rim. Bailey (in press) found that soda-lite from the early naujaite (refers to our upper naujaite) contains more B, Br, S and Be than sodalite from the later naujaite (our lower). Two different Zr-U regression lines reported in Fig. 6 in Bailey et al. (2001) support this separation of the naujaite into two types.
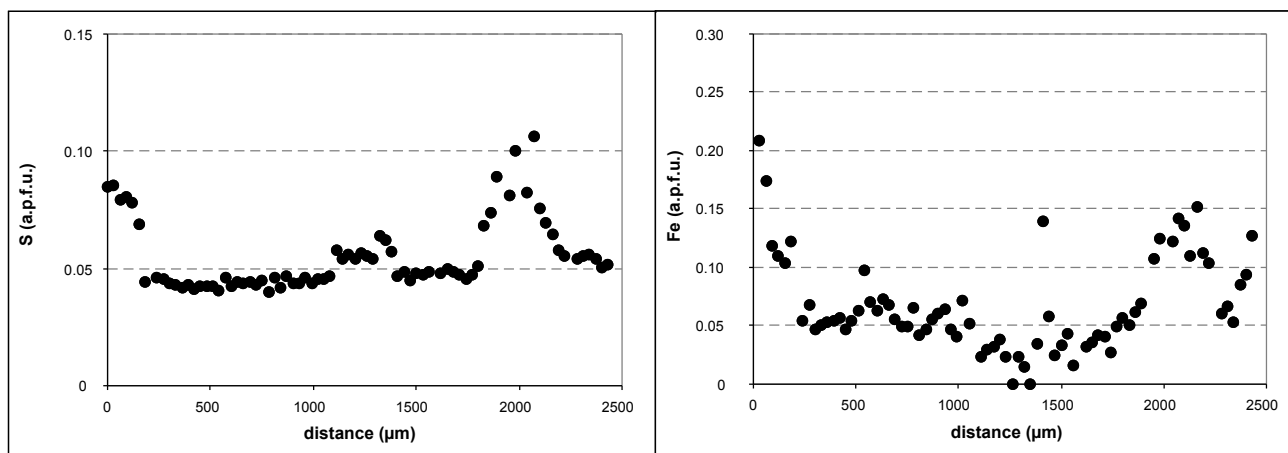
Fig. 7
Diagrams showing zonation of sodalite (from sample I-032) in S and Fe content. Both elements exhibit a similar behaviour with more homogeneous values in the core and increasing values towards the outer rim.

Trace elements were determined using Neutron Activation Analysis (NAA) of hand-picked so-dalite concentrates. In general, the mantle-normalised trace element patterns exhibit strong depletion of elements like Sc, Cr and Co (Fig. 8). HFS elements are weakly and LIL elements are strongly enriched. Because of the aegirine needles enclosed in most sodalites, the resul-ting values are mixtures of sodalite and aegirine. In order to evaluate this problem, we com

pared the analyses to those from later formed large aegirine crystals occurring interstitially in the naujaite (see analyses in Marks et al., 2004a). Trace elements hosted by the sodalite are Rb, Cs and Ba in concentrations up to 500, 22 and 150 ppm, respectively. No stratigraphic trends for these elements are observed. Although some REE are missing in our analyses, it is clear that aegirine is responsible for the measured contents of the REE. The normalised REE patterns are very similar to those from the large arfvedsonite and aegirine crystals enclosing the sodalites (Marks et al., 2004a). Other elements that reflect the influence of the aegirine needles are Zr, Hf, Fe, Sc and Zn.
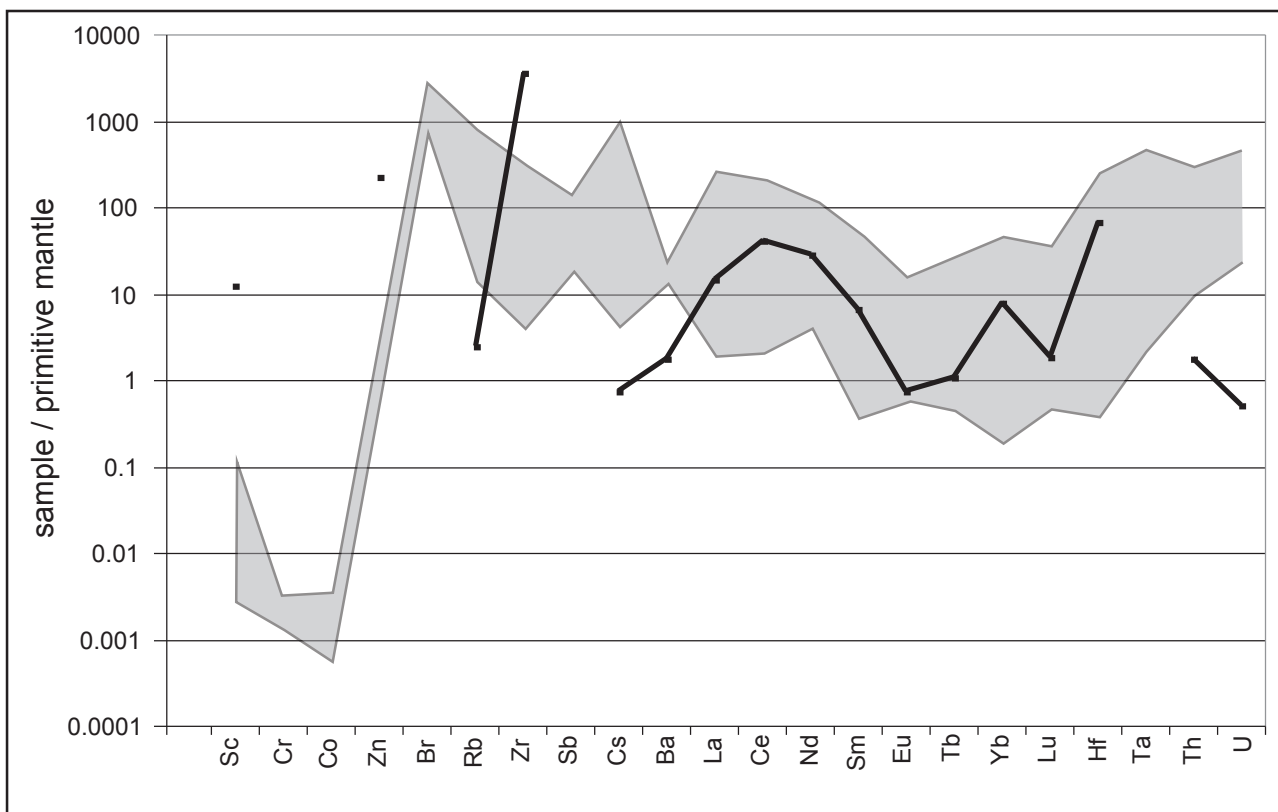
Fig. 8
Trace element pattern of sodalite (shaded area) compared with large interstitial aegirine from the naujaite (black line and dots, data from Marks et al., 2004a). The high variability of most elements is due to different amounts of aegirine needles enclosed in the sodalites. See text for further discussion.

Fluid inclusions in sodalite

The gas content and the composition of the gas trapped in fluid inclusions were summarised by Potter & Konnerup-Madsen (2003). The naujaite contains by far the highest gas contents of the Ilímaussaq rocks (~ 60 cm^3/kg). The gas consists mainly of methane, but other components such as ethane, propane and higher hydrocarbons as well as minor amounts of hydrogen and nitrogen were also found. CO and CO_2 are only present in traces. Konnerup-Madsen et al. (1979) reported very similar bulk values for sodalite from the naujaite, which proves that sodalite is the host of most of the gases.

Primary hydrocarbon-bearing inclusions homogenise at temperatures between –106 °C and –85 °C into the liquid phase. Based on Raman analyses, they contain only methane. Hydrocarbon-bearing inclusions in trails are a mixture of different HC species with methane being the dominant one. Their homogenisation temperatures are higher and exhibit a wide scatter between –80 °C and –10 °C due to variable proportions of higher hydrocarbons. The composition of the secondary HC-bearing inclusions changes with the stratigraphic position of the samples. In the upper parts, the proportion of higher hydrocarbons like ethane and propane is higher. In the lower parts, the fluid is almost pure CH_4. Due to the strong fluorescence of sodalite during Raman analyses, it was not possible to quantify these observations. However, based on Fig. 7A in Konnerup-Madsen et al. (1979), the homogenisation temperatures can be used for an estimation of the HC composition. For the highest measured temperature indicating the highest content of higher hydocarbons, a methane content of 50 to 60 % is derived. This is in fairly good agreement with the values summarised by Potter & Konnerup-Madsen (2003) given the fact that we compare a single inclusion with sodalite bulk values. Fluid inclusions in the sodalites filled with a two-phase aqueous solution are exclusively of secondary origin. Ice melting temperatures are around –20 °C, which corresponds to a salinity of ~22 wt.% NaCl-equiv. The inclusions homogenise over a broad range of temperatures between 50 and 250 °C into the liquid phase.

Discussion

Evolution of the fluid phase

According to the work of Sharp et al. (1989), sodalite crystallisation starts at high temperatures between 800 and 1000 °C, provided the activity of NaCl in the melt is sufficiently high. For the onset of sodalite crystallisation in a naujaite sample from Ilímaussaq, Piotrowsi & Edgar (1970) experimentally determined temperatures of 1190 °C at 1 bar and 900 °C at 1 kbar water pressure, respectively. In their experiments, sodalite is the first phase on the liquidus. The water activity in the melt during sodalite crystallisation was low (Markl et al., 2001a) and fluid inclusions indicate that no aqueous fluid was present during the main period of sodalite formation. If an aqueous fluid phase were expelled from the melt at this stage, NaCl would strongly partition into it (Kilinc & Burnham, 1972) and, hence, become unavailable for sodalite crystallisation. The formation of sodalites from a water-deficient melt is also supported by our fluid inclusion data, which do not show high-temperature aqueous inclusions. Therefore, the primary HC inclusions are interpreted to have formed at a temperature between 800 and 1000 °C.

Several experiments performed at high temperatures and pressures showed that CH_4 fluids

are typical for melts with low oxygen fugacities (e.g. Holloway & Jakobsson, 1986; Scott et al, 2004). Methane and higher hydrocarbons will form spontaneously at mantle P-T-conditions and oxygen fugacities close to the magnetite-wüstite buffer. During ascent to pressures below ~25 kbar, hydrocarbons other than methane become unstable relative to methane (Kenney et al., 2002). Consequently, the primary HC-bearing inclusions in the sodalites contain only methane.
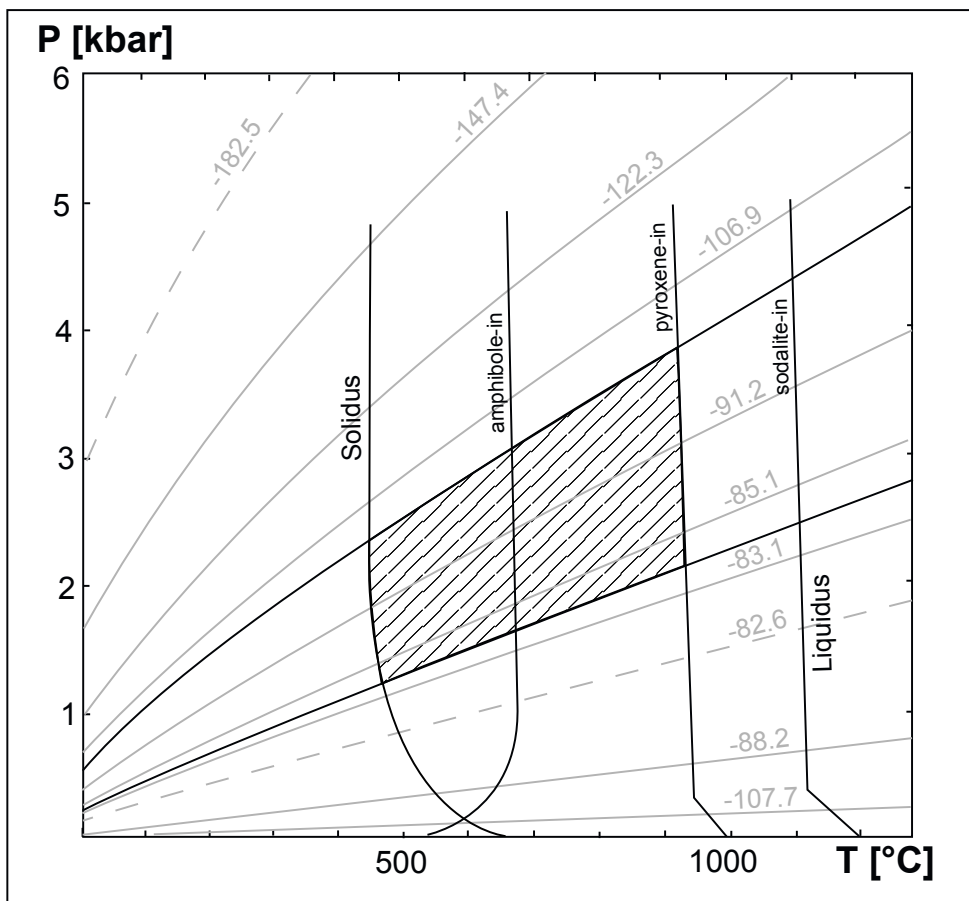
Fig. 9
P-T-diagram with isotherms of homogenisation temperatures of pure methane inclusions (from van den Kerkhof, 1988) and experimentally determined phase relations of the naujaite (from Konnerup-Madsen & Rose-Hansen, 1982). The hatched box expresses the field of formation of the primary hydrocarbon-bearing fluid inclusions in P-T-space.

Some HC-bearing inclusions containing only methane reflect trapping pressures of 3-4 kbar (Fig. 9). This is much deeper than the emplacement level of the intrusion at about 1 kbar. HC-bearing inclusions showing this feature are located exclusively in sodalite parts with aegirine needles. Hence, the aegirine-bearing parts of the sodalites crystallised at considerably higher P-T conditions than the aegirine-free parts, presumably in a deeper magma chamber or during the ascent of the magma, whereas the rims formed during or after the final emplacement. The position of the ν_1 vibration of methane in our Raman spectra also argues for entrapment at higher pressures. At atmospheric pressure, this vibration is located at 2917 cm^{-1}; higher pressures shift the frequency to lower values (Burke, 2001 and references therein). We observed values as low as 2908 cm^{-1} indicating pressures of 3 to 4 kbar, which is in excellent

agreement with the entrapment pressure derived from the homogenisation temperatures. The enormous amount of sodalite present in the naujaite argues for crystallisation from a magma chamber much thicker than today's exposed vertical thickness of the intrusion, i.e. 1700 m (Sørensen, 2001; Sørensen et al, in press). Our data provide evidence for sodalite crystallisation in a deep magma chamber and in an ascending magma.

In general, the solubilities of fluid phases such as H_2O, CO and CO_2 in melts are significantly lower at low fO_2 than under more oxidising conditions (Kadik et al., 2004). Methane in its molecular form is almost insoluble in melts. The equilibration of a CH_4 fluid with a silicate melt is associated with the formation of OH^- and to a lesser extent H_2O. Carbon is present as amorphous or atomic C, but may form Si-C bonds in the melt, which effectively depolymerise the silicate network (Taylor & Green, 1987; Kadik et al., 2004). Water is much more soluble in melts than hydrocarbons. The water activity in the first melt batch was very low (i.e. <0.2) but increased with further fractionation to values between 0.4 and 0.8 in the earlier rocks of the agpaitic magma batch, i.e. pulaskite, foyaite, sodalite foyaite and naujaite (Markl et al., 2001a). During sodalite crystallisation, CH_4 was the dominant fluid phase whereas water remained dissolved in the melt. The water activity increased during fractionation of sodalite and reached the point where an aqueous fluid was expelled from the melt. This aqueous fluid and the still existing hydrocarbon fluid were trapped contemporaneously in the sodalites. Separate inclusion trails lead to the conclusion of their immisciblity. The exsolution of the aqueous fluid may have terminated the formation of sodalite because Cl would strongly partition into such a fluid. Indeed, the salinities of the aqueous inclusions in the Ilímaussaq rocks are moderate to high (up to 60 wt.% NaCl equivalent, Konnerup-Madsen, 2003). Unfortunately, we have no information about the amount of fluid exsolved and we have, therefore, no direct evidence whether the fluid mass was sufficient to remove enough Cl from the melt to stop sodalite crystallization, but we believe our hypothesis to be a geologically realistic one.

The formation of the aqueous fluid inclusions may have been also related to the lujavrite formation, because the amount of aqueous inclusions increases with decreasing distance to lujavrite (Fig. 5, see the samples from drill core II and VI). This model is not in contradiction to the findings of Marks et al. (2004b), who explained the very low δD values of amphiboles by the equilibration with a hydrous fluid that was generated by oxidation of a primary hydrocarbon-bearing fluid, because this equilibration happened at temperatures as low as 350 °C.

The generation of the trapped hydrocarbons by late- to post-magmatic Fischer-Tropsch (FT) type reactions is unlikely for several reasons (see also Beeskow et al., in press). Some of the inclusions are unequivocally identified to be of primary origin based on their textures (Fig. 4c), and they record entrapment pressures higher than the pressure corresponding to the final

emplacement level. This means that these inclusions were enclosed well above temperatures and pressures favourable for a FT type reaction (Anderson, 1984). Although sulphur is known to poison the catalysts that are needed for the FT reaction (Madon & Taylor, 1981), we found abundant HC-bearing inclusions in those sodalites from the lower part of the stratigraphy that contain elevated amounts of S. Furthermore, we did not detect any CO_2 in the inclusions in sodalite, which would be a prerequisite for an FT-type reaction. Bulk analyses show that this species is only present as tiny traces (see Potter & Konnerup-Madsen, 2003).

Ryabchikov & Kogarko (in press) calculated the stable C-H-O fluid phase in agpaitic rocks at fO_2-conditions applicable to Ilímaussaq ($\Delta FMQ= -3$). Their results show that methane is in addition to H_2O the most dominant gas species over a broad range of temperatures in the system C-H-O. Furthermore, their calculated gas composition is in perfect agreement with the sodalite bulk analyses (Potter & Konnerup-Madsen, 2003).

The arguments presented above render the generation of the hydrocarbons by a FT-type reaction unlikely. Konnerup-Madsen (2001) calculated a δ13C value of –4.5 ± 1.5 ‰ PDB for bulk hydrocarbon gases from the Ilímaussaq rocks; this is in excellent agreement with mantle values (Kyser, 1986). The higher hydrocarbons we found in secondary inclusions may have been formed by polymerisation of primary methane. This would also explain the occurrence of H_2 in sodalite bulk analyses (Konnerup-Madsen et al. 1979). According to Des Marais et al. (1981), higher hydrocarbons generated in this way have lower δ13C values than the methane, which has been demonstrated for the higher hydrocarbons in Ilímaussaq (Konnerup-Madsen, 2001).

Sodalite mineral chemistry and melt evolution

The stratigraphic variations of the sulphur content of the sodalite cores are interpreted to reflect Cl depletion during fractionation of sodalite. Different Cl/S ratios in sodalite are hence interpreted to directly reflect different Cl/S ratios in the melt. The brightly luminescing rims reflect local variations in the Cl/S ratios in the residual melt pockets between the sodalite grains floating and solidifying at the roof of the magma chamber. As long as there is enough Cl available in the melt, the incorporation of sulphur in sodalite is minor. When the Cl content decreases with further fractionation, sulphur becomes an important substituent.

Although sphalerite is a common mineral in the naujaites, the Raman measurements indicate the sulphur to be present as $[SO4]^{2-}$ in the sodalites. Incorporation of more reduced sulphur species is known only from Ca-bearing members of the sodalite group, i.e. haüyne and lazurite (Ostrumov et al., 2002; Di Muro et al., 2004). Obviously, the incorporation of sulphur in sodalite as S^{2-} or S^{3-} is related to the Ca component. Despite the low oxygen fugacity in the

agpaitic melt batch (Markl et al., 2001a; Marks & Markl, 2001), S is present as sulphate since sodalite from the naujaite is almost Ca-free. Additionally, the high alkali contents in the melt stabilise the coexistence of sulphate with sulphide at relatively low oxygen fugacities around the FMQ buffer (Baker & Rutherford, 1996). This effect is caused by the formation of Na_2SO_4 groups in the melt even at more reduced conditions (Tsujimura et al., 2004), although the underlying mechanism of this observation are still unclear. Since the initial fO_2 of the agpaitic magma is too low for this sulphate-stabilising effect of the high alkali content in the melt (i.e. ΔFMQ ~ -3), the sulphur content in the sodalite cores from the upper naujaite is relatively low. In contrast, sodalite cores from the lower naujaite and the later formed sodalite rims with bright CL colours contains much more sulphur and hence is interpreted to have formed at higher fO_2 conditions. This increase in fO_2 with fractionation of the agpaitic magma was also documented by Markl et al. (2001a).

Bailey et al. (2001) and Bailey (in press) introduced the idea of a two-stage formation history of the naujaite. Our data support this idea. The sulphur content and the bromine content of the sodalites exhibit changes in the lower part of the naujaite sequence. Bailey (in press) explained the geochemical differences in the naujaites by a layered magma chamber with an extended thickness of several kilometres. Our results are in agreement with this interpretation, but indicate formation of the two types of naujaite from slightly different melt compositions at depth, because the differences in the sodalite core composition are not related to different fluid inclusion populations. We found primary fluid inclusions recording a higher entrapment pressure in both naujaite parts but the composition of sodalites from the two parts is slightly different. It is not unreasonable to assume slightly different melt compositions in a slowly crystallising magma chamber of such a thickness.

Fluorine is enriched in the agpaitic melt during prolonged fractionation and reached its maximum in the kakortokite stage. In the lujavrites, the F content is still high but somewhat lower than in the kakortokites. Due to the low Ca contents and the abundance of Na in the melt, villiaumite (NaF) appears in some parts of the naujaite. Nonetheless, fluorite was found in other parts of the sequence (Fig. 5). Both minerals were not observed together in the same sample. The occurence of fluorite despite the very low Ca contents in the naujaitic melt records the extreme F enrichment in the late melt stages. The variations in Na^+/Ca^{2+} activity (Fig. 10) may be related to the influx of Ca-bearing fluids (Graser et al., in prep.) or to local phenomena dependent on variable crystallisation conditions. In contrast to Cl, Br and I, which are exhausted by the extensive formation of sodalite, the F content of the melt remains high or increases. This process finally leads to the formation of a late-stage villiaumite-rich lujavrite and abundant fluorite in some late-stage veins and hydrothermal alteration zones. Hence, the

naujaite stage fractionates Cl, Br and I from F.

It is interesting to note, that the bottom cumulates (kakortokites), which crystallised after the solidification of the naujaite, contain high amounts of F (up to 2.1 wt.%; Bailey et al., 2001) mainly present as fluorite. Additionally, the contents of Ca and Mg in amphiboles and pyroxenes are significantly higher (Marks et al. 2004a) suggesting the kakortokite formation from a more primitive, replenished melt. Mixing of these two melts, the F-rich residual melt of the roof series (including the naujaite) and the later batch with higher Ca-contents (the kakortokite magma) would lead to the precipitation of abundant fluorite. This mixing probably took place at depth because there is a time gap between both stages. This idea is in agreement with the results of Sørensen et al. (in press) that the roof cumulates and the kakortokite-lujavrite series represent two different melt batches.
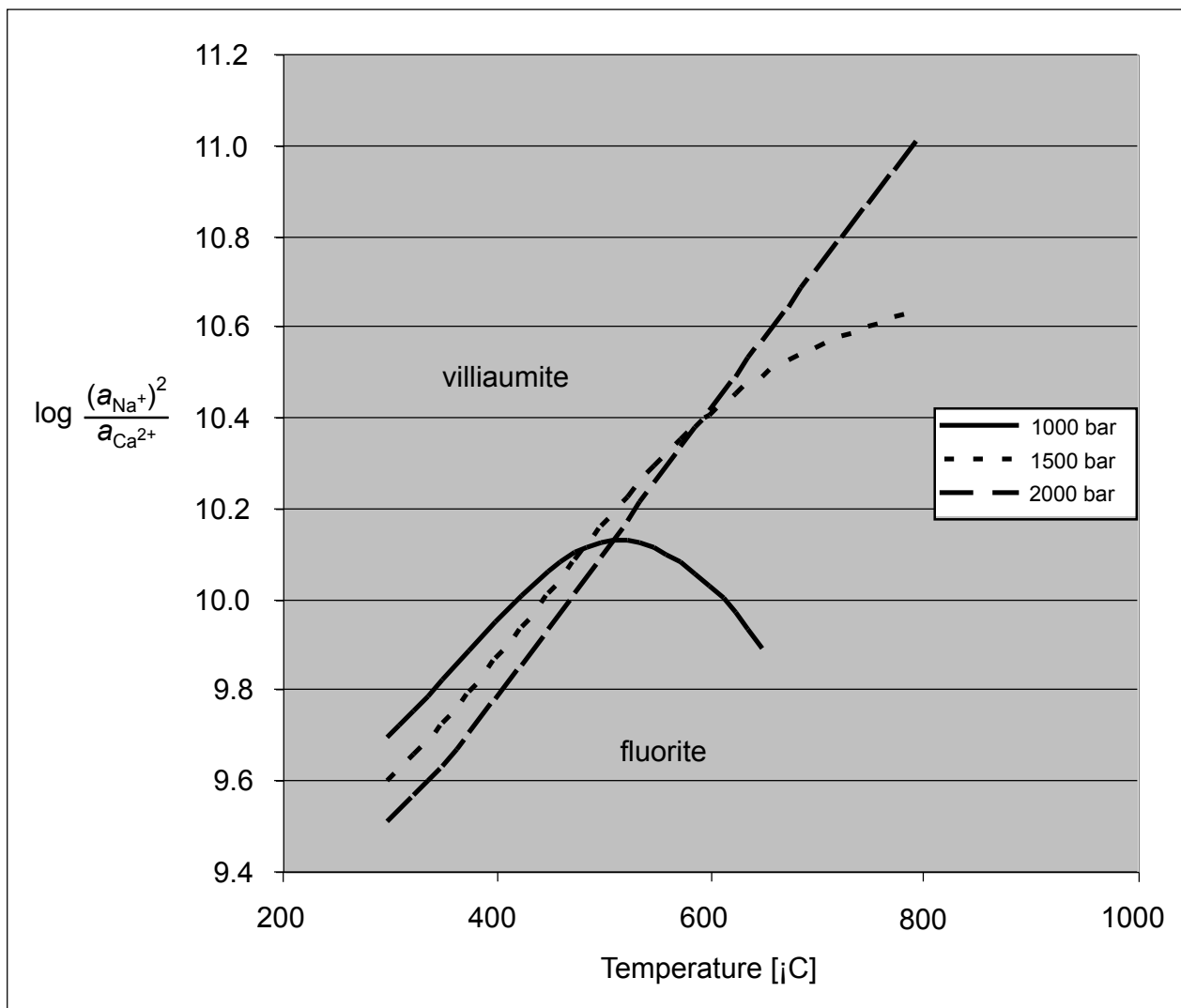
Fig. 10
Diagram of $\log((a\text{Na}^+)2 / a(\text{Ca}^{2+}))$ versus temperature at various pressures for the reaction $2\,\text{NaF} + \text{Ca}^{2+} \rightarrow \text{CaF}_2 + 2\,\text{Na}^+$ calculated with the HCh software (Shvarov & Bastrakov, 1999) and the UNITHERM database. Thermodynamic data of fluorite and villiaumite are from Robie & Hemingway (1995) and that of Ca^{2+} and Na^+ from Shock et al. (1997).

Summary

The naujaite, a sodalite flotation cumulate from the agpaitic Ilímaussaq complex, offers a unique possibility to understand the evolution of the volatile phase during the crystallisation of a large peralkaline magma chamber. The sodalite composition and the fluid inclusion population yield information on the halogen budget of the melt and the composition of the coexisting fluid phase. Two types of fluid inclusions can be found in the sodalite crystals from the naujaite, secondary aqueous inclusions and hydrocarbon-bearing inclusions of both primary and secondary origin. For their entrapment, we prefer a two-stage model in the development of the fluid phase due to the contrasting solubilities of water and hydrocarbons in the melt. From the beginning of sodalite crystallisation, a hydrocarbon fluid clearly was in equilibrium with the melt. The initial water activity was very low but increased with further fractionation. At this stage, sodalite began to crystallise at depths of 10-12 km trapping tiny aegirine needles and the primary hydrocarbon fluid. The NaCl activity in the melt decreased with further fractionation of sodalite from 0.4 to values well below 0.1 (Markl et al., 2001a), while the water activity increased and finally reached the point where an aqueous fluid was expelled from the melt. Since NaCl strongly partitions into the aqueous fluid, the copious formation of sodalite ended with the exsolution of this fluid. Therefore, the aqueous fluid was trapped only as secondary inclusions in sodalite. According to Konnerup-Madsen (2001), the two coexisting fluids are immiscible, and we confirm that in most cases they appear as separate fluid inclusions in the sodalites. Due to the exhaustion of Cl in the melt by the sodalite crystallisation itself and possibly by the exsolution of a NaCl-rich aqueous fluid, sodalite occurs only in smaller quantities in the later formed kakortokites and lujavrites. The high-salinity aqueous fluid trapped in secondary trails in the sodalites seems to be related to the lujavrite because the amount of aqueous inclusions decreases with increasing distance of the sample from the lujavrite. We are therefore convinced that hydrocarbons were the stable fluid phase during crystallisation of all Ilímaussaq rocks, while water-rich fluids may have occurred additionally in the lujavrite and later hydrothermal and pegmatitic stage only.

The sodalite composition reflects the changes in the melt composition during ascent and sodalite fractionation. Except for fluorine, the halogens are effectively scavenged from the melt by the crystallising sodalite. The remaining melt enriched in F was mixed with a following magma batch containing higher amounts of Ca, which resulted in the precipitation of fluorite and the exhaustion of Ca. Later on, the F content of the melt built up again leading to the formation of villiaumite in the latest-formed lujavrites.

Acknowledgements

References

Anderson, R.B., 1984. The Fischer-Tropsch synthesis. Academic Press, New York, USA.

Armstrong, J.T., 1991. Quantitative elemental analysis of individual microparticles with electron beam instruments. In: Heinrich, K.F.J. and Newbury, D.E. (eds.), Electron Probe Quantitation. New York & London, Plenum Press. 261-315.

Bailey, J.C. Geochemistry of elemental boron in the Ilímaussaq alkaline complex, South Greenland. Lithos, in press.

Bailey, J.C., Gwozdz, R., Rose-Hansen, J. & Sørensen, H., 2001. Geochemical overview of the Ilímaussaq complex, South Greenland. In: Sørensen, H. (Ed.), The Ilímaussaq alkaline complex, South Greenland: status of mineralogical research with new results. Geol. Greenl. Surv. Bull. 190, 35-54.

Baker, L.L. & Rutherford, M.L., 1996. Sulfur diffusion in rhyolite melts. Contrib. Min. Petrol. 123, 335–344.

Beeskow, B., Treloar, P.J., Rankin, A.H., Vennemann, T. & Spangenberg, J., A reassessment of models for hydrocarbon generation in the Khibina Mountains, NW Russia. Lithos in press.

Blaxland, A. B., van Breemen, O. & Steenfelt, A., 1976. Age and origin of agpaitic magmatism at Ilimaussaq, south Greenland: Rb-Sr study. Lithos 9, 31-38.

Bodnar, R.J., 1993. Revised equation and table for determining the freezing point depression of $H2O$-NaCl solutions. Geochim. Cosmochim. Acta 57, 683-684.

Burke, E.A.J., 2001. Raman microspectroscopy of fluid inclusions. Lithos 55, 139-158.

Carroll, M.R., 2005. Chlorine solubility in evolved alkaline magmas. An. Geophys. 48, 619-631.

Carroll M.R. & Webster, J.D., 1994 Solubilities of Sulfur, Noble Gases, Nitrogen, Chlorine, and Fluorine in Magmas. In: Carroll, M.R. and Holloway, J.R. (Eds), Volatiles in magmas. Rev. Mineral. 30, 231-279.

Des Marais, D.J., Donchin, J.H., Nehring, N.L. & Truesdell, A.H., 1981. Molecular carbon isotopic evidence for the origin of geothermal hydrocarbons. Nature 292, 826-828.

Di Muro, A., Bonaccorsi, E. & Principe, C., 2004. Complex colour and chemical zonig of sodalite-group phases in a haüynophyre lava from Mt. Vulture, Italy. Min. Mag. 68, 591-614.

Ferguson, J., 1964. Geology of the Ilimaussaq alkaline intrusion, South Greenland. Bull. Grønl. Geol. Unders. 39, 82.

Graser, G. & Markl, G. Ilvaite - Epidote - Hydrogarnet „skarns" record late-magmatic fluid influx into the persodic Ilímaussaq intrusion, South Greenland. in prep.

Greenough, J.D., Lee, C.-Y. & Fryer, B.J., 1999. Evidence for volatile-influenced differentiation in a layered alkali basalt flow, Penghu Islands, Taiwan. Bull. Volcan. 60, 412-424

Holloway, J.R. & Jakobsson, S., 1986. Volatile solubilities in magmas: transport of volatiles from mantles to planet surface. J. Geophys. Res. 91 (B4), D505-D508.

Kadik, A., Pineau, F., Litvon, Y, Jendrzejewski, N., Martinez, I. & Javoy, M., 2004. Formation of carbon and hydrogen species in magmas at low oxygen fugacity. J. Petrol. 45, 1297-1310.

Kenney, J.F., Kutcherov, V.A., Bendeliani, N.A. & Alekseev, V.A., 2002. The evolution of multicomponent systems at high pressures: VI. The thermodynamic stability of the hydrogen-carbon system: The genesis of hydrocarbons and the origin of petroleum. PNAS 99, 10976-10981.

Kilinc, I.A. & Burnham, C.W., 1972. Partitioning of chloride between a silicate melt and coexisting aqueous phase from 2 to 8 kilobars. Econ. Geol. 67, 231-235

Konnerup-Madsen, J., 2001. A review of the composition and evolution of hydrocarbon gases during the solidification of the Ilímaussaq alkaline complex, South Greenland. In: Sørensen, H. (Ed.), The Ilímaussaq alkaline complex, South Greenland: status of mineralogical research with new results. Geol. Greenl. Surv. Bull. 190, 159-166.

Konnerup-Madsen, J., Larsen, E. & Rose-Hansen, J., 1979. Hydrocarbon-rich fluid inclusions in minerals from the alkaline Ilímaussaq intrusion, South Greenland. Bull. Mineral. 102, 642-653.

Konnerup-Madsen, J. & Rose-Hansen, J., 1982. Volatiles associated with alkaline igneous rift activity: fluid inclusions in the Ilimaussaq intrusion and the Gardar granitic complexes (south Greenland). Chem. Geol. 37, 79-93.

Kravchuk, I.F., Kotelnikov, A.R. & Senin, V.G., 2004. Partitioning of volatile (Cl, F, and S) and rare alkali (Rb and Cs) elements in the system aluminosilicate melt-fluid. Geochem. Internat. 42, 1071-1077.

Krumrei, T.V., Villa, I.M., Marks, M., & Markl, G. A 40Ar/39Ar and U/Pb isotopic study of the Ilímaussaq complex, South Greenland: implications for the 40K decay constant and for the duration of magmatic activity in a peralkaline complex. Chem. Geol., in press

Kuleff, I. & Pernicka, E., 2002. INAA of some geological standard reference materials. J. Radioanal. Nucl. Chem. 251, 139-143.

Kyser, T.K., 1986. Stable isotope variation in the mantle. In: Valley, J.W., Taylor, H.P. & O´Neil, J.R. (eds.): Stable isotopes in high temperature geological processes. Rev. Mineral. 16, 141-164.

Larsen, L. M., 1976. Clinopyroxenes and coexisting mafic minerals from the alkaline Ilimaussaq intrusion, south Greenland. J. Petrol. 17, 258-290.

Larsen, L. M., 1977. Aenigmatites from the Ilimaussaq intrusion, south Greenland: Chemistry and petrological implications. Lithos 10, 257-270.

Larsen, L. M., 1981. Chemistry of feldspars in the Ilímaussaq augite syenite with additional data on some other minerals. Rapp. Grønl. Geol. Unders. 103, 31-37.

Lowenstern, J.B., 1994. Dissolved volatile concentrations in an ore-forming magma. Geology 22, 893-896.

Madon, R.J. & Taylor, W.F., 1981. Fischer-Tropsch synthesis on precipitated Fe catalyst. J. Catal. 69, 32-43.

Markl, G., Marks, M, Schwinn, G. & Sommer, H., 2001a. Phase equilibrium constraints on intensive crystallization parameters of the Ilímaussaq Complex, South Greenland. J. Petrol. 42, 2231-   2258.

Markl, G., Marks, M. & Wirth, R., 2001b. The influence of T, aSiO2, fO2 on exsolution textures in Fe-Mg olivine: an example from augite syenite of the Ilímaussaq Intrusion, South Greenland. Am. Mineral. 86, 36-46.

Marks, M. & Markl, G., 2001. Fractionation and assimilation processes in the alkaline augite syenite unit of the Ilímaussaq Intrusion, South Greenland, as deduced from phase equilibria. J. Petrol. 42, 1947-1969.

Marks, M., Halama, R., Wenzel, T. & Markl, G., 2004a. Trace element variations in clinopyroxene and amphibole from alkaline to peralkaline syenites and granites: implications for mineral–melt trace-element partitioning. Chem Geol. 211, 185-215.

Marks, M., Vennemann, T., Siebel, W. & Markl, G., 2004b. Nd-, O-, and H-isotopic evidence for complex, closed-system fluid evolution of the peralkaline Ilímaussaq Intrusion, South Greenland. Geochim. Cosmochim. Acta 68, 3379-3395.

Marr, R.A., Baker, D.R. & Williams-Jones, A.E., 1998. Chemical controls on the solibility of Zr-bearing phases in simplified peralkaline melts and application to the Strange Lake intrusion, Quebec – Labrador. Can. Mineral. 36, 1001-1008.

Metrich, N. & Clocchiatti, R., 1996. Sulfur abundance and its speciation in oxidized alkaline melts. Geochim. Cosmochim. Acta 60, 4151-4160.

Moretti, R., Papale, P. & Ottonello, G., 2003. A model for the saturation of C-O-H-S fluids in silicate melts. Geol. Soc. Spec. Publ. 213, 81-101.

Nielsen, B.L. & Steenfelt, A., 1979. Intrusive events at Kvanefjeld in the Ilímaussaq igneous Complex. Bull. Geol. Soc. Denmark 27, 143-155.

Ostroumov, M., Fritsch, E., Faulques, E. & Chauvet, O., 2002. Étude spectrometrique de la lazurite du Pamir, Tajikistan. Can. Mineral. 40, 885-893.

Petersilie, I.A. & Sørensen, H., 1970. Hydrocarbon gases and bituminous substances in rocks from

the Ilímaussaq alkaline intrusion, South Greenland. Lithos 3, 59-76.

Piotrowsi, J.M. & Edgar, A.D., 1970. Melting relations of undersaturated alkaline rocks from South Greenland. Medd. Grønl. 181, 1-62.

Potter, J & Konnerup-Madsen, J., 2003. A review of the occurrence and origin of abiegenic hydrocarbons in igneous rocks. In: Petford, N. & McCaffrey, K.J.W. (Eds.). Hydrocarbons in crystalline rocks. Geol. Soc. London Spec. Pub. 214, 151-173.

Potter, J., Rankin, A.H. & Treloar, P.J., 2004. Abiogenic Fischer-Tropsch synthesis of hydrocarbons in alkaline igneous rocks; fluid inclusions, textural and isotopic evidence from the Lovozero complex, N.W. Russia. Lithos 75, 311-330.

Poulsen, V., 1964. The sandstones of the Precambrian Eriksfjord Formation in South Greenland. Rapp. Grønl. Geol. Unders. 2, 16.

Robie, R.A. & Hemingway, B.S., 1995. Thermodynamic properties of minerals and related substances at 298.15 K and 1 Bar (105 Pascals) pressure and at higher temperatures. US Geol. Surv. Bull. 2131, 461 pp.

Rose-Hansen, J. & Sørensen, H., 2002. Geology of the lujavrites from the Ilímaussaq alkaline complex, South Greenland, with information from seven bore holes. Med. Grønl. Geosci. 40, 58 pp

Rose-Hansen, J., Sørensen, H. & Watt, W.S., 2001. Inventory of the literature on the Ilímaussaq alkaline comlex, South Greenland. Dan. Grønl. Geol. Unders. Rapp. 2000/57, 38 pp. + CD-ROM.

Ryabchikov, I.D. & Kogarko, L.N. Magnetite compositions and oxygen fugacities of the Khibina magmatic system. Lithos, in press.

Salvi, S. & Williams-Jones, A.E. 1997. Fischer-Tropsch synthesis of hydrocarbons during sub-solidus alteration of the Strange Lake peralkaline granite, Quebec/Labrador, Canada. Geochim. Cosmochim. Acta 61, 83-99.

Salvi, S. & Williams-Jones, A.E. Alteration, HFSE mineralisation, and hydrocarbon formation in peralkaline igneous systems: Insights from the Strange Lake Pluton, Canada. Lithos in press.

Schmitt, A.L., Trumbull, R.B., Dulski, P. & Emmermann, R., 2000. Zr-Nb-REE mineralization in peralkaline granites from the Amis Complex, Brandberg (Namibia): Evidence for magmatic pre-enrichment from melt inclusions. Econ. Geol. 97, 399-413.

Scott, H.P., Hemley, R.J., Mao, H.K., Herschbach, D.R., Fried, L.E. Howard, W.M. & Bastea, S., 2004. Generation of methane in the Earth´s mantle: In situ high pressure-temperature measurements of carbonate reduction. PNAS 101, 14023-14026.

Sharp, Z.D., Helffrich, G.R., Bohlen, S.R. & Essene, E.J., 1989. The stability of sodalite in the system $NaAlSiO_4$-NaCl. Geochim. Cosmochim. Acta 53, 1943-1954.

Shock, E.L., Sassani, D.C., Willis, M. & Sverjensky, D.A., 1997. Inorganic species in geological fluids: Correlations among standard molal thermodynamic properties of aqueous ions and hydroxide complexes. Geochim Cosmochim Acta 61, 907-950.

Shvarov, Y.V. & Bastrakov, E., 1999. HCh: A software package for geochemical equilibrium modeling. User's guide. Australian Geological Survey Organisation, Department of Industry, Science and Resources.

Sørensen, H., 1966. On the magmatic evolution of tha alkaline igneous province of South Greenland. Rapp. Grønl. Geol. Unders. 7, 1-19.

Sørensen, H., 2001. Brief introduction to the geology of the Ilímaussaq alkaline complex, South Greenland, and its exploration history. In: Sørensen, H. (Ed.), The Ilímaussaq alkaline complex, South Greenland: status of mineralogical research with new results. Geol. Greenl. Surv. Bull. 190, 7-24.

Sørensen, H., Bohse, H. & Bailey, J.C. The origin and mode of emplacement of lujavrites in the Ilímaussaq alkaline complex, South Greenland. Lithos, in press.

Sørensen, H. & Larsen, L.M., 1987. The Ilimaussaq Intrusion; progressive crystallization and formation of layering in an agpaitic magma. In: Fitton, J.G. & Upton, B.G.J. (Eds.), Alkaline igneous rocks. Geol. Soc. Spec. Publ. 30, 473-488.

Stevenson, R., Upton, B.G.J. & Steenfelt, A., 1997. Crust-mantle interaction in the evolution of the Ilímaussaq Complex, South Greenland: Nd isotopic studies. Lithos 40, 189-202.

Taylor, W.R. & Green, D.H., 1987. The petrogenetic role of methane: Effect on liquidus phase relations and the solubility mechanism of reduced C-H volatiles. In: B.O. Mysen (Ed.), Magmatic Processes: Physicochemical Principles. Geochem. Soc. Spec. Publ. 1, 121-137.

Tsujimura, T., Xue, X., Kanzaki, M. & Walter, M.J., 2004. Sulfur speciation and network structural changes in sodium silicate glasses: Constraints from NMR and Raman spectroscopy. Geochim. cosmochim. acta 68, 5081 - 5101.

Upton, B.G.J., Emeleus, C.H., Heaman, L.M., Goodenough, K.M. & Finch, A.A., 2003. Magmatism of the mid-Proterozoic Gardar Province, South Greenland: chronology, petrogenesis and geological setting. Lithos 68, 43-65.

Ussing, N.V., 1912. Geology of the country around Julianehaab, Greenland. Medd. Grønl. 38, 426.

van den Kerkhof, A.M., 1988. Phase transitions and molar volumes of CO2 - CH4 - N2 inclusions. Bull. Mineral. 111, 257-266.

Webster, J.D. & De Vivo, B., 2002. Experimental and modeled solubilities of chlorine in aluminosilicate melts, consequences of magma evolution, and implications for exsolution of hydrous chloride melt at Mt. Somma-Vesuvius. Am. Mineral. 87, 1046-1061.

Evolution of a strongly layered peralkaline rock from the Ilímaussaq intrusion, South Greenland: implications for the origin of magmatic layering

Thomas V. Krumrei, Tina Rudolf and Gregor Markl

Eberhard Karls Universität Tübingen,

Institut für Geowissenschaften, Wilhelmstr. 56,

D-72074 Tübingen, Germany

Abstract

The Ilímaussaq intrusion, South Greenland, belongs to a suite of evolved intrusives in the mid-Proterozoic Gardar Province. It was formed in 4 stages, of which the last two produced the majority of the intrusion's volume. The rocks from these two melt batches are highly evolved agpaites with (Na+K)/Al ratios up to 1.8. Most of the rocks show magmatic layering to different extent, but the so-called kakortokite, a nepheline syenite consisting of arfvedsonitic amphibole, eudialyte, alkali feldspar and nepheline, show a spectacular recurrence of black, red and white layers, which is due to regular changes in the modal contents of the above-named minerals. These three-layer units recur 29 times.

The layering within a unit is a normal one with the densest mineral at the bottom and the lighter minerals following upwards. All four minerals crystallised contemporaneously and appear to be separated from each other only by their different densities. Since the viscosity and the density of the magma were low, only a very small proportion of crystals in the range of 0.1 to 0.3 % could remain suspended in the melt before gravity force them to settle down. Therefore, crystallisation from 600 m of magma is needed to produce enough crystals to build up the average unit thickness of 8 m. Between the formation of the units must have been a temporal hiatus, because there are sharp contacts between the units, whereas the transition within a unit between the differently coloured varieties is gradual. The recurrence of the unit is thought to be due to volatile pressure variations caused by eruptive activity that lead to oscillations of the liquidus temperature of the melt around its actual temperature. The volatile release stopped the crystallisation of the four cumulus minerals. After eruption, the system is closed again when the hydrostatic pressure exceeds the internal pressure in the magma chamber and the buoyancy of the light fluids. When the liquidus temperature is forces below the temperature of the melt by the increasing volatile pressure, contemporaneous crystallisation occurred until the next eruption.

Since the proportion of the crystals formed in each cycle is insignificant compared to the total magma volume, the bulk chemistry of the melt is hardly changed by crystallisation and separation of the crystals. Consequently, the minerals record only minor evolutional trends within the stratigraphy.

Introduction

Repetitive layering is a common feature in large mafic intrusions such as the Skaergaard intrusion, East Greenland (McBirney and Noyces, 1979; Maaløe, 1987; Naslund et al., 1991), the Stillwater Complex, Montana (Hess, 1960; Muerer and Boudreau, 1996) or the Great

Dyke, Zimbabwe (Wilson, 1996). Layering is, however, less common in more evolved rocks like granites, but there are some examples (e.g. Barrière, 1981). In highly evolved rocks such as the Ilímaussaq intrusion, layering becomes more commonly again (Wang and Merino, 1993). In one of the most evolved intrusions at all, the strongly peralkaline Ilímaussaq complex, repetitive layering occurs in a such regular way as is not even seen in the large layered intrusions. In the so-called kakortokite, a peralkaline nepheline syenite, 29 three-layer units with a relatively uniform thickness of several metres (8 m in average) crop out (Bohse et al., 1971). Each unit is made up of a black, a red and a white layer, coloured according to the dominant mineral, i.e. arfvedsonitic amphibole, eudialyte and alkali feldspar, respectively.

To explain the recurrence of layering in general, several models were established. Oscillations of the melt temperature produced during the cooling of the magma are one possible reason. As an origin for these temperature oscillations, Brandeis et al. (1984) suggested interactions between the release of latent heat, heat conduction and crystallisation rate, whereas Allègre et al. (1981) identified a delayed response of the crystallisation rate to temperature changes. McBirney and Noyces (1979) and Maaløe (1987) explained this phenomenon by temperature-controlled changes in the nucleation rate. Another process, which was put forward to account for repetitive layering is Ostwald ripening (Boudreau, 1987; McBirney et al., 1990). Further, Wang and Merino (1993) showed that the feedback between mineral growth rates and the concentrations of reactant species can also cause the repetition of layering and pointed out that this model works especially well in magmas with high alkali contents, which is true for the Ilímaussaq melt. Finally, layering in the rocks was attributed to reflect layering in the crystallising melt (e.g. Wörner and Schmincke, 1984; Wilson and Larsen, 1985).

Several students of the Ilímaussaq alkaline complex presented models on the origin of the recurrence of layering in the kakortokites. Larsen & Sørensen (1987) explained the layering by a multiply layered magma chamber. In this model, the magma layers crystallised beginning at the lowermost layer successively in upward direction and crystallisation is caused by the transfer of thermal energy and volatiles to next overlying magma layer. Sørensen (1968) invoked oscillatory changes of the liquidus temperature around the temperature of the magma that are also caused by the migration of volatiles and thermal energy but in an unlayered magma. Periodic overturns of the magma by convection were suggested by Upton (1961) and Bohse et al. (1971) to be the cause of the recurrence of the three-layer units.

We examined the mineral chemistry of the amphiboles from the black layers systematically throughout the stratigraphy of the kakortokite. Further, we discuss the fluid dynamics in the magma chamber and we present a model for the origin of the recurrence of the layering,

which is based on the model presented by Sørensen (1968).

Geology

Magmatism in the Gardar Province, South Greenland, is closely related to rifting between 1350 and 1140 Ma. Based on U-Pb chronology, two main periods of magmatic activity around 1280 Ma and between 1180 and 1140 Ma, respectively, can be separated (Upton et al., 2003). During these time spans, several alkaline to peralkaline plutonic complexes and a large number of dykes with variable compositions intruded the Ketilidian (1.7 - 1.8 Ga) granitic basement rocks (Julianehåb granite). The Ilímaussaq intrusion belongs to the second of
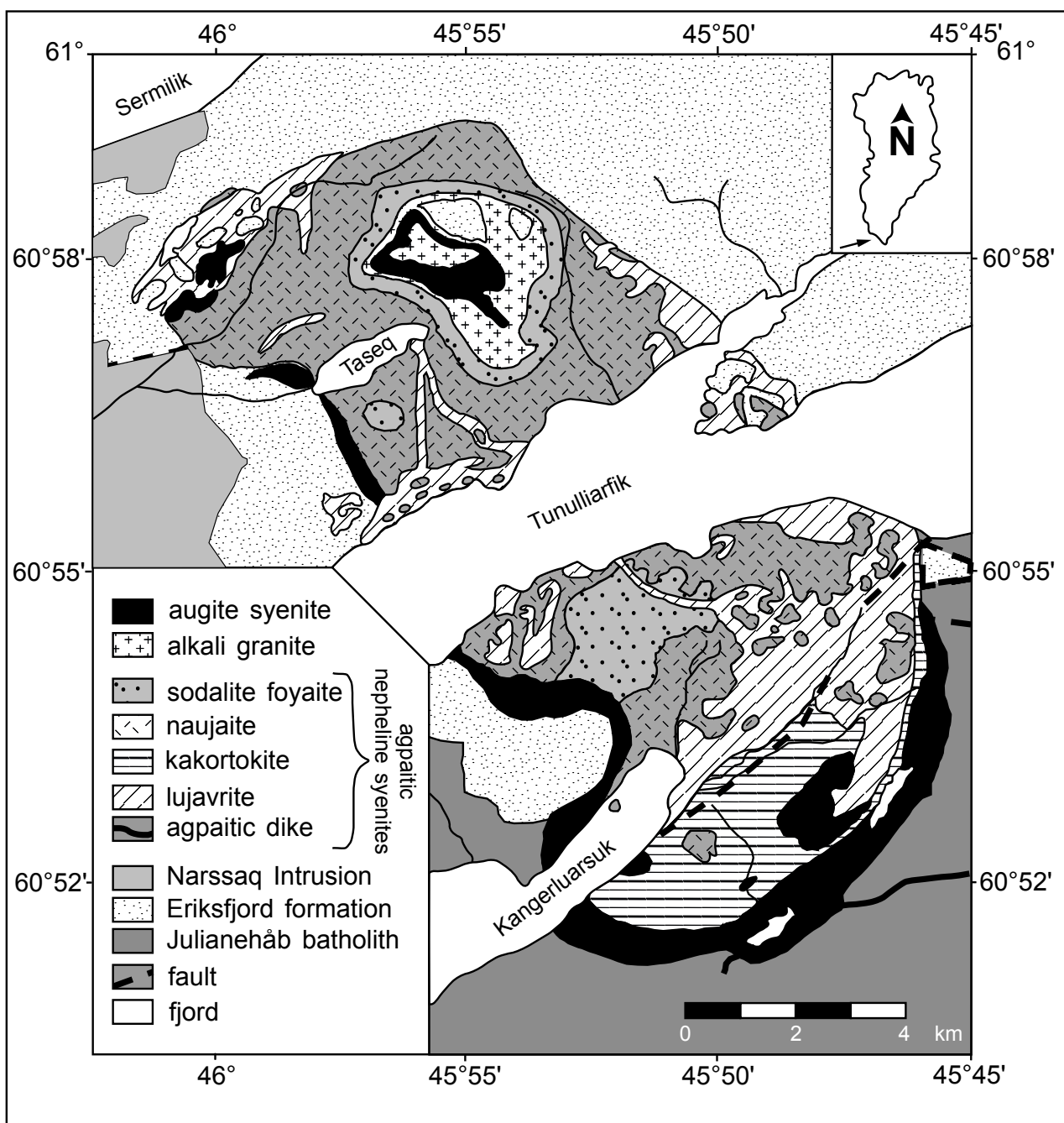
Fig. 1 Geological map of the Ilímaussaq intrusion, modified after Ferguson (1964).

these periods (Blaxland et al., 1976). Krumrei et al. (2006) dated the complex at 1161 ± 5 Ma using the Ar-Ar technique on amphiboles. It consists of alkaline to peralkaline, mostly agpaitic rocks (Fig. 1). Controlled by early fault systems (Sørensen, 1966), the complex intruded at the contact between the Julianehåb granite and the late-Gardar Eriksfjord basalts and sandstones (Poulsen, 1964). The intrusion level was shallow and no metamorphic overprint at all has changed the mineralogy of the rocks (Upton et al., 2003).

Four pulses of magma intruded successively to 3 - 4 km depth (Larsen, 1976; Bailey et al.,1981; Sørensen, 2006). The first one produced a silica-saturated to slightly under-saturated augite syenite, which is now found in parts of the intrusion as the outer shell and as xenoliths within the agpaitic rocks. Subsequently, a sheet of a peralkaline granite (called alkali granite in the literature on Ilímaussaq) intruded the augite syenite. According to Marks et al. (2004b), it represents a more evolved and crustally contaminated equivalent of the augite syenite that possibly assimilated 10 to 15 % of Archeaen lower crustal rocks. In the third and fourth stage, various nepheline syenites were formed mostly by low-pressure in situ fractionation of a broadly phonolitic melt. They contain nepheline, eudialyte, sodalite, alkali feldspar, aegirine and arfvedsonite in various proportions as well as rare minerals like rinkite, aenigmatite, neptunite and others. These agpaites make up the major part of the complex and can be subdivided into a roof series that was formed from the third melt batch (pulaskite, foyaite, sodalite foyaite and naujaite, from the roof downwards), a bottom series (kakortokites) and the most evolved rocks (lujavrites) in between, both crystallised from the fourth stage. The current interpretation is that the roof and the bottom series are cumulates. The first formed by downward crystallisation and flotation of minerals less dense than the melt, the latter by gravitational separation after the solidification of the roof series and the residual melts intruded the roof cumulates along fractures (Larsen & Sørensen, 1987).

One of the agpaitic syenites, the so-called kakortokite, is a strongly layered body of approximately 200 m thickness (280 m if the slightly layered and the transitional layered kakortokites above the main kakortokite are added). It appears only in the southern part of the intrusion separated from the rest by an upthrusting fault (Fig. 2), but most probably this rock is underlying also the northern part of the intrusion. The kakortokite grades successively into the overlying aegirine lujavrites. It is the lowermost exposed rock of the Ilímaussaq intrusion, but more cumulates are suspected to be below, as they are indicated by gravitational and magnetic anomalies (Blundell, 1978; Forsberg and Rasmussen, 1978).
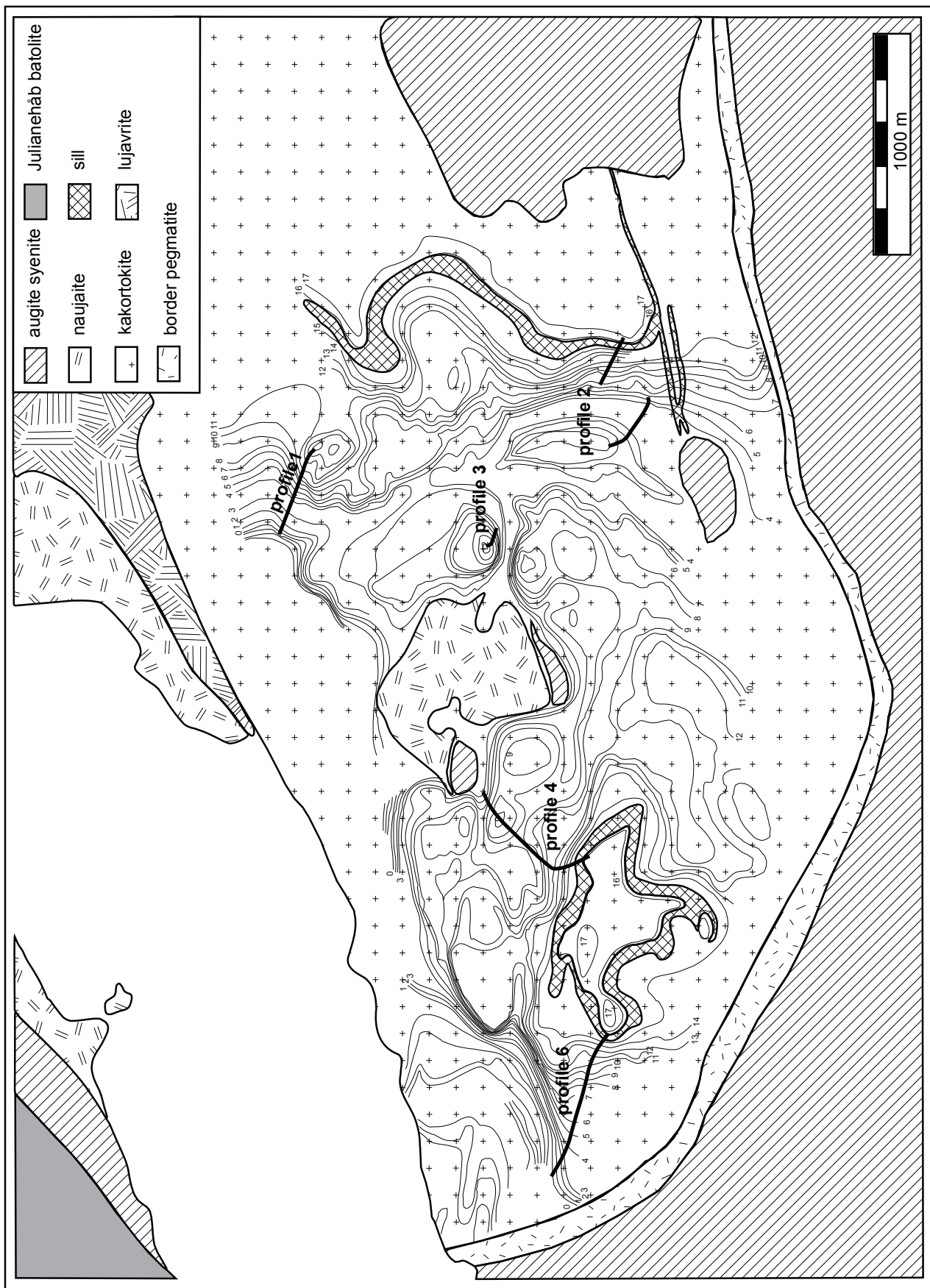
Fig. 2 Geological map showing of the southern part of the Ilímaussaq intrusion in more detail including the layering and the location of the sample profiles. Modified from Bohse et al. (1971).

Petrography of the kakortokites

The kakortokite consists of twenty-nine units and each unit can be subdivided into a black, a red, and a white layer. In principle, the three types consist of the same minerals in variable proportions. The black is the lowermost of the three layers and it is dominated by arfvedsonitic amphiboles. The red one in the middle gains its colour by abundant eudyalite and the uppermost white variety consists mainly of alkali feldspar and nepheline. There is a sharp contact between the black type and the white variety below. In contrast, the transition from black to red and from red to white is gradual. The red layer is not always fully developed. In some units, it forms only lenses between the black and the white layers and in places, it is completely absent. Most of the units remain very constant in their structure and thickness across the whole exposed kakortokite. In average, one three-layer unit is ~8 m in thickness. Close to the margins of the intrusion the dip of the layers becomes steeper and the layering becomes more and more enigmatic. Bohse et al. (1971) numbered the 29 units from -11 to +17 using a prominent unit that they gave the number 0 for reference. In layer +3, large xenoliths from the augite syenite and the naujaite can be found, which were detached from the rocks above by a roof collapse (e.g. Larsen and Sørensen, 1987). The following units upwards are bent above the xenoliths and the units below show sagging and compaction features (see Fig. 2a in Schönenberger et al., 2006 for a photo) proving the cumulate character of the rock. Furthermore, sedimentary structures induced by flows (i.e. trough banding and current bedding) are visible close to the margins of the intrusion, around the large xenoliths in unit +3 and in the lowermost exposed units.

Nepheline, alkali feldspar and eudialyte occur in all three varieties as cumulus phases, whereas arfvedsonite and aegirine appear as abundant cumulus material only in the black layers (Fig. 3a-d). The amphiboles in the red and white layers are in most cases grown from intercumulus melt (Sørensen, 1969). Common late- or post-magmatic minerals are albite, analcime, sodalite and others. In general, the grain sizes of the cumulus minerals are in most samples the same. Amphiboles form anhedra usually 5 mm long and alkali feldspars occur in a similar size. Eudialyte grains are normally between 1 and 2 mm in diameter (Fig. 3b and c) and primary nepheline is present as 2 mm long prisms (Fig. 3c). A few samples are more fine-grained with about half the reported grain sizes, e.g. layer 0 from profile 6 and layer +4 from profile 1. Eudialyte is often heavily altered and replaced by minerals like catapleite, pectolite, analcime, fluorite and others. Aegirine and arfvedsonite appear in some samples to be in equilibrium (Fig. 3a), in others aegirine replaces arfvedsonite and *vice versa*. Alkali feldspar is occasionally overgrown by analcime and albite (Fig. 3d).

Several profiles were taken sampling the black arfvedsonite-rich kakortokite varieties

from units 0 to +16 (Fig. 2). The lower units were excluded because they are only badly exposed in the field.
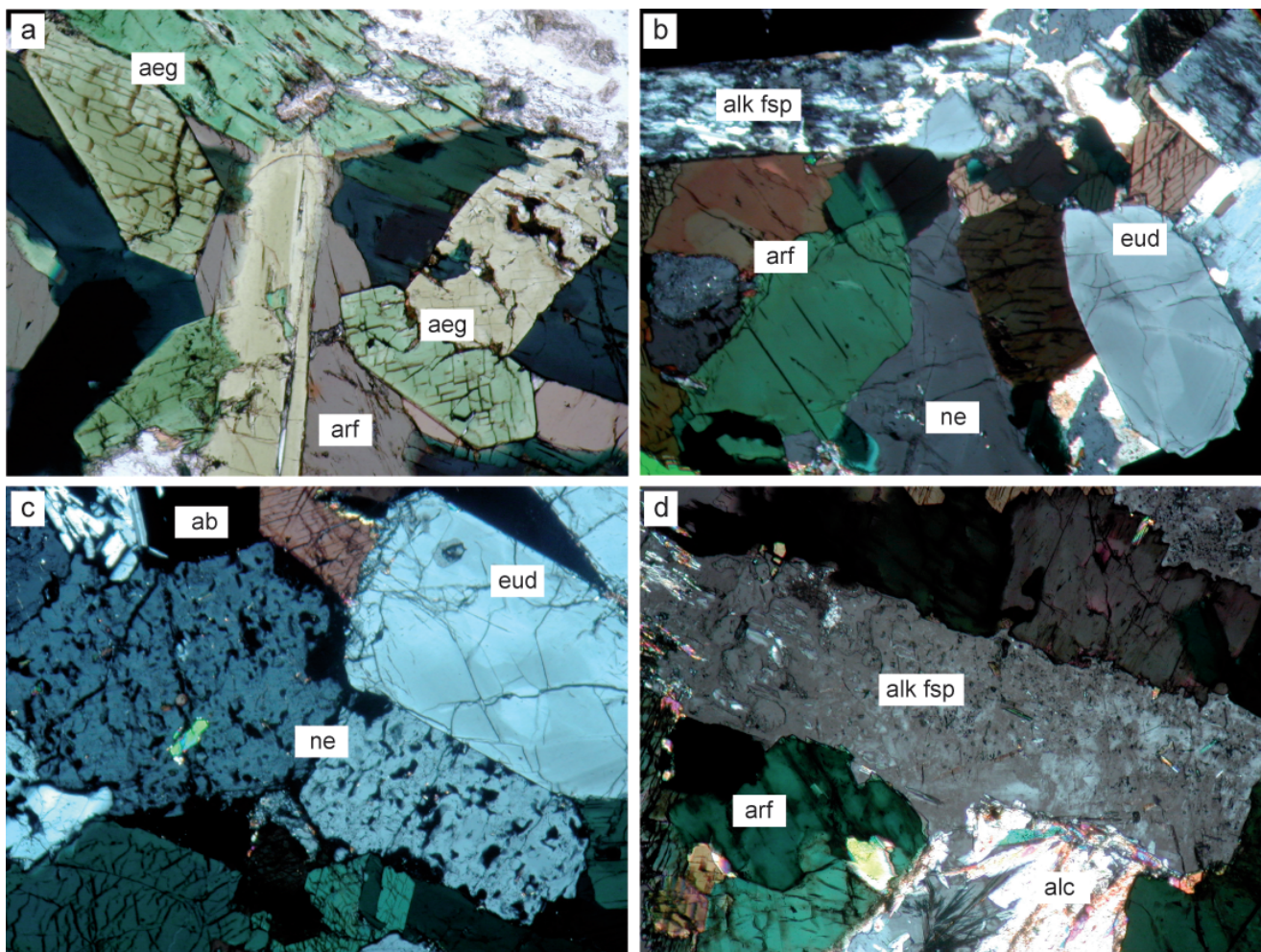
Fig. 3 Photomicrographs showing the phase relations and reaction textures in the black kakotokite. The length of the photos is 10 mm. a) aegirine (aeg) and arfvedsonite (arf) in equilibrium texture. Both are euhedral but aegirine crystallised earlier than arfvedsonite. b) The crystallisation sequence in this eudialyte (eud), alkali feldspar (alk fsp), arfvedsonite and nepheline (ne). The large euhedral eudialyte shows a typical sector zonation. Nepheline occurs only interstitially. c) Euhedral eudialyte and nepheline. The latter shows a blotchy alteration. In the upper left corner late-formed small albite (ab) laths are visible. d) Large alkali feldspar with typical exsolution textures. In the lower right corner, analcime (alc) replaces the alkali feldspar.

Methods

Electron Microprobe

Major element compositions of amphiboles were determined using a JEOL 8900 electron microprobe at the Institut für Geowissenschaften, Universität Tübingen, Germany. For calibration, both natural and synthetic standards were used. The beam current was 15 nA and the acceleration voltage was 15 kV. The counting time on the peak was 16 s for major elements, and 30-60 s for minor elements. Background counting times were half of the peak counting times. The peak overlap between the Fe $L\eta$ and F $K\alpha$ lines was corrected for. Data reduction was performed using the internal $\phi\rho Z$ procedures of JEOL (Armstrong, 1991). Mean values of the amphibole composition are presented in Tab. 1.

Table 1 Chemical composition of selected amphibole grains measured with electron microprobe.

wt %	unit +4, profile 3, grain 3									unit 0, profile 2, grain 4										
SiO_2	47.21	47.65	48.10	48.23	48.46	48.39	48.40	49.03	49.19	47.86	47.69	48.24	48.40	47.87	48.23	48.22	47.78	47.41	47.67	47.08
TiO_2	0.68	0.71	0.75	0.67	0.64	0.66	0.65	0.71	0.66	0.85	0.72	0.83	0.80	0.69	0.68	0.74	0.69	0.59	0.63	0.78
Al_2O_3	2.71	2.68	2.66	2.74	2.54	2.56	2.19	1.83	1.82	3.22	2.94	2.81	2.72	2.98	2.98	2.86	3.01	4.07	3.21	3.15
Li_2O	0.26	0.20	0.26	0.23	0.25	0.23	0.31	0.19	0.23	0.10	0.11	0.15	0.11	0.07	0.14	0.10	0.11	0.16	0.11	0.13
FeO	34.45	34.33	34.30	33.85	34.73	34.69	34.73	34.28	34.07	33.71	33.87	33.59	33.66	34.11	33.52	34.14	33.82	33.00	34.04	34.01
MnO	0.73	0.68	0.69	0.62	0.66	0.71	0.75	0.76	0.77	0.72	0.73	0.69	0.75	0.74	0.64	0.65	0.65	0.63	0.67	0.73
MgO	0.53	0.55	0.51	0.53	0.51	0.58	0.59	0.55	0.57	0.64	0.73	0.63	0.66	0.70	0.80	0.74	0.81	0.68	0.76	0.54
CaO	1.49	1.36	1.36	1.33	1.24	1.37	1.61	1.38	1.45	1.30	1.77	0.99	1.06	2.07	1.35	1.19	1.78	1.42	1.92	1.88
Na_2O	7.75	7.96	7.99	7.78	8.09	7.95	7.53	7.35	7.31	7.83	7.59	7.92	7.88	7.48	7.86	8.02	7.59	7.42	7.55	7.60
K_2O	1.84	1.64	1.71	2.00	1.75	1.84	2.28	2.62	2.67	1.94	1.87	2.06	2.05	1.82	1.89	1.80	1.88	2.49	1.87	1.68
ZrO_2	0.10	0.13	0.12	0.13	0.15	0.13	0.11	0.02	0.30	0.19	0.23	0.17	0.11	0.25	0.19	0.18	0.21	0.49	0.22	0.21
Cl	b.d.	0.01	b.d.	b.d.	0.01	b.d.	b.d.	b.d.	b.d.	0.02	0.02	0.02	0.01	0.01	0.01	0.02	0.02	0.01	0.02	0.01
F	0.25	0.29	0.48	0.19	0.39	0.21	0.26	0.14	0.39	0.57	0.73	0.69	0.82	0.73	0.87	0.90	0.79	0.72	0.76	0.62
Total	**98.62**	**98.66**	**99.55**	**98.85**	**100.00**	**99.86**	**100.13**	**99.29**	**99.95**	**99.18**	**99.26**	**99.15**	**99.28**	**99.70**	**99.51**	**99.78**	**99.38**	**99.45**	**99.69**	**98.74**

formulae based on 16 cations and 23 oxygens

Si	7.463	7.527	7.540	7.592	7.556	7.547	7.552	7.715	7.716	7.537	7.534	7.603	7.630	7.543	7.582	7.567	7.537	7.456	7.498	7.475
Al	0.505	0.499	0.491	0.508	0.467	0.471	0.403	0.340	0.336	0.598	0.547	0.522	0.505	0.553	0.552	0.529	0.560	0.754	0.595	0.589
Ti	0.080	0.085	0.088	0.079	0.074	0.077	0.077	0.084	0.078	0.101	0.086	0.098	0.095	0.082	0.080	0.087	0.081	0.070	0.075	0.093
Li	0.165	0.126	0.164	0.148	0.159	0.143	0.194	0.118	0.145	0.066	0.071	0.097	0.068	0.043	0.091	0.062	0.068	0.099	0.071	0.084
Fe^{3+}	1.305	1.154	1.169	1.055	1.202	1.176	1.249	0.943	0.933	0.945	0.949	0.980	0.917	0.852	0.959	0.998	0.939	0.979	0.973	1.005
Mg	0.126	0.129	0.119	0.124	0.118	0.134	0.137	0.130	0.132	0.149	0.171	0.148	0.155	0.165	0.187	0.174	0.190	0.159	0.178	0.127
Fe^{2+}	3.250	3.381	3.327	3.401	3.326	3.349	3.283	3.568	3.536	3.495	3.526	3.447	3.521	3.643	3.448	3.483	3.522	3.362	3.505	3.511
Mn	0.098	0.090	0.092	0.083	0.087	0.094	0.098	0.101	0.102	0.096	0.098	0.092	0.101	0.098	0.085	0.086	0.087	0.084	0.089	0.099
Ca	0.252	0.230	0.229	0.224	0.207	0.229	0.269	0.233	0.244	0.219	0.300	0.167	0.179	0.349	0.227	0.200	0.301	0.239	0.324	0.320
Na	2.377	2.439	2.429	2.375	2.445	2.405	2.277	2.241	2.222	2.392	2.324	2.419	2.409	2.285	2.395	2.440	2.321	2.261	2.301	2.340
K	0.371	0.330	0.342	0.402	0.348	0.366	0.454	0.526	0.534	0.390	0.377	0.414	0.412	0.366	0.379	0.360	0.378	0.500	0.375	0.340
Zr	0.008	0.010	0.009	0.010	0.011	0.010	0.008	0.001	0.023	0.015	0.018	0.013	0.009	0.019	0.015	0.014	0.016	0.037	0.017	0.016
Cl		0.002			0.002					0.005	0.005	0.006	0.003	0.004	0.003	0.005	0.004	0.004	0.005	0.004
F	0.124	0.146	0.236	0.092	0.190	0.105	0.129	0.067	0.191	0.282	0.365	0.344	0.407	0.363	0.431	0.444	0.395	0.360	0.378	0.311
Sum	**16.000**	**16.000**	**16.000**	**16.000**	**16.000**	**16.000**	**16.000**	**16.000**	**16.000**	**16.000**	**16.000**	**16.000**	**16.000**	**16.000**	**16.000**	**16.000**	**16.000**	**16.000**	**16.000**	**16.000**

b.d. = below detection limit

Table 1 Continued.

wt % — groups: columns 1–14 = unit +6, profile 6, grain 3; columns 15–24 = unit +8, profile 1, grain 2

	1	2	3	4	5	6	7	8	9	10	11	12	13	14	15	16	17	18	19	20	21	22	23	24
SiO_2	47.73	47.93	47.95	47.78	47.60	47.36	47.11	48.06	47.81	48.55	48.43	48.22	48.16	48.81	48.82	49.30	47.68	47.94	48.60	48.44	47.91	48.19	48.00	48.80
TiO_2	0.57	0.53	0.53	0.53	0.57	0.63	0.58	0.63	0.59	0.67	0.57	0.60	0.64	0.55	0.52	0.58	0.66	0.64	0.62	0.67	0.76	0.64	0.69	0.62
Al_2O_3	2.49	2.33	2.31	2.32	2.39	2.77	2.73	2.75	2.77	2.66	2.57	2.55	2.55	2.46	2.02	1.60	2.43	2.43	2.46	2.52	2.59	2.53	2.48	2.35
Li_2O	0.18	0.12	0.18	0.19	0.16	0.15	0.23	0.15	0.20	0.18	0.15	0.16	0.16	0.16	0.26	0.22	0.24	0.24	0.24	0.22	0.23	0.20	0.26	0.20
FeO	34.15	34.04	34.20	34.04	34.27	34.12	34.29	34.27	34.14	34.24	34.16	34.34	34.31	34.23	34.30	34.20	34.60	34.87	34.73	34.55	34.49	34.37	34.71	33.97
MnO	0.75	0.68	0.69	0.64	0.71	0.72	0.63	0.68	0.61	0.63	0.67	0.68	0.70	0.71	0.71	0.69	0.70	0.69	0.59	0.66	0.63	0.65	0.73	0.75
MgO	0.59	0.69	0.66	0.65	0.67	0.66	0.68	0.70	0.70	0.67	0.63	0.57	0.50	0.47	0.62	0.60	0.59	0.69	0.69	0.70	0.67	0.65	0.65	0.82
CaO	1.79	1.94	1.91	1.87	1.86	2.25	2.21	2.23	2.16	1.49	1.81	1.83	1.85	1.74	1.20	1.37	1.44	1.50	1.40	1.40	1.42	1.57	1.47	1.00
Na_2O	7.61	7.56	7.56	7.56	7.57	7.38	7.39	7.49	7.46	7.90	7.66	7.67	7.69	7.74	7.76	7.25	7.88	7.94	8.04	8.05	7.96	7.89	7.92	7.96
K_2O	1.76	1.66	1.74	1.73	1.74	1.72	1.74	1.72	1.78	1.78	1.79	1.73	1.67	1.74	2.19	2.78	1.73	1.71	1.71	1.67	1.70	1.66	1.76	2.10
ZrO_2	0.20	0.14	0.16	0.14	0.16	0.22	0.21	0.26	0.22	0.17	0.15	0.17	0.21	0.14	0.02	0.17	0.13	0.16	0.07	0.12	0.13	0.12	0.07	0.05
Cl	b.d.	0.01	0.02	0.01	b.d.	0.02	0.01	0.01	0.02	0.01	b.d.	0.01	0.01	0.01	0.01	b.d.	b.d.	0.01	b.d.	b.d.	b.d.	b.d.	0.01	b.d.
F	0.37	0.52	0.63	0.74	0.72	0.41	0.50	0.63	0.56	0.65	0.48	0.64	0.50	0.61	0.45	0.42	0.31	0.74	0.81	0.80	0.82	0.64	0.56	0.70
Total	98.61	98.44	98.97	98.67	98.80	98.76	98.85	99.96	99.47	100.00	99.40	99.54	99.32	99.75	99.49	99.68	98.93	100.12	100.54	100.32	99.82	99.59	99.92	99.76

formulae based on 16 cations and 23 oxygens

	1	2	3	4	5	6	7	8	9	10	11	12	13	14	15	16	17	18	19	20	21	22	23	24
Si	7.570	7.625	7.598	7.599	7.562	7.514	7.468	7.545	7.532	7.591	7.621	7.596	7.596	7.667	7.658	7.754	7.517	7.499	7.562	7.554	7.515	7.567	7.505	7.633
Al	0.465	0.437	0.431	0.435	0.447	0.518	0.510	0.509	0.514	0.490	0.477	0.473	0.474	0.455	0.373	0.296	0.452	0.448	0.451	0.463	0.479	0.468	0.457	0.433
Ti	0.068	0.063	0.064	0.063	0.068	0.075	0.069	0.075	0.070	0.078	0.067	0.071	0.076	0.065	0.062	0.069	0.079	0.075	0.072	0.078	0.089	0.075	0.081	0.072
Li	0.112	0.080	0.113	0.124	0.103	0.095	0.145	0.097	0.125	0.112	0.093	0.099	0.102	0.101	0.166	0.137	0.150	0.153	0.152	0.139	0.143	0.129	0.165	0.123
Fe^{3+}	1.035	0.914	1.009	1.024	1.055	0.983	1.153	0.935	1.010	1.008	0.913	0.957	0.939	0.867	1.147	0.938	1.244	1.281	1.188	1.158	1.197	1.094	1.278	1.104
Mg	0.139	0.164	0.157	0.154	0.158	0.157	0.161	0.165	0.163	0.156	0.147	0.133	0.117	0.110	0.145	0.140	0.139	0.161	0.161	0.163	0.156	0.152	0.152	0.192
Fe^{2+}	3.494	3.615	3.523	3.503	3.498	3.544	3.393	3.564	3.488	3.469	3.582	3.566	3.586	3.630	3.353	3.560	3.318	3.280	3.331	3.348	3.327	3.419	3.261	3.340
Mn	0.101	0.091	0.093	0.086	0.096	0.096	0.084	0.091	0.082	0.083	0.089	0.091	0.094	0.094	0.094	0.092	0.093	0.091	0.078	0.088	0.084	0.087	0.097	0.100
Ca	0.304	0.331	0.324	0.319	0.317	0.382	0.375	0.375	0.365	0.250	0.305	0.309	0.313	0.293	0.202	0.231	0.243	0.251	0.233	0.234	0.239	0.264	0.246	0.168
Na	2.340	2.332	2.324	2.330	2.331	2.269	2.273	2.280	2.278	2.395	2.336	2.344	2.351	2.359	2.359	2.211	2.408	2.407	2.427	2.433	2.421	2.403	2.402	2.413
K	0.356	0.337	0.352	0.351	0.353	0.348	0.352	0.344	0.358	0.355	0.359	0.348	0.336	0.349	0.438	0.558	0.348	0.341	0.339	0.332	0.340	0.333	0.351	0.419
Zr	0.016	0.011	0.013	0.011	0.013	0.017	0.016	0.020	0.017	0.013	0.011	0.013	0.016	0.011	0.002	0.013	0.010	0.012	0.005	0.009	0.010	0.009	0.005	0.004
Cl		0.003	0.005	0.004		0.005	0.003	0.002	0.006	0.002		0.002	0.002	0.003	0.001			0.002					0.003	
F	0.186	0.259	0.315	0.374	0.362	0.204	0.253	0.315	0.278	0.319	0.237	0.321	0.248	0.301	0.222	0.208	0.156	0.368	0.400	0.397	0.405	0.320	0.279	0.348
Sum	16.000	16.000	16.000	16.000	16.000	16.000	16.000	16.000	16.000	16.000	16.000	16.000	16.000	16.000	16.000	16.000	16.000	16.000	16.000	16.000	16.000	16.000	16.000	16.000

Table 1 Continued.

wt %

	unit +12, profile 2, grain 3										unit +16, profile 6, grain 1							
SiO_2	47.37	47.45	47.49	47.44	47.66	47.64	47.51	47.58	48.06	49.30	47.49	47.33	46.68	47.52	46.79	46.70	47.06	46.65
TiO_2	0.60	0.61	0.64	0.65	0.64	0.63	0.62	0.64	0.66	0.70	0.58	0.61	0.62	0.61	0.62	0.63	0.81	0.92
Al_2O_3	2.47	2.42	2.52	2.54	2.47	2.43	2.66	2.63	2.79	2.95	2.61	2.69	2.76	2.56	2.74	3.04	2.75	2.86
Li_2O	0.20	0.20	0.27	0.23	0.20	0.22	0.27	0.23	0.25	0.32	0.25	0.23	0.26	0.21	0.27	0.24	0.21	0.28
FeO	34.53	34.54	34.49	34.57	34.57	34.79	34.08	34.12	33.96	33.94	33.62	33.74	34.14	34.20	34.27	34.23	34.03	34.22
MnO	0.67	0.64	0.67	0.68	0.64	0.70	0.74	0.75	0.74	0.69	0.73	0.77	0.79	0.73	0.75	0.68	0.69	0.71
MgO	0.53	0.54	0.59	0.56	0.55	0.56	0.54	0.52	0.52	0.55	0.47	0.46	0.46	0.48	0.45	0.48	0.46	0.48
CaO	1.42	1.26	1.39	1.47	1.39	1.42	1.52	1.48	1.28	1.29	1.66	1.87	2.16	1.74	2.32	2.36	2.16	2.14
Na_2O	7.83	7.73	7.91	7.88	7.93	7.92	7.82	7.79	8.01	8.23	7.65	7.53	7.37	7.62	7.37	7.40	7.45	7.46
K_2O	1.71	2.01	1.73	1.67	1.64	1.70	1.71	1.77	1.72	1.69	1.73	1.73	1.73	1.76	1.64	1.61	1.62	1.69
ZrO_2	0.14	0.19	0.20	0.16	0.18	0.19	0.17	0.21	0.18	0.15	0.19	0.18	0.37	0.15	0.46	0.74	0.27	0.31
Cl	0.01	b.d.	b.d.	0.01	0.01	0.01	0.01	0.01	b.d.	0.02	b.d.	b.d.	b.d.	b.d.	b.d.	b.d.	b.d.	0.01
F	0.74	0.69	0.69	0.80	0.77	0.72	0.66	0.55	0.55	0.53	0.57	0.60	0.67	0.67	0.73	0.71	0.68	0.74
Total	**98.69**	**98.78**	**99.22**	**99.19**	**99.11**	**99.47**	**98.92**	**98.80**	**99.30**	**101.12**	**98.16**	**98.28**	**98.63**	**98.75**	**99.05**	**99.40**	**98.68**	**99.13**

formulae based on 16 cations and 23 oxygens

	unit +12, profile 2, grain 3										unit +16, profile 6, grain 1							
Si	7.524	7.530	7.492	7.499	7.538	7.507	7.515	7.533	7.552	7.589	7.571	7.547	7.442	7.547	7.440	7.402	7.497	7.402
Al	0.462	0.453	0.469	0.473	0.460	0.451	0.496	0.491	0.517	0.535	0.490	0.506	0.519	0.479	0.513	0.568	0.516	0.535
Ti	0.072	0.073	0.076	0.078	0.076	0.075	0.073	0.076	0.078	0.081	0.069	0.073	0.074	0.073	0.074	0.075	0.097	0.110
Li	0.129	0.131	0.169	0.145	0.125	0.142	0.169	0.144	0.159	0.199	0.163	0.148	0.169	0.134	0.172	0.155	0.133	0.180
Fe^{3+}	1.213	1.229	1.300	1.245	1.172	1.258	1.214	1.153	1.140	1.088	1.081	1.056	1.191	1.095	1.164	1.117	1.018	1.211
Mg	0.126	0.129	0.139	0.132	0.129	0.132	0.126	0.122	0.121	0.125	0.111	0.109	0.109	0.114	0.106	0.114	0.109	0.113
Fe^{2+}	3.374	3.354	3.250	3.325	3.400	3.327	3.294	3.365	3.323	3.281	3.401	3.443	3.361	3.447	3.393	3.420	3.516	3.330
Mn	0.090	0.087	0.089	0.091	0.086	0.093	0.100	0.101	0.098	0.090	0.099	0.104	0.107	0.098	0.101	0.091	0.093	0.096
Ca	0.242	0.214	0.235	0.249	0.236	0.240	0.258	0.251	0.215	0.213	0.284	0.319	0.369	0.296	0.395	0.401	0.369	0.364
Na	2.412	2.379	2.418	2.414	2.433	2.419	2.397	2.391	2.440	2.455	2.365	2.329	2.279	2.347	2.272	2.274	2.302	2.294
K	0.346	0.407	0.348	0.337	0.331	0.342	0.345	0.357	0.345	0.332	0.352	0.352	0.352	0.357	0.333	0.326	0.329	0.342
Zr	0.011	0.015	0.015	0.012	0.014	0.015	0.013	0.016	0.013	0.011	0.015	0.014	0.029	0.012	0.036	0.057	0.021	0.024
Cl	0.001			0.003	0.002	0.002	0.002	0.002		0.005								0.002
F	0.369	0.348	0.344	0.397	0.383	0.360	0.330	0.274	0.273	0.259	0.289	0.301	0.336	0.334	0.368	0.354	0.341	0.369
Sum	**16.000**	**16.000**	**16.000**	**16.000**	**16.000**	**16.000**	**16.000**	**16.000**	**16.000**	**16.000**	**16.000**	**16.000**	**16.000**	**16.000**	**16.000**	**16.000**	**16.000**	**16.000**

b.d. = below detection limit

Table 2 Mean values of amphibole trace element composition.

sample	O-2-S	O-4-S	O-6-S	4-1-S	4-2-S	4-3-S	4-4-S	4-6-S	6-1-S	6-2-S	6-4-S	6-6-S	8-1-S	8-2-S
n	11	8	10	15	9	4	6	9	9	13	11	10	11	10
Li	950.2	1461.0	463.6	813.8	986.6	244.5	1052.0	885.4	986.6	813.0	717.0	941.3	921.9	891.5
Be	13.48	23.76	8.68	7.27	10.23	14.62	12.56	24.35	15.78	11.95	15.08	5.37	9.11	12.60
Ca	8622	9502	13318	14397	12384	10143	10087	12968	11023	72429	10224	11645	10855	10494
Sc	7.59	11.16	10.65	12.09	8.13	7.46	5.85	8.38	7.13	8.76	7.45	7.84	8.75	8.17
Zn	853.1	883.6	802.6	803.5	832.9	770.3	1007.5	839.9	767.7	852.0	760.8	779.9	825.5	970.5
Ga	35.3	32.4	31.9	34.5	36.0	33.5	39.8	31.8	31.8	37.0	35.9	30.1	31.8	34.2
Rb	45.1	44.4	44.8	47.0	43.6	50.9	42.8	52.9	46.9	44.0	58.4	41.9	45.0	47.2
Sr	14.06	16.69	19.21	22.56	17.06	15.30	14.83	19.71	16.90	130.15	14.51	17.64	16.55	17.28
Y	7.90	7.29	8.79	11.84	10.55	11.80	17.72	14.20	7.78	86.19	14.36	10.11	10.30	10.35
Zr	1310	1372	1477	1845	1240	1003	930	1141	908	1329	1218	1256	1280	1505
Nb	129.1	156.6	160.3	186.9	140.0	152.3	111.4	101.2	116.7	171.1	142.1	138.1	144.1	136.5
Sn	62.0	43.3	44.2	50.0	51.0	37.7	48.0	51.5	46.2	58.4	94.7	46.8	49.2	57.2
Cs	0.19	b.d.	0.12	0.16	b.d.	0.14	0.38	0.32	0.18	b.d.	1.02	b.d.	0.05	0.08
Ba	5.06	6.38	4.18	6.29	3.68	3.37	5.15	3.32	4.63	4.79	5.46	3.28	4.55	4.15
La	11.21	14.61	14.69	20.91	12.60	9.98	9.78	13.94	11.04	45.85	11.14	12.33	12.70	12.98
Ce	28.0	33.5	35.1	49.6	30.7	23.4	23.0	30.1	24.8	99.4	23.4	31.0	29.8	30.8
Pr	3.65	4.12	4.69	6.64	4.22	3.06	3.13	3.83	3.23	14.59	3.19	4.10	3.97	3.95
Nd	13.58	15.07	16.48	23.19	15.07	9.64	11.44	13.91	11.33	70.32	11.68	14.47	14.75	14.93
Sm	1.88	2.11	2.17	3.55	2.51	1.46	2.05	2.04	1.59	14.15	1.88	2.10	2.14	2.27
Eu	0.18	0.16	0.14	0.21	0.15	0.12	0.17	0.14	0.11	1.24	0.14	0.15	0.16	0.16
Gd	1.05	0.99	0.95	1.41	1.25	0.94	1.46	1.17	0.72	13.42	1.19	1.10	1.02	1.17
Tb	0.13	0.14	0.15	0.21	0.13	0.15	0.30	0.20	0.11	1.37	0.19	0.15	0.15	0.16
Dy	1.07	1.03	1.13	1.54	1.32	1.49	2.20	1.55	0.77	8.76	1.81	1.42	1.26	1.32
Ho	0.32	0.30	0.37	0.43	0.44	0.34	0.63	0.54	0.26	1.77	0.54	0.41	0.44	0.38
Er	1.90	1.75	2.18	2.42	2.26	2.14	2.64	2.59	1.67	5.66	2.51	2.22	2.27	2.21
Tm	0.55	0.56	0.63	0.75	0.68	0.62	0.67	0.77	0.54	1.05	0.71	0.63	0.66	0.63
Yb	6.81	7.09	7.58	9.76	8.47	8.00	8.52	9.07	6.17	9.85	7.87	7.35	7.63	7.52
Lu	1.52	1.54	1.96	2.38	1.91	1.85	1.87	2.04	1.36	2.02	1.74	1.66	1.66	1.74
Hf	30.5	29.0	41.2	46.0	32.0	25.8	21.6	25.4	19.9	35.5	29.5	31.2	31.1	43.3
Ta	1.91	2.10	3.15	3.08	2.34	1.69	1.79	2.06	1.67	2.51	3.93	2.29	2.32	2.12
Pb	1.34	2.04	2.57	2.53	2.44	3.59	2.19	2.59	2.02	10.52	2.72	2.74	2.07	2.55

b.d. = below detection limit

Table 2 continued.

sample	8-4-S	8-6-S	12-2-S	12-3-S	12-4-S	12-6-S	16-1-S	16-2-S	16-4-S	16-6-S
n	9	12	9	10	9	8	5	9	6	5
Li	336.9	713.4	932.5	547.2	41.4	1070.4	591.0	855.7	646.8	1103.0
Be	7.67	14.99	11.09	12.54	1.06	4.86	15.32	8.10	13.88	8.47
Ca	13511	12179	9679	9901	17349	11502	9651	9179	12023	9595
Sc	8.39	6.52	6.73	6.66	6.00	7.91	7.51	6.13	7.02	7.01
Zn	500.0	506.1	767.4	864.4	142.1	780.9	957.6	951.9	862.2	1037.8
Ga	31.2	29.8	31.1	32.4	32.8	30.4	35.5	34.7	33.4	37.9
Rb	23.7	56.7	40.5	45.4	0.1	48.1	47.9	44.8	43.5	54.6
Sr	7.20	14.30	14.69	17.13	5.55	18.07	18.54	15.88	20.38	19.74
Y	10.33	11.34	8.88	10.15	5.42	11.19	9.94	10.07	11.69	11.03
Zr	3300	1116	1230	1269	1717	1229	1166	808	1792	1065
Nb	40.9	70.2	128.7	131.0	5.8	153.4	157.0	114.8	167.3	138.1
Sn	293.9	122.3	47.0	45.7	188.6	45.4	51.4	43.8	51.7	38.6
Cs	0.09	0.32	0.06	0.06	0.04	b.d.	0.07	0.15	0.19	0.19
Ba	2.15	3.33	2.76	3.45	0.28	3.11	4.96	3.78	4.73	3.91
La	6.52	9.20	8.69	11.46	8.56	13.56	13.70	10.11	19.22	14.12
Ce	17.2	21.9	22.4	23.7	25.5	32.0	32.3	22.2	40.1	32.2
Pr	2.58	3.13	2.98	3.58	3.99	4.52	4.18	3.03	5.19	3.64
Nd	10.97	11.86	11.19	11.87	15.52	16.24	14.24	11.04	17.94	12.37
Sm	2.10	2.01	1.68	1.77	2.61	2.46	2.17	1.57	2.46	1.29
Eu	0.16	0.23	0.13	0.11	0.18	0.15	0.13	0.12	0.15	0.09
Gd	1.24	1.40	0.80	1.06	1.34	1.15	0.85	0.97	1.27	0.56
Tb	0.21	0.19	0.12	0.18	0.18	0.15	0.13	0.23	0.17	0.07
Dy	1.51	1.75	0.85	1.27	1.18	1.35	1.24	1.48	1.34	0.63
Ho	0.40	0.45	0.30	0.46	0.21	0.51	0.36	0.35	0.46	0.27
Er	1.94	2.18	1.94	2.16	0.81	2.61	1.91	1.59	2.57	1.88
Tm	0.53	0.60	0.55	0.63	0.24	0.71	0.65	0.46	0.66	0.72
Yb	6.79	6.71	6.70	7.25	2.85	9.18	7.24	5.26	8.00	8.78
Lu	1.65	1.58	1.48	1.66	0.83	1.87	1.67	1.12	1.93	2.02
Hf	107.0	28.5	30.0	34.7	34.9	30.9	35.1	17.7	37.9	27.8
Ta	0.92	1.20	2.08	2.31	0.22	2.39	2.29	1.83	3.62	0.71
Pb	1.73	1.82	1.32	2.00	0.83	2.96	3.03	2.71	3.58	2.22

b.d. = below detection limit

Laser-ICP-MS

In situ laser ablation inductively coupled plasma mass spectrometer (LA-ICP-MS) analyses of REE and other trace elements were performed at the Universität Würzburg using an Agilent 7500i ICP-MS equipped with a 266-nm Nd-YAG laser (Merchantek 266 LUV). The laser beam diameter at the sample surface was approximately 50 μm. All measurements were made using Thermo Elemental PlasmaLab btime-resolved analysisQ (TRA) data acquisition software with a total acquisition time of 45 s per analysis, allowing about 20 s for background followed by 25 s for laser ablation. NIST 612 (Pearce et al., 1997) glass was used for instrument calibration, and NIST 614 and NIST 640 were used as secondary standards. Si was used as an internal standard to correct the ablation yield differences between and during individual analyses on both standards and samples. The results are given in Tab. 2.

Results

Formula calculations of the amphiboles are based on 16 cations and 23 oxygens. The calculations result systematically in under-occupied C-sites and over-occupied A-sites for which (a) significant Li-contents in the amphiboles (Marks et al. 2004a) that cannot be measured by the microprobe and (b) the poor matrix correction of the microprobe for this special type of amphiboles resulting in too high Na contents are responsible (Pfaff, unpubl. data). Therefore, we performed a correction of the Na-content and calculated the Li-content. The first is based on the assumption that sites A and B of the amphibole lattice are only occupied by Na, Ca, and K and are completely filled by these elements. This assumption is consistent with the findings that arfvedsonites and nyböites usually have no or only very little vacancies (Leake et al., 1997). The measured amount of Ca and K was subtracted from the three A- and B-sites and the remaining number was attributed to Na. The calculation of the Li is based on the assumption that Li occupies only the C-site of the amphibole lattice. Since the C-site is under-occupied and all other major elements in the amphiboles were measured, we assumed that the remaining space until the C-site is completely filled corresponds to the Li-content. Cros-schecks with Li measurements with La-ICP-MS (Tab. 2) show excellent agreement between the calculated and the measured values.

According to the amphibole nomenclature of Leake et al. (1997), most measured amphiboles refer to arfvedsonite and only some are ferric-ferronyböite, which is typical of the highly evolved peralkaline rocks of the Ilímaussaq intrusion (Larsen, 1976; Marks et al. 2004a). In principal, the amphiboles are rich in Na and Fe and contain high amounts of the trace elements Zr, Zn, and Li. Fe^{3+}/Fe^{2+} ratios vary between 0.20 and 0.40 with some higher values in the uppermost sample from profile 1. Ca (2.8 – 0.8 wt.-%) and Mg (1.0 – 0.4 wt.-%)
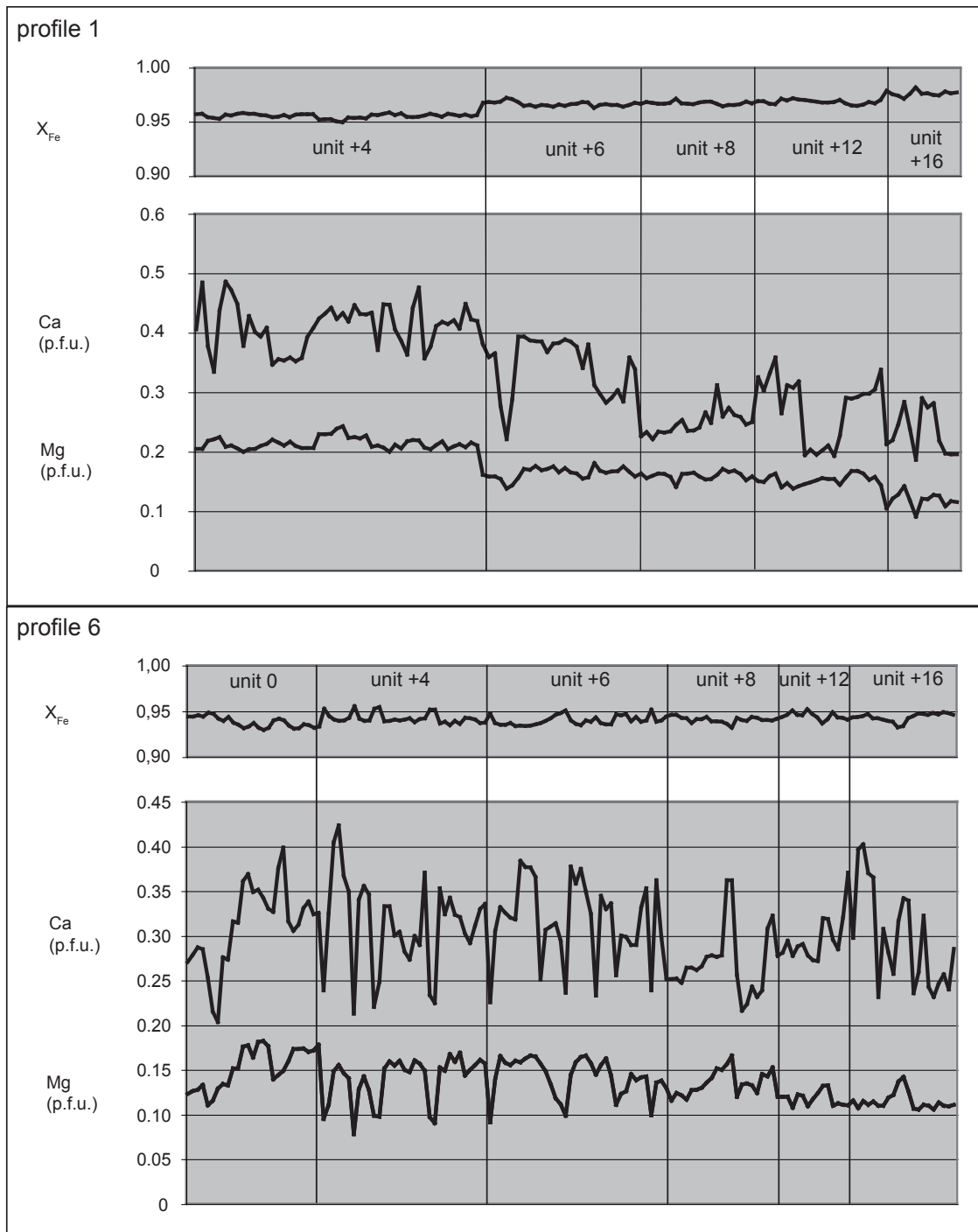
Fig. 4 Selected chemical profiles of amphibole measurements by microprobe through the kakortokite sequence comparing profiles 1 and 6. In profile 1, Mg and Ca show a slight decrease with stratigraphical height whereas XFe increases. In contrast, no chemical trends are obvious in profile 6. Analyses, which show the features of the second amphibole generation (i.e. high K values), are excluded from these diagrams. The samples within a unit are not arranged stratigraphically. Note the much larger scatter of the amphibole composition within one unit in profile 6.

contents are low.

Andersen et al. (1981) found the mineral composition to be constant throughout the kakortokite sequence. In contrast, Larsen (1976) reported in the amphiboles a decrease in the Mg-content with stratigraphical height and Steenfeld and Bohse (1975) showed an increase in U in the eudialytes. Our results also show systematic chemical trends in the amphiboles and less pronounced in the eudialytes (Rudolf, unpubl. data). Although the scatter

of some element concentrations, e.g. of Ca and Mg, within one unit is high due to zonations in the amphiboles, there are clear correlations with the stratigraphic height of the samples (Fig. 4). These correlations are, however, only visible in some of the profiles and appear to depend on the distance of the profile to the margin of the intrusion. The profile most distant to it, i.e. profile 1, exhibits the clearest trends and the profile closest to the margin lacks any stratigraphical trend (profile 6). X_{Fe} remains constant around 0.94 in profile 6. This is significantly lower than the lowermost sample from profile 1, which starts at 0.955 and increases upwards to almost 0.98. Furthermore, Ca is constant over profile 6, admittedly with a high scatter within one layer expressing the zonation of the crystals, and fluctuates around 0.3 atoms per formula unit (a.p.f.u.). In profile 1, the within-layer scatter is much less and there is a progression from 0.4 a.p.f.u. in the lowermost sample to 0.2 a.p.f.u. at the top reflecting the evolution of the melt from which the amphiboles crystallised. Mg behaves very similar to Ca and Li shows an inverse behaviour, i.e. it increases with fractionation but remains constant in the marginal profile.
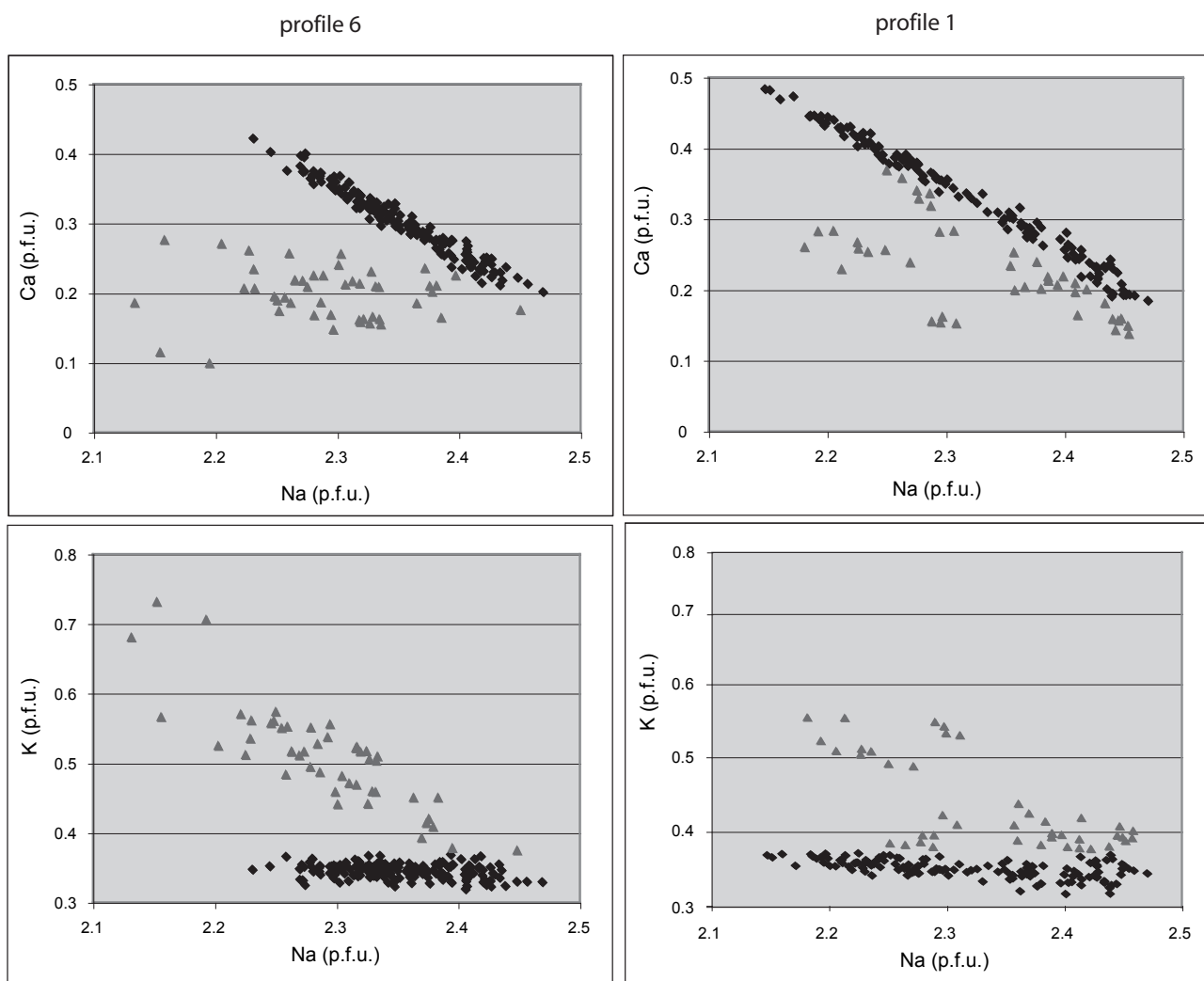
Fig. 5 Diagrams showing the two amphibole generations expressed by different trends in Ca/Na and K/Na plot, respectively. See text for discussion.

In the plots K vs. Na and Ca vs. Na (Fig. 5), two different amphibole generations are visible. The younger generation has significantly higher contents of K and lower values of Al and Ca of which the latter is independent from the Na content. Microprobe analyses showing these features stem in most cases from the very rim of the amphibole grains. The vast majority of the analyses belong to the older generation with low and constant K values, a higher content of Al and Na-Ca values that follow a sharp trend. Chemical profiles of amphibole grains with the high-K generation at the rim show that the change is an abrupt one (Fig. 6). This indicates that the two generations were formed with a temporal hiatus. Here again, differences in the different profiles are visible. The younger generation occurs frequently in profile 6 and only subordinately in the other profiles.
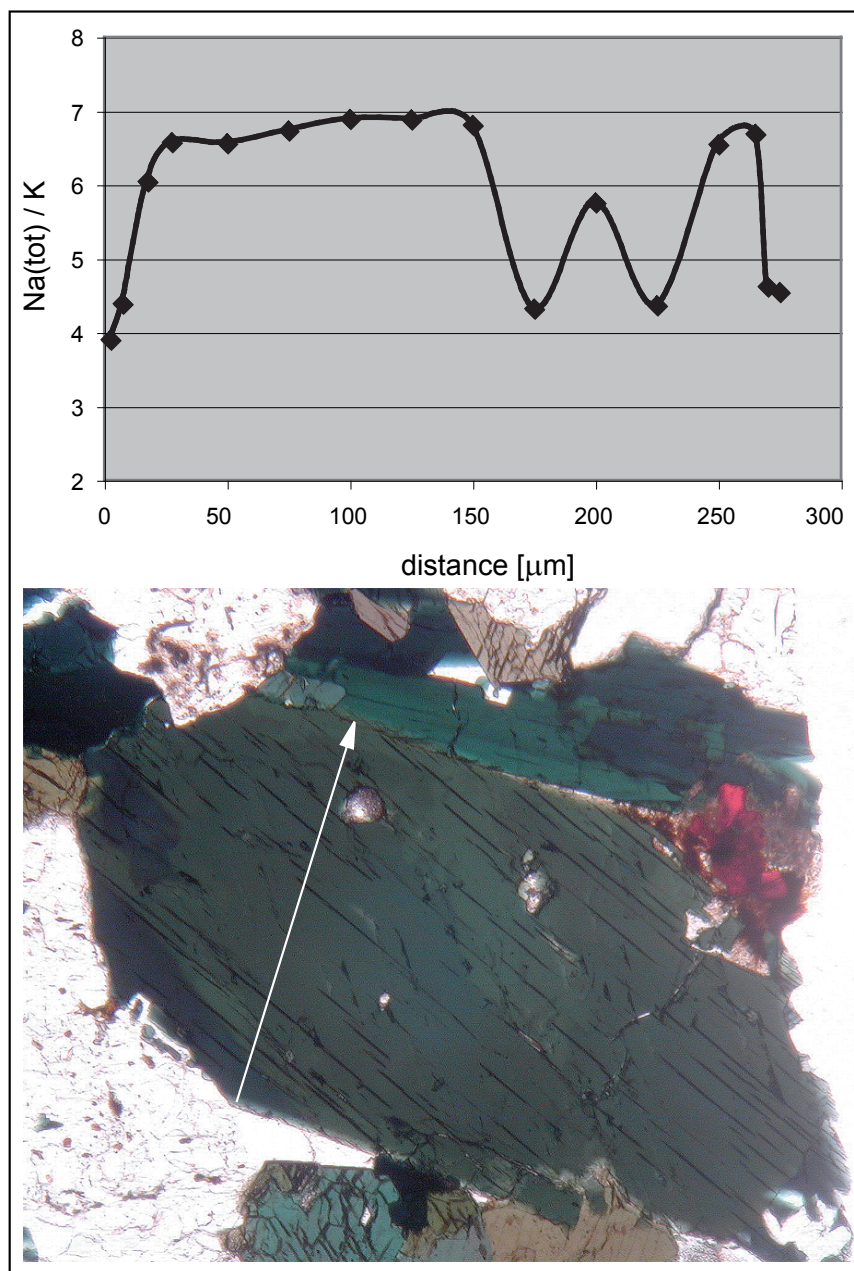
Fig. 6 Profile of a single amphibole grain from unit +6, profile 1. The white arrow in the photomicrograph indicate the direction of the measurement. Note the abrupt changes in the Na/K ratio at the rim and also around the inclusion.

The trace element composition of the amphiboles follows in general the features outlined above for the main elements. There are only some enigmatic stratigraphic trends, for instance Sc tends to decrease with the stratigraphic height (Fig. 7), but the two amphibole generations differ significantly in their composition. The older generation is characterised by low Sn and high Li and Pb contents and the younger one has lower Sc and almost insignificant Li values (Fig. 8).
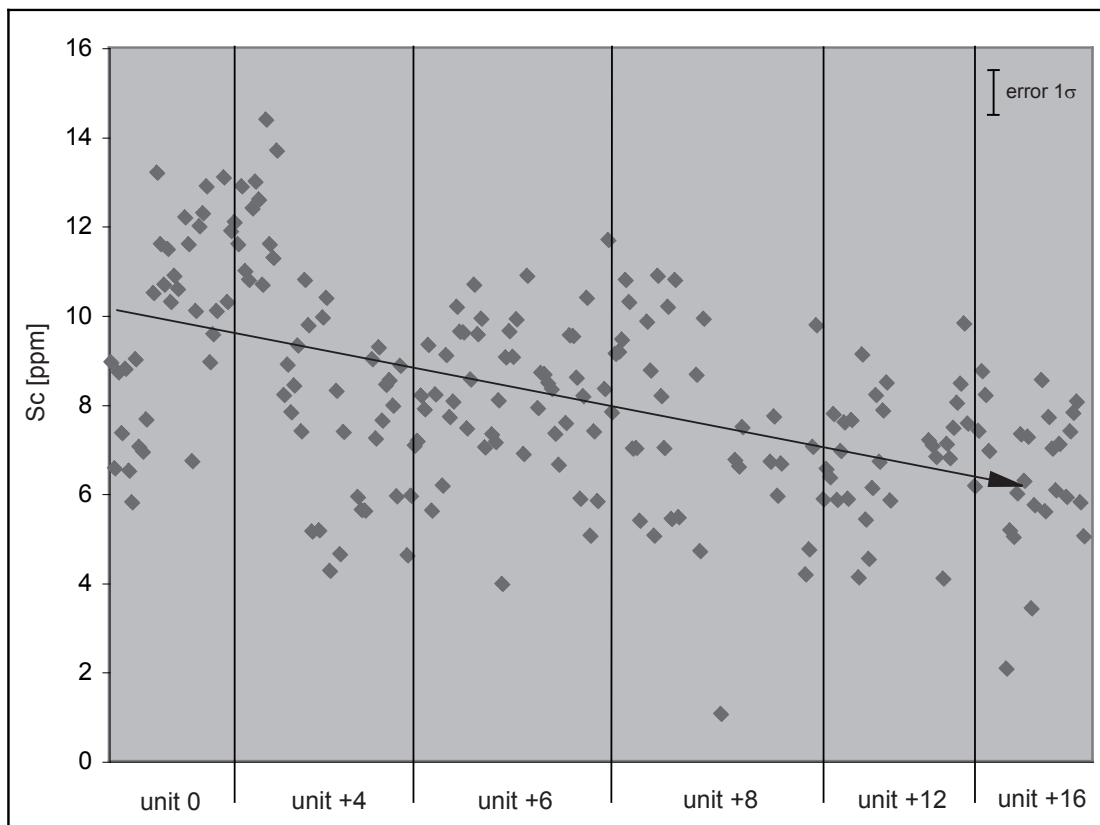
Fig. 7 Stratigraphic arrangement of Sc in the amphiboles measured by La-ICP-MS. Again, within one unit there is a large scatter of the values, but nonetheless a slight decrease with stratigraphic height is obvious.
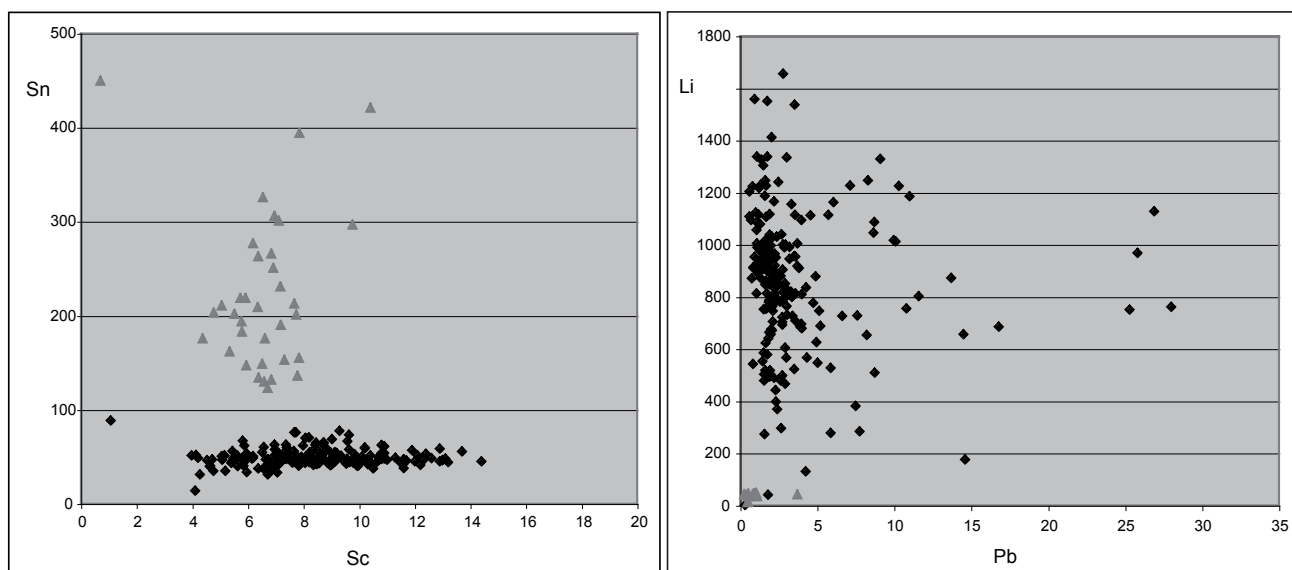
Fig. 8 Trace element plots of Sn vs. Sc and Li vs. Pb showing the two different amphibole generations. Values are in ppm.

Convection in the melt or not?

It is a matter of discussion, of which kind movements in the magma are and no concluding statement was established yet (see Latypov, 2003 for a review). Brandeis and Marsh (1989) and Hort et al. (1999) showed in their experiments for liquids cooled from above, that thermal convection decreases relatively quick and finally wanes completely after the liquid's superheat is gone. Their results cannot be assigned completely to natural magma systems because magmas usually do not contain significant amounts of superheat and have instead temperatures close to the liquidus. However, other workers come to the opposite result and provide evidence that thermal convection will be vigorous and compositional convection and crystal sedimentation will further enhance the convection (e.g. Martin et al., 1987; Jaupart and Tait, 1995).

Before we discuss both models with respect to the Ilímaussaq intrusion and in particular the kakortokite-lujavrite sequence therein, we look at the geology and the conditions under which this magma batch intruded. If one takes into account that the kakortokites and the lujavrites are geochemically closely related to each other and developed from one magma batch, then an estimation of the thickness of the magma chamber must include both rocks. A reconstruction of the magma chamber from the outcropping rocks gives a thickness of 700 to 800 m and most probably this magma chamber comprised the total horizontal extent of the intrusion, i.e. 17 x 8 km. Since the bottom of the intrusion is not exposed, this vertical extent of 700 – 800 m has to be regarded as a minimum estimation. Nonetheless, the magma chamber had clearly a disk-like geometry. Consequently, the heat loss will almost exclusively occur through the roof. Since the rocks forming the roof of the kakortokite-lujavrite sequence, namely pulaskite, foyaite, sodalite foyaite and naujaite, were formed from the earlier magma batch, there may have been residual heat from it within the roof rocks and the surrounding of the intrusion. The temperature of the roof at the time of intrusion of the fourth magma batch can only be estimated roughly, because the time gap between the two events is unknown. Ar-Ar dating gave evidence that the time interval between the two events was short (Krumrei et al., 2006), but the occurrence of naujaite xenoliths in unit +3 shows undoubtedly that the roof sequence was cooled below its solidus of approximately 500 °C (Konnerup-Madsen and Rose-Hansen, 1982) when the fourth magma batch intruded. However, the residual heat from the earlier magma batch resulted in lower thermal gradients between melt and country rocks and a thermal equilibrium is established faster than without the pre-heating. Also, the bottom of the magma chamber would have had elevated temperatures. Although the underlying rocks are not exposed today, geophysical data provided evidence for are larger mafic body at depth that probably represents more cumulates (Blundell, 1978; Forsberg and Rasmussen,

1978). This body may act together with a generally elevated geothermal gradient, as it is typical for rift settings, a source of heat from below.

First we follow the approach that predicts vigorous convection in the melt for a long period of time (e.g. Martin et al., 1987; Jaupart and Tait, 1995). Using the temperatures of the peralkaline magma (Sørensen, 1968; Larsen 1976), the magma densities and viscosities for dry and water-rich compositions (Larsen & Sørensen, 1987), the flow regime within the magma chamber expressed by the thermal Rayleigh number can be estimated (Bartlett, 1969). The calculation of the Rayleigh number for this magma results in very high numbers between 10^{12} and 10^{13}, which are a consequence of the low viscosity of the peralkaline magma. Despite the much lower temperature the viscosity is similar to that of basalt. As shown by Martin et al. (1987), the thermal Rayleigh number as calculated above gives only minimum estimates. If heat flux through the roof of the magma chamber and crystal settling is taken into account, the number will be orders of magnitude higher. Consequently, the formation of convection cells is very unlikely and the movement of the magma within the chamber is expected to have been rather chaotic. Also the surprisingly constant thickness of the units over a horizontal extension of more than 4 km argues against magma movement in discrete convection cells, which would have been numerous because of the low height and the large horizontal extension of the magma chamber.

According to the work of several authors (eg. Martin et al., 1987; Latypov, 2003), crystallisation will occur mainly in boundary layers, either at the roof or, more preferably, at the bottom of the magma chamber. Due to the high movement rates of the magma, the concept of crystallisation in boundary layers cannot explain the thickness of the units, the gradation of the minerals and the repetition of the layering because the stability of the boundary layers is very limited. We will discuss this below in more detail.

As shown above, the concept of vigorously convecting magma seems to be not applicable to the kakortokites. Therefore, we examine now the other model that predicts rather quiescent conditions regardless which Rayleigh number was calculated (Brandeis and Marsh, 1989; Hort et al. 1999). The elevated temperatures in the surrounding of the fourth intrusive batch resulted - as explained above - in a lower thermal gradient between melt and the walls and this in turn resulted in a less vigorous thermal convection soon after intrusion because thermal convection is driven by temperature contrasts. Nonetheless, the movements in the magma were strong enough to form currents resulting in the sedimentary features found in the lower kakortokites. Obviously, convection decreased rapidly with time because structures

like trough banding and current bedding are only visible in the lowermost units and very close to the margin of the kakortokites. The roof collapse producing the xenoliths in unit +3 may have intensified the movements for a while, because unit +4 contains once again numerous features indicating magmatic flow (Bohse et al., 1971). In general, the settling of the crystals seems to have happened in rather quiescent conditions. We therefore conclude that thermal convection played only a minor role and convection in the melt was mainly driven by crystal settling. Since natural melts usually do not contain significant amounts of superheat (in contrast to the liquids used in most of the analogue experiments) and have instead temperatures close to the liquidus, the kakortokite melt would already start with the quiescent phase of the model by Hort et al. (1999). In this model, movements close to the margin were detected even after the loss of the superheat, when the rest of the melt volume was more or less quiescent. Hort et al. explained this by the thermal gradient that developed at the margin because of the imperfect insulation of their experiment. Exactly the same is seen in the kakortokites. We find the undisturbed layering in the centre and features of magma flow close to the margins. At the very margins, the layering becomes enigmatic and more fine-scaled.

Place of crystallisation

According to the work of several authors (eg. Martin et al., 1987; Latypov, 2003), crystallisation will occur mainly in boundary layers, either at the roof or, more preferably, at the bottom of the magma chamber. The high movement rates of the magma would allow the thermal boundary layers to develop a thickness in the range of tenths of centimetres or at most a few metres. The compositional boundary layer would be only several millimetres thick (Martin et al., 1987). When the boundary layers achieve their critical thickness, they become unstable and the evolved melt therein will mix with the main magma body. Since the volume of the melt within the boundary layer is very small compared to that of the total melt, the effect on the bulk composition of the melt is insignificant. Only multiply repeated growth, crystallisation and breakdown will change the composition of the magma to such an extent that it starts to influence the composition of the liquidus minerals. However, it is hard to imagine, how this model of crystallisation can explain the order of crystallisation and the repetition of this order recorded in the kakortokites.

In contrast to the findings of Campbell (1978) and McBirney and Noyces (1979) that crystallisation mainly takes place at the bottom of the magma chamber, the crystallisation of the cumulus minerals in the kakortokites must have happened somewhere above the final settling horizon, since several features in the rocks can only be explained by crystal settling, for instance the fact that the layering bends above the large xenoliths in unit +3 or the density

grading of the minerals. Using formula (1) in Sparks et al. (1993), the critical concentration of crystals in the melt can be calculated that determines whether the crystals can sink down or remain suspended in the melt. At values below this critical concentration, the newly formed crystals float in the melt. At values above it, the crystals settle down. Using the density for a fluid-saturated melt (2290 kg*m^{-3}, from Larsen and Sørensen, 1987), typical densities for the minerals (2590, 2600, 2950, and 3440 kg*m^{-3} for nepheline, alkali feldspar, eudialyte and arfvesonite, respectively), a typical coefficient of thermal expansion (5*10^{-5} K^{-1}, from Sparks et al., 1993) and assuming a temperature gradient in the melt pile of 7 K, the resulting critical concentrations are 0.30, 0.29. 0.16, and 0.10 % for nepheline, alkali feldspar, eudialyte, and arfvesonite, respectively. This means that, besides the large temperature gradient from top to bottom, crystallisation from approximately 600 m of the magma pile is needed to produce enough crystals to build the average unit thickness of 8 m, if we assume that 70 % of the unit's volume is cumulus material and the rest formed from intercumulus liquids. Crystallisation from a magma layer or a boundary layer of several meters or less in thickness is not sufficient and would result in cumulate horizons in centimetre scale only. Additionally, the calculated thickness of the three differently coloured horizons of each unit is in good agreement with the actual average thickness relations reported by Bohse et al. (1971). The black and red layers have similar thicknesses and the white layer is several times thicker than the others.

In addition to the above-named densities of melt and minerals, we used for the calculation of the settling velocity a viscosity of 139 Pa*s (Larsen and Sørensen, 1987) and an equivalent radius of the grains of 1.5 mm. Due to the low viscosity of the melt and the relatively high density contrast between mineral grains and the melt, the settling velocities of crystals are high, i.e. between 0.9 and 3.5 m per day. Assuming contemporary crystallisation of all cumulus minerals from the whole magma column and in the same proportions everywhere, the contrast in the settling velocity for the different minerals would allow for the formation of well-sorted horizons of each mineral (Fig. 9). In fact, if one calculates the modal composition of this hypothetical cumulates after one mineral has completely settled down, the values are in excellent agreement with the actual modal compositions of the three kakortokite varieties reported by Ferguson (1967) and Sørensen (1968). Although the calculation of the settling velocity assumes settling in a quiescent medium, the general statement of good separation of the different minerals from each other holds also in a moving medium, since the relative velocities of the different minerals will not change. But in this case, the sorting of minerals would be enhanced because the movement of the melt will keep minerals less dense longer in suspension than the denser minerals.
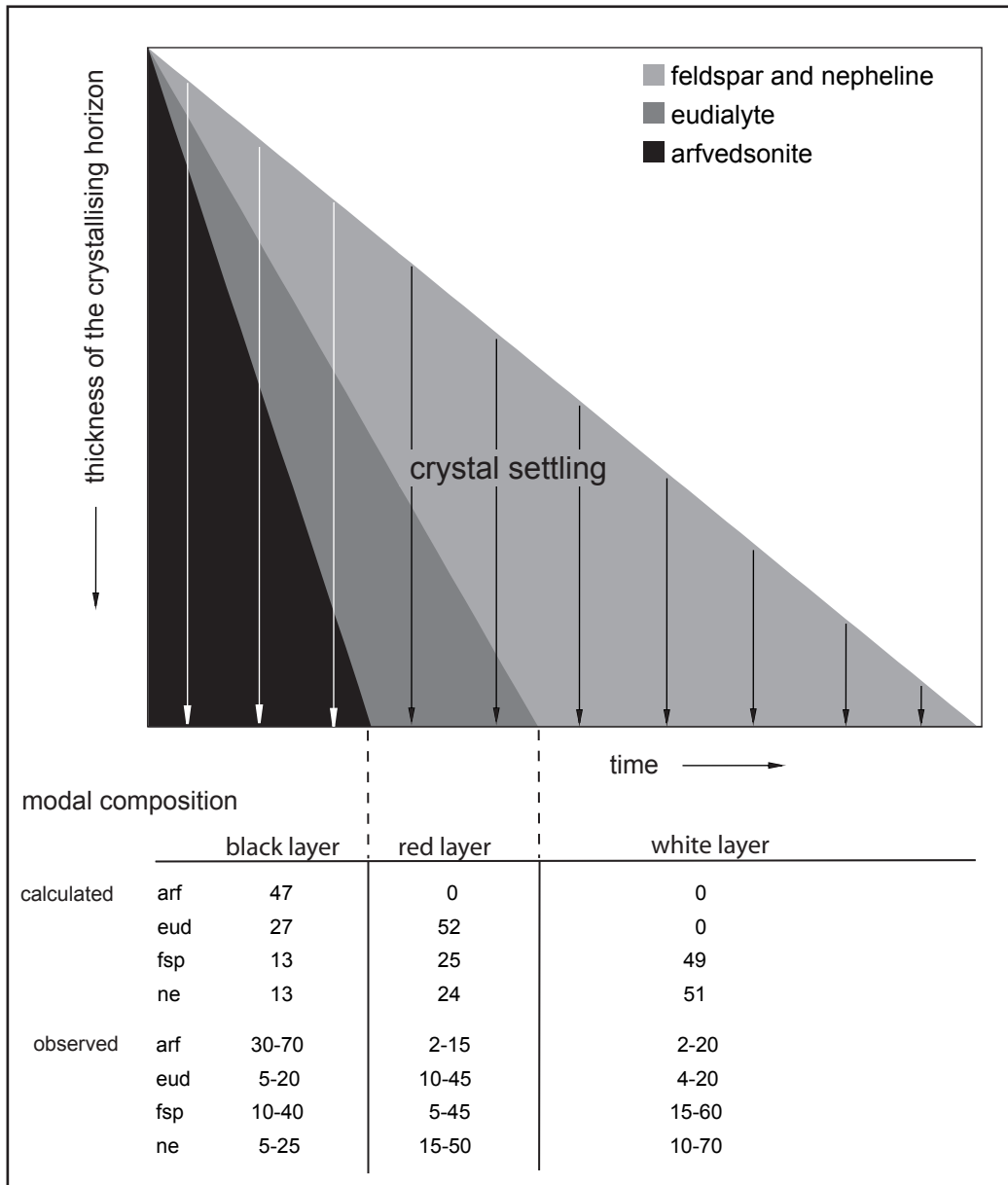
modal composition

		black layer	red layer	white layer
calculated	arf	47	0	0
	eud	27	52	0
	fsp	13	25	49
	ne	13	24	51
observed	arf	30-70	2-15	2-20
	eud	5-20	10-45	4-20
	fsp	10-40	5-45	15-60
	ne	5-25	15-50	10-70

Fig. 9 Diagram showing the different settling velocities of the different minerals assuming homogeneous nucleation and crystallisation. For the calculation we used the viscosity of the fluid-saturated melt from Sørensen and Larsen (1987), a thickness of the crystallising horizon of 600 m and an average equivalent radius of the crystals of 1.5 mm. The resulting settling velocities are 3.5, 2.0, 0.95, and 0.91 m/day for arfvedsonite, eudialyte, alkali feldspar, and nepheline, respectively. The latter two are plotted together, because they have nearly the same velocity. It takes ~650 days until all crystals are settled down. The modal proportions of the four minerals calculated from this diagram using the critical crystal concentration and the actually observed values (Ferguson, 1967; Sørensen 1968) are in excellent agreement.

Chemical trends in the amphiboles

The two amphibole generations expressed by their Na/K and Na/Ca ratios and the differing trace element contents (Fig. 5 and 8) were also found in amphiboles from late-stage pegmatites from Ilímaussaq (Müller-Lorch et al., 2007). The authors explained this observation with the hypothesis that the amphibole generation with low K values was formed in the presence of alkali feldspar that buffered the activities of Na and K. Once the melt evolved towards more differentiated conditions, analcime replaces the alkali feldspar as a stable phase. Sin

ce analcime does, in contrast to alkali feldspar, not incorporate significant amounts of K, the amphiboles would have to incorporate it. As analcime is a typical intercumulus phase in the kakortokites and the high-K analyses are typically from the amphibole rims, we assign the two amphibole generations in the kakortokite to the same process: the activities of Na and K in the main magma were buffered by alkali feldspar that crystallised contemporaneously with amphibole. In the highy evolved intercumulus melt, alkali feldspar was no longer a stable phase and analcime formed instead. The occurrence of the high-K amphibole generation is independent of the unit the sample comes from, but not independent of the sampling profile. The profile closest to the intrusion's margin has a significantly higher amount of amphibole with high K contents, which may be related to movements of intercumulus melt towards the margin of the intrusion induced by the load of the growing kakortokite pile. This squeezed-out intercumulus melt can further be related to the numerous pegmatitic structures in the so-called "border pegmatite", which is an up to 100 m wide zone interpreted as the contact facies of the kakortokite (Sørensen et al., 2006) although it can be found also at higher stratigraphical levels (Sørensen, 2006). The distribution of K, Na, and Ca in the grains supports the formation of the two generations with a temporal hiatus, because the changes in the element contents are not smooth but abrupt. The chemical change occurs preferably at the rim of the amphibole grains but also in the interior of a grain, which is then related to inclusions (Fig. 6). If the changes were due to a continuous process like the evolution of the melt, the change in the chemistry would be also continuous and not step-like as it is seen in the amphiboles. Besides the chemical trends in the amphiboles related to late-stage processes, also differentiation trends of ortho-magmatic origin were found. In almost all profiles the amphiboles record normal fractionation trends in terms of decreasing Mg and Ca values, increasing Li and Na contents and increasing X_{Fe} and Fe^{3+}/Fe^{2+} ratio with stratigraphical height. The latter is consistent with increasing oxygen fugacity during fractionation reported by Markl et al. (2001). In parts, these trends (e.g. for Mg) are already reported in the literature (Larsen, 1976). What is new is the finding of a different behaviour depending on the sample location and the distance to the margin of the intrusion. The amphiboles from profile 6 taken relatively close to the margin exhibit none of the fractionation trends except a small increase in Li and Fe^{3+}/Fe^{2+} ratio. Since the preferred mechanism of incorporation of Li in the arfvedsonites is the coupled substitution of $Li + Fe^{3+} = 2 Fe^{2+}$, this combination is not surprising. This means that the marginal melt participated in the increase in the oxygen fugacity but not in the chemical evolution. To explain this, one could argue for an influence of the nearby augite syenite, but as the amphiboles from the intrusion's centre have in the lowermost samples higher Ca and Mg contents, i.e. are somewhat more primitive than the amphiboles throughout the entire

marginal profile, this is unlikely. An influence of the augite syenite would result in more elevated Ca and Mg contents. Furthermore, there is the border pegmatite, which shields the evolving melt from the augite syenite (Fig. 2).

A possible explanation for the chemical differences depending on the distance to the margin is the different movement conditions in the magma as it was found by Hort et al. (1999). In their experiments, an upward directed flow of magma (respectively the analogue liquid) occurred close to the margins, and this movement is two orders of magnitude faster than the movement in the centre of the cooling liquid. They attributed this flow to a heat flux through the walls of the tank. However, this movement is not convection in discrete convection cells; it is rather a slow magma movement that is only visible at the margins. When the stream reaches the roof of the chamber, the up-flowing material mixes with the main body and since the volume of this upflow is almost insignificant compared to the main body, the movement carries away in the main body. Since a magmatic system is usually not heated through the walls like the liquid in this experiment but looses thermal energy through it, the flow is directed in the opposite direction, namely downwards. Applying the model to the Ilímaussaq intrusion, this down-flowing material stems from the upper part of the chamber and is consequently somewhat richer in volatiles. Therefore, the amphiboles from the marginal profile show a somewhat less primitive composition than those from the lowermost layers in the centre of the kakortokite (constantly around 0.13 p.f.u. Mg in profile 6 and a development from 0.21 to 0.11 p.f.u. Mg in profile 1). The composition of this material remains relatively constant, because the volatile-rich melt may not take part in the bulk crystallisation due to the lowering of the liquidus temperature by the volatiles.

We note that the amphibole trends within the kakortokite are minor compared to the development upwards. There are distinct changes in mineral and whole-rock chemistry when the kakorokites grade into the overlying lujavrites (Andersen et al., 1981; Pfaff, unpubl. data). These changes are also reflected in the petrography. The rocks become much more fine-grained and cumulate features die out upwards.

Origin of the recurrence of magmatic layering in the kakortokites

The layering in the kakortokite is a normal one with the densest minerals at the bottom (arfvedsonite) and the less dense minerals following upwards (eudialyte, feldspar and nepheline). From the petrography it is obvious that all cumulus minerals (arfvesonite, eudialyte, alkali feldspar and nepheline) crystallised at the same time and were separated from each other only by their different settling rate, although it is known that mafic minerals need less undercooling to nucleate than felsic minerals (Carmichael et al., 1974). The discussions and

calculations shown above demonstrate, that crystallisation from the whole magma was at stagnant or only slowly convecting conditions explains the thickness of the units, the thickness of the layers and their modal mineralogy very well. We will, therefore, use this setting as a basis for discussing the recurrence of the three-layer units for at least 29 times.

Larsen & Sørensen (1987) explained the layering by a multiply layered magma chamber. Their model is based on the formation of double-diffusive magma layers that allow heat and exsolved fluid to migrate upwards. Loosing fluids and heat to the next layer on top will cause crystallisation in the layer below, because of the now elevated liquidus temperature of the melt in this layer. This model also explains the repetition of the three-layer units. It fails to explain the bending of the layers above the huge xenoliths. Furthermore, crystallisation from a relatively thin melt horizon would not produce enough material to build up layers several metres thick. Another model to explain the recurrence of the layering was presented by Sørensen (1968), who invoked oscillatory changes of the liquidus temperature around the temperature of the magma caused by the migration of volatiles and thermal energy. Upton (1961) and Bohse et al. (1971) invoked periodic overturns of the magma by convection to be the cause of the recurrence of the three-layer units.

Together with the movement conditions in the melt discussed above, these findings point to an unlayered magma chamber. However, crystallisation from the total magma volume is energetically unlikely because homogeneous nucleation would by needed (Dowty, 1980). Lauder (1964) suggested that in a non-convecting system nucleation takes place at least in major parts of a magma chamber and Marsh (1998) lined out that nuclei may always be present in magmas with liquidus temperature, i.e. saturated magmas. The absence of resorption features in the cumulus minerals proves that the melt was saturated or oversaturated. This would imply that only some kind of activation is needed controlling crystallisation in an oscillatory way.

The temperature of the magma is not likely to vary abruptly to generate nucleation of all four cumulus minerals in the melt. Pressure changes, however, can lower the liquidus easily. Indeed, some authors suggested that there may have been a surface expression of the Ilímaussaq intrusion in terms of extrusive or eruptive activity (Ussing, 1912; Ferguson, 1964), although there are no remnants left today. Nonetheless, we argue for this volcanic activity because it would explain the recurrence of the units as a consequence of the frequent pressure release by the eruptions. Earlier workers (e.g. Sørensen, 1968) rejected this model because the sealing of the vent after a pressure release seemed unlikely. To overcome this problem, we draw an analogy to a model, which is used to explain the periodic activity

of geysers (e.g. White, 1967). With time, the pressure a system that is capable to develop a gaseous phase increases due to the formation of a low-density high-volume phase. When the internal pressure exceeds the hydrostatic pressure, this phase can escape leading to an abrupt pressure decrease in the system. After the steam is gone, the system will tranquilise and be closed again by the hydrostatic pressure. Subsequently, the internal pressure rises again, the next eruption occurs and so forth. In the melt of the kakortokite-lujavrite stage that was very enriched in volatiles, we can imagine a similar system: crystallisation led to an enrichment of volatiles in the remaining melt lowering its liquidus temperature by the pressure increase in the system. Subsequently, crystallisation occurred and the newly grown mineral grains could settle at the bottom. The down-sinking crystals caused movements in the melt that are directed in the opposite direction, i.e. upwards leading to the homogenisation of the residual melt. Cooling would have also resulted in an increase in pressure because the lower the melt's temperature the lesser volatiles could it hold in solution. At a time, the internal pressure combined with the buoyancy of the light fluids exceeded the hydrostatic pressure and a certain amount of volatiles or of extremely volatile-enriched melt from the roof of the chamber escaped, the pressure dropped suddenly leading to the formation of bubbles of volatiles. Since the volatile content of a melt affects its liquidus temperature strongly, the lost of volatiles resulted in an increase of the liquidus temperature and consequently crystallisation stopped. When the violence of the eruption slows down and the overpressure was gone, the hydrostatic pressure sealed the vent and the next cycle began.

Indeed, the melting experiments with the Ilímaussaq rocks accomplished by Piotrowski and Edgar (1970) and Sood and Edgar (1970) showed, that the volatile pressure has a strong impact on the liquidus temperature of the melt. They found for the foyaite, which is considered to be similar to the kakortokite, a liquidus temperatures of ~1100 °C and ~870 °C at atmospheric pressure and 1 kbar water pressures, respectively.

Conclusions

We present a comprehensive dataset of amphibole analyses from the strongly layered kakortokite unit of the peralkaline Ilímaussaq intrusion, South Greenland. In the light of these new data, we examined the conditions of crystallisation in the magma chamber and developed a new approach to explain the recurrence of the layering.

The calculations of the flow regime in the magma chamber and of the crystallisation indicate that crystallisation from 70-80 % of the magma volume is needed to explain the thickness of the units. Due to the low viscosity of the melt, only a very small proportion of crystals could be hold suspended in the melt. The calculations of the proportions of each cumulus

mineral are in excellent agreement with the findings in the field. The crystallisation itself is believed to have been caused by variations in the volatile pressure, which were in turn caused by eruptive escapes of volatiles or strongly volatile-enriched melt. These eruptions occurred frequently similar to geysers and are therefore responsible for the recurrence of the units. Because of the very small amount of crystals crystallised at each cycle, the changes in the mineral chemistry are minor but nonetheless detectable. The chemical evolution becomes much more articulate when the conditions changed drastically, which leads to other textures and other minerals in the rocks, e.g. the ceasing of the layering, flow textures, much more fine-grained rocks, etc. The structures in the rocks argue for crystallisation in a quiescent medium with some more movements at the beginning that may be a remnant of the intrusion process of the melt. At the walls of the intrusion, a slow down-flow of volatile-enriched melt from the roof may have occurred explaining the distance-dependent differences in the mineral chemistry of the amphiboles.

Acknowledgements

References

Allègre C.J., Provost A. and Jaupart C. (1981). Oscillatory zoning: a pathological case of crystal growth. Nature 294, 223-228.

Andersen S., Bailey J.C. and Bohse H. (1981). Zr-Y-U stratigraphy of the kakortokite-lujavrite sequence, southern Ilímaussaq intrusion. Rapp. Grønl. Geol. Unders. 103, 69-76.

Armstrong J.T. (1991). Quantitative elemental analysis of individual microparticles with electron beam instruments. In: Heinrich, K.F.J. and Newbury, D.E. (eds.), Electron Probe Quantitation. New York & London, Plenum Press. 261-315.

Bartlett R.W. (1969). Magma convection, temperature distribution, and differentiation. Amer. J. Sci. 267, 1067-1082.

Bailey J.C., Gwozdz R., Rose-Hansen J. and Sørensen H. (2001). Geochemical overview of the Ilímaussaq alkaline complex, South Greenland. In: H. Sørensen (ed.). The Ilímaussaq alkaline complex, South Greenland: status of mineralogical research with new results. Geol Greenl. Surv. Bul. 190, 35-54.

Barrière M. (1981). On curved laminae, graded layers, convection currents and dynamic crystal sorting in the Ploumanac'h (brittany) subalkaline granite. Contr. Mineral. Petrol. 77, 214-224.

Blaxland A. B., van Breeman O. & Steenfelt A. (1976). Age and origin of agpaitic magmatism at Ilimaussaq, south Greenland: Rb-Sr study. Lithos 9, 31-38.

Blundell D.J. (1978). A gravity survey across the Gardar Igneous Province, SW Greenland. J. Geol. Soc. London 135, 545– 554.

Bohse, H., Brooks, C.K., and Kunzendorf, H. (1971) Field observations on the kakortokites of the Ilímaussaq intrusion, South Greenland, including mapping and analyses by portable X-ray fluorescence equipement for zirconium and niobium. Rapp. Grønl. Geol. Unders. 38, 43 pp.

Boudreau A.E. (1987). Pattern formation during crystallisation and the formation of fine-scale layering. In: I. Parsons (ed.) Origin of igneous layering. Reidel, Dordrecht, 453-471.

Brandeis G.Jaupart C. and Allègre C.J. (1984). Nucleation, crystal growth and the thermal regime of cooling magmas. J Geophys. Res. 89 (B12), 10161-10177.

Brandeis G. and Marsh B.D. (1989). The convective liquidus in a solidifying magma chamber: a fluid dynamic investigation. Nature 339, 613-616.

Campbell I.H. (1978). Some problems with cumulus theory. Lithos 11, 311-321.

Carmichael I.S.E., Turner, F.J. and Verhoogen J. (1974). Igneous petrology. McGraw-Hill, New York.

Dowty E. (1980). Crystal growth and nucleation theory and the numerical simulation of igneous crystallisation. In: R.B. Hargraves (ed.) Physics of magmatic processes, Princeton University Press, Princeton, USA, 419-485.

Ferguson J. (1964). Geology of the Ilimaussaq alkaline intrusion, South Greenland. Bull. Grønl. Geol. Unders. 39, 82 pp.

Forsberg R. and Rasmussen K.L. (1978). Gravity and rock densities in the Ilímaussaq area, South Greenland. Rapp. Grønl. Geol. Unders. 90, 81– 84.

Hess H.H. (1960). Stillwater igneous complex. Geol. Soc. Am. Mem. 80, 230 pp.

Hort, M., Marsh B.d., Resmini R.g. and Smith M.k. (1999). Convection and crystallization in a liquid cooled from above: an experimental and theoretical study. J. Petrol. 40, 1271-1300.

Japart C. and Tait S. (1995). Dynamic of differentiation in magma reservoirs. J. Geophys. Res. 100, 17617-17636.

Konnerup-Madsen J. and Rose-Hansen J. (1982). Volatiles associated with alkaline igneous rift activity: fluid inclusions in the Ilimaussaq intrusion and the Gardar granitic complexes (South Greenland). Chem. Geol. 37, 79–93.

Krumrei T.V., Villa I.M., Marks M., and Markl G. (2006) A ^{40}Ar/^{39}Ar and U/Pb isotopic study of the Ilímaussaq complex, South Greenland: implications for the ^{40}K decay constant and for the duration of magmatic activity in a peralkaline complex. Chem. Geol. 227, 258-273.

Larsen L. M. (1976) Clinopyroxenes and coexisting mafic minerals from the alkaline Ilimaussaq intrusion, south Greenland. J. Petrol. 17, 258-290.

Larsen L.M. and Sørensen H. (1987) The Ilímaussaq intrusion – progressive crystallisation and formation of layering in an agpaitic magma. In: Fitton, J.G. & Upton B.G.J. (Eds.), Alkaline Igneous Rocks. Geol. Soc. Sp. Publ. 30, London, 473-488.

Lauder W.R. (1964). `Mat´ formation and crystal settling in magma. Nature 202, 1100-1101.

Leake B.E., Wooley A.R, Arps C.E.S., Birch W.D., Gilbert M.C., Grice J.D., Hawthorne F.C., Kato A., Kisch H.J., Krivovichec V.G., Linthout K., Laird J., Mandarino J., Maresch W.V., Nickel E.H., Rock N.M.S., Schumacher J.C., Smith D.C., Stephenson N.C.N., Ungaretti L., Whittake E.J.W., and Youzhi, G. (1997). Nomenclature of amphiboles; report of the Subcommittee on Amphiboles of the International Mineralogical Association Commission on New Minerals and Mineral Names. Europ. J. Mineral. 9, 623-651.

Maaløe S. (1987). Rhythmic layering of the Skaergaard intrusion. In: Parsons, I. (ed.) Origins of igneous layering. Reidel, Dordrecht, 247-262.

Markl, G., Marks, M., Schwinn, G., Sommer, H., 2001a. Phase equilibrium constraints on intensive crystallization parameters of the Ilímaussaq Complex, South Greenland. J. Petrol. 42, 2231–2258.

Marks M., Halama R., Wenzel T., and Markl G. (2004a). Trace element variations in clinopyroxene and amphibole from alkaline to peralkaline syenites and granites: implications for mineral–melt trace-element partitioning. Chem. Geol. 211, 185-215.

Marks M., Vennemann T., Siebel W., and Markl G. (2004b). Nd-, O-, and H-isotopic evidence for complex, closed-system fluid evolution of the peralkaline Ilímaussaq Intrusion, South Greenland. Geochim. Cosmochim. Acta 68, 3379-3395.

Marsh B.D. (1998). On the interpretation of crystals size distributions in magmatic systems. J. Petrol. 39, 553-599.

Martin D., Ross W.G., and Campbell I.H. (1987). Compositional and thermal convection in magma chambers. Contrib. Mineral. Petrol. 96, 465-475.

McBirney A.R. and Noyces R.M. (1979). Crystallisation and layering of the Skaergaard intrusion. J. Petrol. 20, 485-554.

McBirney A.R., White C.M. and Boudreau A.E. (1990). Spontaneous development of concentric layering in a solidified siliceous dike, East Greenland. Earth-Sci. Rev. 29, 321-330.

Müller-Lorch D., Marks M.A.W. and Markl G. (2007). Na and K distribution in agpaitic pegmatites.

Lithos 95, 315-330.

Muerer W.P. and Boudreau A.E. (1996). Petrology and mineral composition of the middle banded series of the Stillwater Complex, Montana. J. Petrol. 37, 583-607.

Naslund H.R., Turner P.A. and Keith D.W. (1991). Crystallisation and layer formation in the middle zone of the Skaergaard intrusion. Bull. Geol. Soc. Denmark 38, 165-171.

Pearce N.J.G., Perkins W.T., Westgate J.A., Gorton M.P., Jackson S.E, Neal C.R., Chenery S.P. (1997). A compilation of new and published major and trace element data for NIST SRM 610 and NIST SRM 612 glass reference materials. - Geostandards Newsletter, 21, 115-144.

Piotrowsi J.M. and Edgar A.D. (1970). Melting relations of undersaturated alkaline rocks from South Greenland compared to those of Africa and Canada. Medd. Grønl. 181, 62 pp.

Poulsen V. (1964). The sandstones of the Precambrian Eriksfjord Formation in South Greenland. Rapp. Grønl. Geol. Unders. 2, 16 pp.

Schönenberger J., Marks M., Wagner T., and Markl G. (2006). Fluid–rock interaction in autoliths of agpaitic nepheline syenites in the Ilímaussaq intrusion, South Greenland. Lithos 91, 331 – 351.

Sood M.K. and Edgar A.D. (1970). Melting relations of undersaturated alkaline rocks from the Ilímaussaq intrusion and Grønnedal-Ìka complex South Greenland, under water vapour and controlled partial oxygen pressure. Medd. Grønl. 181, 41 pp.

Sørensen H. (1966). On the magmatic evolution of tha alkaline igneous province of South Greenland. Rapp. Grønl. Geol. Unders. 7, 1-19.

Sørensen H. (1968). Rhythmic igneous layering in peralkaline intrusions. An essay review on Ilímaussaq (Greenland) and Lovozero (Kola, USSR). Lithos 2, 261-283.

Sørensen H. (2006). The Ilímaussaq alkaline complex, South Greenland – an overview of 200 years research and an outlook. Med. Grønl. Geosci. 45, 70 pp.

Sørensen H., Bohse H. and Bailey J.C. (2006). The origin and mode of emplacement of lujavrites in the Ilímaussaq alkaline complex, South Greenland. Lithos 91, 286-300.

Sparks R.S., Huppert H.E., Koyaguchi T., and Hallworth M.A. (1993). Origin of modal and rhythmic igneous layering by sedimentation in a convecting magma chamber. Nature 361, 246-249.

Steenfeld A. and Bohse H. (1975). Variations in the content of uranium in eudialyte from the differentiated alkaline Ilímaussaq intrusion, South Greenland. Lithos 8, 39-45.

Upton B.G.J. (1961). Textural features of some contrasted igneous cumulates from South Greenland. Bull. Grønl. Geol. Unders. 29.

Upton B.G.J., Emeleus C.H., Heaman L.M., Goodenough K.M., and Finch A.A. (2003). Magmatism of the mid-Proterozoic Gardar Province, South Greenland: chronology, petrogenesis and geological setting. Lithos 68, 43-65.

Ussing N.V. (1912). Geology of the country around Julianehaab, Greenland. Medd. Grønl. 38, 426 pp.

Wang Y. and Merino E. (1993). Oscillatory magma crystallization by feedback between the concentrations of the reactant species and mineral growth rates. J. Petrol. 34, 369-382.

Wilson A.H. (1996). The great dyke of Zimbabwe. In: G. Cawhorn (ed.) Layered intrusions. 365-402.

Wilson J.R. and Larsen S.B. (1985) Two-dimensional study of a layered intrusion – the Hyllingen Series, Norway. Geol. Mag. 122, 97-124.

White D.E. (1967). Some priciples of geyser activity, mainly from Steamboat Springs, Nevada. Am. J. Sci. 265, 641-684.

Wörner G. and Schmincke H.-U. (1984). Mineralogical and chemical zonation of the Laacher See tephra sequence (East Eifel, W. Germany). J. Petrol. 25, 805-835.